AN ANALYTICAL AND EXPERIMENTAL INVESTIGATION OF VORTEX-TYPE FLUID MODULATORS

by

David N. Wormley

S.B., Massachusetts Institute of Technology
(1962)

S.M., Massachusetts Institute of Technology
(1964)

SUBMITTED IN PARTIAL FULFILLMENT

OF THE REQUIREMENTS FOR THE

DEGREE OF DOCTOR OF PHILOSOPHY

AT THE

MASSACHUSETTS INSTITUTE OF TECHNOLOGY

OCTOBER, 1967

Signature of Author . . . . . .
Department of Mechanical Engineering, October, 1967

Certified by. . . . . .
Thesis Supervisor

Accepted by . . . . . .
Chairman, Departmental Committee on Graduate Students

AN ANALYTICAL AND EXPERIMENTAL INVESTIGATION OF VORTEX-TYPE FLUID MODULATORS

David N. Wormley

Submitted to the Department of Mechanical Engineering on October 27, 1967, in partial fulfillment of the requirements for the degree of Doctor of Philosophy.

Abstract

An analytical and experimental study of the steady-state characteristics of vortex valves which operate in the incompressible flow regime was conducted. The first part of the study considered the effects of fluid properties and geometry on the characteristics of the valve as viewed from the valve ports and led to the establishment of a valve design procedure. The second part of the study consisted in the investigation of the flow field within the vortex chamber.

As a result of the study of valve port characteristics it was found that the nondimensional valve characteristic was essentially independent of Reynolds number, chamber length, and supply port area if each of these parameters was within a specified broad range of values. The nondimensional valve characteristic was found to depend primarily upon two ratios -- the valve exit to chamber radius ratio and the ratio of the control port area to the exit port area. As a result of the experimental and analytical studies of valve characteristics, a procedure was developed for designing single exit valves which operate in the incompressible flow regime. The design procedure provides a systematic method of progressing from a set of input specifications which include the valve maximum control flow and pressure and maximum supply flow and pressure requirements to a specification of each of the critical dimensions in a prototype valve. As a part of the procedure, the prototype valve characteristic is checked to determine if multiple values of total flow exist at the cutoff value of control flow.

As part of the experimental study of the flow field within the vortex chamber a series of flow visualization photographs were taken and the pressure distribution across the valve chamber was measured for a number of inlet flow conditions. The flow visualization studies indicated that at sufficiently high vortex strengths all of the flow

passing through the chamber was contained in the chamber end wall boundary layers and that a region near the chamber midplane existed through which no radial flow passed. From the pressure profile data it was determined that at high vortex strengths substantial losses occurred in the mixing of the inlet flows with the main chamber flow.

A momentum integral analysis was developed for the flow in the valve main chamber. The analysis could be used to predict the pressure distribution across the chamber to the chamber exit given the flow conditions at chamber periphery. Pressure profiles computed with the aid of the analysis agreed closely with experimental profiles.

Thesis Supervisor: Herbert H. Richardson

Title: Associate Professor of Mechanical Engineering

ACKNOWLEDGEMENTS

The members of the Mechanical Engineering Department have provided a unique and very rewarding educational experience for me during the past eight years. The many contributions of the Department members are greatly appreciated. Especially helpful in the leading to a completion of my doctoral thesis investigation has been the assistance of the members of the Engineering Projects Laboratory.

In particular, I would like to express my sincere gratitude to the following persons:

Professor H. H. Richardson who as Thesis Advisor has provided invaluable guidance and encouragement throughout the investigation. His counsel and continuing interest in my professional development are warmly appreciated.

Professors S.Y. Lee, P.G. Hill, and J.L. Smith Jr. who as Thesis Committee members have contributed valuable advice and criticism through their spirited discussions.

Professors R. W. Mann and H. M. Paynter who have been so instrumental in providing a unique educational experience.

Roger Humphrey, Jens Jorgensen, and Adam Bell, who as fellow students and colleagues have provided so many timely suggestions.

Pat Perry who cheerfully and expertly typed the final manuscript.

My wife, Shirley, whose patience has seemed without limit.

I wish to acknowledge the M.I.T. Computation Center for the use of its facilities.

This thesis was supported in part by the U.S. Air Force under contract AF 33(615)-3601, and Harry Diamond Laboratory, under contract DAAG39-67-C-0019, and sponsored by the Division of Sponsored Research of M.I.T.

TABLE OF CONTENTS

	Page
ABSTRACT	2
ACKNOWLEDGEMENTS	4
LIST OF FIGURES	10
LIST OF TABLES	13
NOMENCLATURE	14
PART I INTRODUCTION AND SUMMARY	18
CHAPTER 1 THE PROBLEM	19
1.1 Introduction	19
1.2 The Vortex-Type Fluid Modulator	20
1.3 The Variety of Vortex-Type Devices	26
1.4 Scope of the Investigation	27
CHAPTER 2 SUMMARY OF RESULTS	29
2.1 Introduction	29
2.2 Summary of Studies Leading to a Vortex Valve Design Procedure	29
2.3 Summary of Studies of the Flow Field in Short Vortex Chambers	34
2.4 Recommendations for Further Research	39
PART II THE FLUID MODULATOR PORT-CHARACTERISTICS	41
CHAPTER 3 THE INVISCID VALVE MODEL	42
3.1 Derivation of the Characteristic Equation	42
3.1.1 The Inlet Ports	42
3.1.2 The Valve Main Chamber	45

Page

3.1.3 The Exit Port 46

3.1.4 The Inviscid Valve Characteristic 47

CHAPTER 4 EXPERIMENTAL VALVE CHARACTERISTICS 55

4.1 Introduction 55

4.2 The Experimental Apparatus 55

4.3 The Experimental Results 59

4.3.1 The Influence of Reynolds Number 60

4.3.2 The Influence of Geometry 63

4.3.2.1 The Control Port Area 63

4.3.2.2 The Supply Port Area 67

4.3.2.3 The Exit Port Area 69

4.3.2.4 The Chamber Length 73

4.3.2.5 The Chamber Radius 75

4.4 Determination of Vortex Valve Maximum and Minimum Flow Properties 77

4.5 Comparison of Experimental Data with the Results of the Inviscid Theory 85

CHAPTER 5 VORTEX VALVE DESIGN 90

5.1 Introduction 90

5.2 The Design Procedure 91

5.2.1 Input Specifications 92

5.2.2 Nondimensional Performance Parameters 93

5.2.3 Selection of Prototype Valve Dimensionless Geometric Parameter Values 93

5.2.4 Existence of Multiple Values of Total Flow at the Cutoff Value of Control Flow 96

Page

5.2.5 The Values of the Valve Critical Dimensions . . . 103

5.2.6 Sketch of the Prototype Valve Characteristic . . 105

5.2.7 Summary of the Design Procedure 105

5.3 Design Example 105

5.4 Influence of Valve Dynamic Behavior on Valve Design . . 109

5.5 Construction of a Prototype Valve 112

5.6 The Vortex Valve as a Circuit Component 117

PART III STUDIES OF THE FLOW FIELD IN THE VORTEX CHAMBER 129

CHAPTER 6 EXPERIMENTAL STUDIES OF THE FLOW FIELD IN SHORT VORTEX CHAMBERS 130

6.1 Introduction 130

6.2 Flow Visualization Studies 131

6.3 End Wall Static Pressure Distributions 142

6.4 Effective Chamber Outer Wall Tangential Velocity 153

CHAPTER 7 ANALYTICAL INVESTIGATION OF THE FLOW FIELD IN SHORT VORTEX CHAMBERS 158

7.1 Introduction 158

7.2 Formulation of the Flow Model 161

7.2.1 The Developing Flow Region 161

7.2.2 The Developed Flow Region 173

7.2.3 Specification of the Velocity Profile Functions and the Shear Law 176

7.3 Solution of the Vortex Chamber Equations 180

7.4 Comparison of Predicted and Experimental Pressure Profiles 189

Page

7.5 Requirements of an Analytical Method of Predicting Vortex Valve Characteristics 194

APPENDICES

APPENDIX A TABULATION OF TEST CONDITIONS 196

APPENDIX B CONTROL PORT PRESSURE-FLOW CHARACTERISTICS 198

BIBLIOGRAPHY 200

BIOGRAPHICAL NOTE 205

LIST OF FIGURES

		Page
1.1	Sketch of a Conceptual Vortex Valve	21
1.2	Typical Vortex Valve Characteristics	23
3.1	Vortex Valve Inlet, Main Chamber, and Exit Regions	43
3.2	The Influence of h/r_e and A_s/A_e on the Maximum Valve Flow	50
3.3	The Inviscid Valve Characteristics	52
4.1	Photograph of the Four Inch Test Valve	56
4.2	Vortex Valve Test Flow Loop	58
4.3	The Influence of Reynolds Number on the Valve Characteristics	61
4.4	The Influence of Control Port Area on the Valve Characteristic	64
4.5	Correlation of Valve Characteristics for Various Control Port Areas	66
4.6	The Influence of Supply Port Area on the Valve Characteristic	68
4.7	The Influence of Exit Radius on the Valve Characteristic. . .	
4.8	The Dual Exit Valve Characteristic	72
4.9	The Influence of Chamber Length on the Valve Characteristic	74
4.10	The Influence of Chamber Radius on the Valve Characteristic	76
4.11	Photograph of Maximum and Minimum Flow Test Apparatus	78
4.12	Vortex Valve Turndown Ratio	82
4.13	Vortex Valve Cutoff Control Pressure Ratio	83

		Page
4.14	Valve Quiescent Power Drain Ratio	84
4.15	Comparison of Inviscid and Experimental Valve Characteristics	86
5.1	Vortex Valve Cutoff Flow Characteristics	95
5.2	Characteristics of Prototype Valve A and Valve B	97
5.3	Determination of the Existence of Multiple Values of Total Flow at the Cutoff Control Flow	100
5.4	Vortex Valve Cutoff Flow Characteristics	102
5.5	Summary of Design Procedure	106
5.6	Sketch of Prototype Hydraulic Valve Characteristic	110
5.7	Photograph of One Inch Chamber Diameter Planar Valve . . .	114
5.8	Characteristic of the Planar Valve	115
5.9	Vortex Valve Bridge Circuits	118
5.10	Determination of the Family of Valve Characteristics. . . .	120
5.11	Derivation of Supply Port Input Characteristics	121
5.12	The Supply Port Input Characteristics	122
5.13	Derivation of Exit Port Output Characteristics	124
5.14	The Exit Port Output Characteristics	125
5.15	Derivation of Half Bridge Characteristics	126
5.16	The Half Bridge Characteristics	127
6.1	Photograph of Seven Inch Chamber Diameter Valve	132
6.2	Flow Conditions for the Flow Visualization Photographs . .	133
6.3	Flow Visualization Photograph #1, $\frac{v_o^+}{u_o} = 407$	135
6.4	Flow Visualization Photograph #2, $\frac{v_o^+}{u_o} = 215$	136
6.5	Flow Visualization Photograph #3, $\frac{v_o^+}{u_o} = 58$	137
6.6	Flow Visualization Photograph #4, $\frac{v_o^+}{u_o} = 24$	138

		Page
6.7	Interpretation of the Flow Visualization Photographs	141
6.8	Photograph of the Pressure Profile Test Apparatus	144
6.9	Experimental Pressure Profile in the 0.25 Inch Exit Radius Dual Exit Chamber.	148
6.10	Experimental Pressure Profile in the 0.25 Inch Exit Radius Single Exit Chamber	149
6.11	Experimental Pressure Profile in the 0.50 Inch Exit Radius Single Exit Chamber	150
6.12	Influence of Ideal Ratio of Peripheral Tangential to Radial Velocity on the Jet Recovery Factor	156
7.1	The Developing and Developed Flow Regions	162
7.2	Experimental Velocity Profiles from the Data of Savino and Keshock.	167
7.3	Comparison of Velocity Profiles from Data of Savino and Keshock with Analytical Profiles	178
7.4	Analytical Flow Properties of the Vortex Chamber for BLC = 0.01	183
7.5	Analytical Flow Properties of the Vortex Chamber for BLC = 0.05	184
7.6	Circulation Distribution in the Vortex Chamber	187
7.7	Comparison of Analytical and Experimental Pressure Profiles for the 0.25 Inch Exit Radius Dual Exit Chamber	190
7.8	Comparison of Analytical and Experimental Pressure Profiles for the 0.25 Inch Exit Radius Single Exit Chamber	191
7.9	Comparison of Analytical and Experimental Pressure Profiles for the 0.5 Inch Exit Radius Single Exit Chamber	192

LIST OF TABLES

Page

4.1 Comparison of Predicted Values of $\bar{W}_o^+$ and $\bar{P}_c^+$ with Experimental Data 88

6.1 Tabulation of Pressure Profile Test Conditions 147

NOMENCLATURE

A_c	total tangential control port area
A_e	total chamber exit area
A_o	chamber outer periphery curtain area
A_s	total radial supply port area
BLC	boundary layer coefficient defined in equation 7.51
BLC^*	modified boundary layer coefficient defined in equation 7.52
C_c	control port discharge coefficient
C_e	exit port discharge coefficient
C_t	equivalent friction factor
C_s	supply port discharge coefficient
D	chamber diameter
$f(\eta)$	velocity profile function
$g(\eta)$	velocity profile function
G	geometric constant defined in equation 3.17
h	chamber height
p_c	control port pressure measured relative to valve exhaust pressure
p_{cc}	control port pressure at cutoff measured relative to valve exhaust pressure
p_e	pressure at radius r_e measured relative to valve exhaust pressure
p_o	pressure at radius r_o measured relative to valve exhaust pressure

p_s	supply pressure to valve measured relative to valve exhaust pressure
p_t	pressure tap pressure, gage
p_{dg}	valve exhaust pressure, gage
p_{sg}	valve supply pressure, gage
$\bar{P} = \frac{p}{p_s}$	a nondimensional pressure
$\bar{P} = \frac{p}{\rho u_o^2}$	a nondimensional pressure
$\bar{P}_c^+$	nondimensional pressure at $\bar{W}_o = 0.707$
Q_{AV}	average volumetric flow rate
Q_c	volumetric control flow
Q_s	volumetric supply flow
Q_t	volumetric total flow
$\overline{QP}$	cutoff quiescent power drain ratio
r_e	exit radius
r_o	chamber radius
R_w	maximum flow Reynolds number
T	chamber fill time
TR	valve turndown ratio
u	radial velocity defined positive in + r direction
u_e	radial velocity at r_e defined positive in - r direction
u_o	radial velocity at r_o defined positive in - r direction
u_s	secondary velocity coefficient
u_δ	primary velocity coefficient
U	nondimensional primary radial velocity coefficient defined positive in - r direction

U_s	nondimensional secondary velocity coefficient defined positive in - r direction
v	tangential velocity
v_δ	tangential velocity at $y = \delta$
v_e	tangential velocity at r_e
v_o	tangential velocity at r_o
v_o^+	ideal peripheral tangential velocity
v_w	tangential velocity at chamber outer periphery
V_t	effective total velocity at chamber midplane
V_∞	free stream tangential velocity
w	axial velocity
W_c	control mass flow rate
W_{cc}	control mass flow rate at cutoff
W_o	total mass flow rate
W_m	maximum mass flow rate
W_s	supply mass flow rate
$\bar{W} = \frac{W}{W_m}$	nondimensional flow rate
$\bar{W}_c^+$	nondimensional control flow at $\bar{W}_o = 0.707$
$\alpha_1 \ldots \alpha_5$	velocity profile coefficients
γ	geometric constant defined in equation 3.12
Γ	nondimensional circulation
δ	boundary layer thickness
$\bar{\delta}$	nondimensional boundary layer thickness
ϵ	jet recovery factor
μ	operating fluid viscosity

η	ratio of axial displacement to boundary layer thickness
λ	ratio outer periphery tangential to radial velocity
π	3.1416
ρ	operating fluid density
τ_r	shear stress in radial direction
τ_t	shear stress in tangential direction
$\bar{\tau}_{rw}$	nondimensional end wall shear stress in radial direction
$\bar{\tau}_{tw}$	nondimensional end wall shear stress in tangential direction

PART I

INTRODUCTION AND SUMMARY

CHAPTER 1

THE PROBLEM

1.1 Introduction

In the past few years considerable interest has developed in fluidics, or no moving part fluid devices. Much of the interest in fluidic devices stems from their potential reliability and insensitivity to extreme environmental conditions of temperature, radiation, shock, or vibration. Many of the fluidic devices which have been developed utilize a relatively constant-power primary flow stream which is modulated by a relatively low power level secondary flow stream. These types of fluid modulators include both proportional and digital amplifiers such as beam deflection proportional and wall attachment bistable amplifiers as well as impact modulators and turbulence amplifiers. Although these fluid amplifiers are attractive for signal level applications and can perform many of the common digital logic functions, their constant input power consumption precludes their use in high power level applications in which quiescent power drain is an important consideration. One fluid amplifier -- the vortex amplifier -- has been developed in which the input power consumption may be modulated. The vortex amplifier, or the vortex valve, is the subject of the present study.

1.2 The Vortex-Type Fluid Modulator

A conceptual vortex amplifier is sketched in Figure 1.1. The amplifier consists of a short cylindrical chamber with an exit port in the center of one end plate (in some cases dual exits are used with an exit in both the top and bottom plate) and two types of inlet ports -- a supply port which injects fluid radially into the chamber and a control port which injects fluid tangentially into the chamber. In valve operation under the condition of zero control flow, supply flow proceeds directly from the valve supply ports to the valve exit port with negligible pressure drop across the chamber. In this condition the pressure at the valve exit orifice is essentially supply pressure and maximum flow passes through the valve. When control flow is injected tangentially into the chamber, a tangential velocity is imparted to the fluid at the outer edge of the chamber. As the fluid moves toward the center of the chamber, conservation of angular momentum requires that its tangential velocity increase and ideally a potential vortex is formed. The flow field of the vortex creates a pressure drop across the valve chamber between the supply ports and the exit orifice and in effect increases the resistance to flow through the valve. As the tangential control flow is increased, the strength of the vortex in the main chamber is increased and the total flow through the valve is decreased. The vortex valve is basically a flow amplifier in which a relatively small tangential control flow is used to modulate the relatively large total flow through the valve. Typical nondimensional vortex valve

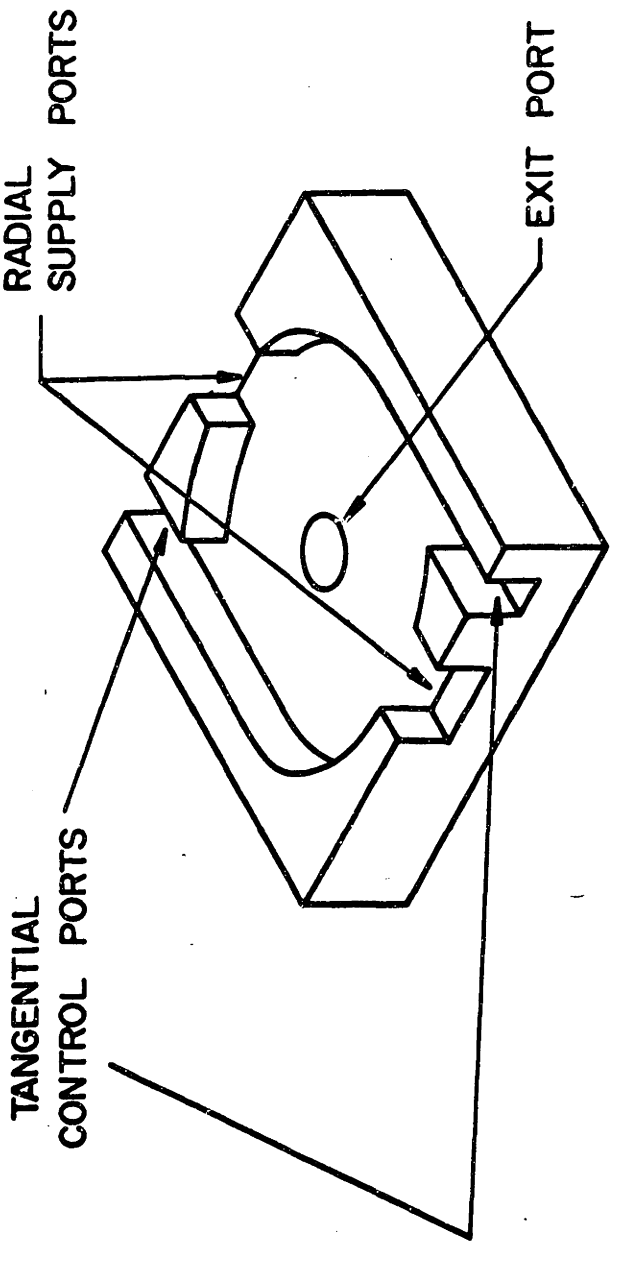

Fig. 1.1. Sketch of a Conceptual Vortex Valve.

characteristics in which the flows are normalized with respect to the flow through the valve at zero control flow are plotted in Figure 1.2 for the case of constant valve supply and exhaust pressures. The two characteristics which have been plotted are labeled as proportional and bistable and represent typical characteristics obtainable with various valve geometries. Some properties of these characteristics are of particular interest. In both the bistable and proportional characteristics the cutoff point is of interest. The cutoff point is defined as the point on the characteristic where sufficient control flow has been added to the valve to shut off the supply flow completely. At this point on the characteristic the total flow through the valve is equal to the control flow. Some common figures of merit for vortex valve performance relate the pressure and flow conditions at cutoff to those at the maximum flow condition. The valve turndown ratio TR, which is equal to the reciprocal of the nondimensional cutoff control flow $\bar{W}_{cc}$, represents the ratio of the maximum to minimum valve flow. The cutoff control pressure ratio $\bar{P}_{cc}$ is the ratio of the valve control port pressure at cutoff to the valve supply pressure where both pressures are measured relative to the valve exhaust pressure. For valves operated in the incompressible flow regime, the product $\bar{P}_{cc}\bar{W}_{cc}$ of the nondimensional cutoff control pressure ratio and cutoff control flow is the cutoff quiescent power drain ratio $\overline{QP}$ and represents the ratio of the valve power consumption at cutoff to the power consumption at the maximum flow condition.

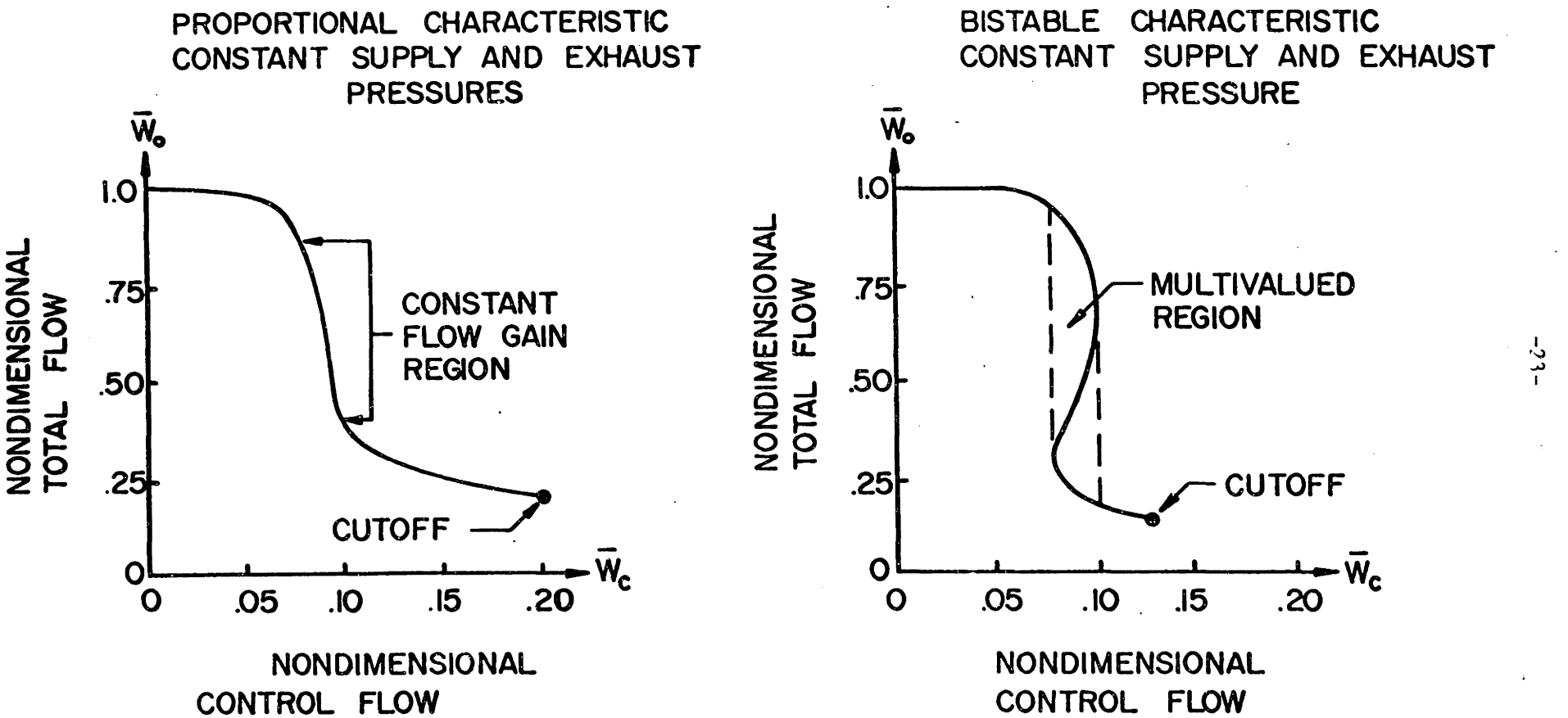

Fig. 1.2. Typical Vortex Valve Characteristics.

An additional parameter of interest in the proportional valve is the incremental flow gain $\frac{\Delta W_o}{\Delta W_c}$. It is noted that the flow gain is usually negative; i.e. an increase in control flow decreases the valve total flow. It is also noted that the incremental flow gain of the valve is strongly dependent upon where on the valve characteristic it is measured since the vortex valve characteristic is highly nonlinear. In a given proportional valve characteristic the incremental flow gain may vary from a value near zero at the valve maximum and minimum flow points to a value exceeding several hundred in the middle flow range of the valve. The valve characteristic has been called proportional simply because over a part of its total flow range the incremental flow gain is finite and nearly constant.

In the bistable valve characteristic of Figure 1.2 the flow gain is not constant and finite over any significant part of the valve characteristic and varies from zero to infinity. The bistable characteristic also contains a region in which multiple values of total flow exist for a given value of control flow. In some cases a valve will tend to support sustained oscillations when the control flow is set so that the valve operates in the multivalued flow region. This valve characteristic has been called bistable because essentially only two stable operating points exist -- a flow level near the maximum flow and a flow level near the minimum flow.

Although the valve characteristics presented here are plotted as total flow versus control flow to illustrate the basic flow amplification properties of the valve, other common ways of presenting

valve characteristics are to plot total flow versus control pressure for constant supply and exhaust pressures, or total flow versus supply pressure for selected values of control flow or pressure, with constant valve exhaust pressure.

Studies of the vortex valve which have provided some valuable data on the influence of geometry and fluid properties on the valve characteristics have been described in References 1, 2, and 10. Mayer (10)* has shown that the characteristic measured on a given vortex valve operating in the compressible flow regime can be scaled to find the characteristic of the valve operating at a different supply, exhaust, or control pressure level. He has also described a procedure by which vortex valve characteristics can be scaled with respect to control port area. Gebben (1) has studied the effects of control port area and supply pressure level in a single valve with a fixed radius ratio on the valve cutoff characteristics. In a study to build an optimum turndown ratio valve Koerper (2) has presented data which is primarily concerned with the influence of geometry on the valve cutoff pressure and flow properties.

Because the vortex valve is unique among fluidic elements with respect to its ability to modulate input power consumption, it has found use in a number of applications for which jet interaction amplifiers are not attractive. References 3, 4, 5, 6, 7, 8, 12 and 13

---

* Numbers in ( ) refer to references listed in Bibliography.

describe a variety of vortex valve applications including the fabrication of a fluidic servovalve, the design of flight control systems, nuclear rocket engine control systems and others. In some of these references vortex valves with vented outlet flow receivers (5,6) have been described and valves with center tap pressure pick ups (3,8) have been tested in an effort to develop valves which act as pressure amplifiers.

The property which most severely limits the application of the vortex valve is the requirement that the valve control port pressure be greater than the valve supply pressure. This property of the valve imposes some restrictions on the ability to stage vortex valves with the result that for some signal level applications vortex valves are less attractive than other types of fluidic devices.

1.3 The Variety of Vortex-Type Devices

Although the vortex valve has received considerable attention only in the last few years other devices utilizing vortex-type flows have been of interest to researchers for the past few decades. A large number of studies have been conducted on a wide variety of vortex-type devices including the cyclone separator (15), the Ranque-Hilsch tube (16), the gaseous vortex reactor (17), and vortex whistle (18). More recently, interest has also been devoted to studies of a counter vortex oscillator (38), digital flow meter (39), and vortex rate gyroscope (40). Reference 10 contains a graph showing the rapid rate of increase in publications concerning vortex-type devices from 1920 to 1967. The literature is so profuse on

vortex-type devices that it is impractical to discuss each study in detail in this thesis. Studies of vortex phenomena which are directly applicable to parts of the present investigation are referenced in the appropriate parts of the thesis.

1.4 Scope of the Investigation

Although vortex related devices have been studied for more than three decades and vortex amplifiers have been under intensive study since 1961, no procedure has been developed for vortex valve design. The development of a purely analytical design procedure has been prohibited to date by the lack of an adequate description of the complex and many faceted three dimensional flow fields existing in the vortex valve inlet, main chamber, and exit regions. The development of a semi-empirical design procedure has been hampered by the lack of adequate and complete experimental data which indicates the influence of fluid properties and valve geometry on the valve characteristic. In the present investigation the solutions to two strongly coupled, but somewhat distinct, problems are sought:

Problem 1

The development of sufficient analytical and experimental information concerning vortex valve characteristics as viewed from the valve ports to establish a technique for designing vortex valves.

Problem 2

The investigation of the flow field within the valve to provide a basic understanding of valve

behavior and provide a basis for the development of a complete rational model for vortex valve behavior.

In seeking the solutions to these two problems, the investigation has been limited in scope primarily to a consideration of the steady-state characteristics of single exit valves which operate in the incompressible flow regime.

In the investigation of Problem 1 an experimental study is undertaken to determine the influence of geometry and fluid properties on the vortex valve characteristics. The experimental data from this investigation is coupled with the results of an idealized analysis of the vortex valve to generate a semi-empirical procedure for designing vortex valves. In the investigation of Problem 2 the scope of the investigation is limited primarily to an investigation of the flow in the valve main chamber. An investigation which included a comprehensive study of the main chamber region as well as the inlet and exit regions of the valve was not feasible within the scope of the present investigation. Effort was concentrated in the investigation of the valve main chamber region because an adequate understanding of this region appeared at the onset of the investigation to be a prerequisite for future studies leading to a complete rational model of the vortex chamber valid for both steady state and dynamic performance.

CHAPTER 2

SUMMARY OF RESULTS

2.1 Introduction

In the preceding section of this thesis two problems have been posed. The solution to Problem 1 required the development of a vortex valve design procedure while the solution to Problem 2 required an investigation of the flow field within the valve chamber. The work conducted in the effort to solve Problem 1 is described in Chapters 3, 4 and 5 of the thesis. Chapters 3 and 4 provide the basic analytical and experimental work required for the design procedure which is developed in Chapter 5. Chapter 5 has been written so that it can be read independently of Chapters 3 and 4. A summary of these three chapters is included in Section 2.2 of this chapter.

The work concerned with the solution to Problem 2 is described in Chapters 6 and 7. Chapter 6 describes the basic experimental investigation which provided the physical insight of the flow in the vortex chamber required to formulate the analytical model developed in Chapter 7. The results of Chapters 6 and 7 are summarized in Section 2.3 of this chapter.

2.2 Summary of Studies Leading to a Vortex Valve Design Procedure

In this section the results of an analytical and experimental investigation of the steady-state characteristics of vortex valves

operating in the incompressible flow regime are summarized. As a result of these studies a procedure has been developed for designing vortex valves.

In the analytical part of the investigation an idealized model of the vortex valve was formulated which is based upon the assumptions that the flow in the valve main chamber is steady, incompressible, and inviscid and that the mixing of the inlet flows to the valve is lossless. As a result of the analysis it was found that the inviscid valve characteristic was primarily a function of the valve radius ratio $\frac{r_e}{r_o}$ and the control to exit port area ratio $\frac{A_c}{A_e}$. The inviscid valve characteristic was essentially independent of valve chamber length and supply port area if these two quantities were sufficiently large. The inviscid valve characteristic, which is multivalued over almost the complete flow range, agreed closely with experimental valve characteristics at large values of total flow and agreed poorly at low values of total flow (near the minimum flow point on the characteristic). The values of control pressure and flow required at 70.7% maximum flow which were predicted by the inviscid analysis agreed within 15% of experimentally measured values over a wide range of valve geometries. The ability of the inviscid analysis to predict the pressure and flow requirements at 70.7% maximum flow provides one part of the information required to determine if multiple values of total flow exist at the cutoff value of control flow in a prototype valve.

The purpose of the experimental investigation was to determine the influence of fluid properties and valve geometry on the

incompressible valve characteristic. The tests were conducted primarily on single exit valves. As a result of tests conducted with both air and water, it was found that the nondimensional valve characteristic is maximum flow Reynolds number and supply pressure level independent for valves operated at maximum flow Reynolds numbers (Reynolds number based on maximum valve weight flow, chamber diameter, and operating fluid viscosity) greater than 7'50 and for values of supply pressure sufficiently low so that the flow in the valve can be considered incompressible. No upper limiting value of Reynolds number was found at which the nondimensional valve characteristic became significantly dependent upon Reynolds number. At the highest Reynolds number tested in the investigation of 3300, the nondimensional valve characteristic showed no dependence upon maximum flow Reynolds number. Data in the literature which is referenced in the thesis suggests that the nondimensional valve characteristic may continue to be maximum flow Reynolds number independent, or very weakly dependent upon Reynolds number for values of maximum flow Reynolds number which are 3-4 times the largest Reynolds number tested in this investigation. The fact that the nondimensional valve characteristic is maximum flow Reynolds number and supply pressure level independent under the conditions specified above indicates that the nondimensional valve characteristic measured on a given valve geometry at constant supply and exhaust pressures is a universal characteristic which can be used to determine the valve dimensional characteristics for a wide range of both supply and exhaust pressures and operating fluids. This result has provided the basis for the design procedure developed in the investigation and

for the evaluation of fluid circuits containing vortex valves which operate under varying supply and exhaust pressure levels.

Tests conducted to determine the influence of geometry on the valve characteristic indicated that the nondimensional valve characteristic depended primarily upon the valve radius ratio $\frac{r_e}{r_o}$ and control to exit port area ratio $\frac{A_c}{A_e}$. As the valve radius ratio was increased by increasing the exit radius, the value of nondimensional control flow required at each point on the characteristic decreased while the value of nondimensional control pressure increased. It was also noted that as $\frac{r_e}{r_o}$ increased, the valve characteristic tended to become multivalued and agree closely with the inviscid valve characteristic over a greater flow range. As the valve control to exit port area was increased by increasing the control port area, the value of nondimensional control flow required at each point on the characteristic increased and the value of nondimensional control pressure decreased. It was found that the effect of control port area on the valve characteristic could be successfully scaled with respect to the parameter $\bar{W}_c/\sqrt{A_c/A_e}$ for variations in control port area of at least a factor of two.

The value of valve supply port area was not found to influence the valve characteristic significantly if the valve supply port area was greater than three times the exit port area. The valve characteristic was also independent of the value of valve chamber length within the range of chamber lengths tested in the investigation which included $0.144 \frac{h}{r_o} < 0.64$ with $2 \leq \frac{h}{r_e}$.

Since vortex valve characteristics could be reduced to a function of only two variables $\frac{A_c}{A_e}$ and $\frac{r_e}{r_o}$ under the conditions in which the maximum flow Reynolds number, valve chamber length, and valve supply port area are within the bounds specified above, it was feasible to determine a map of valve cutoff characteristics. A series of experiments was conducted with a single exit valve geometry to determine valve turndown ratio, cutoff control pressure ratio, and cutoff quiescent power drain ratio for a wide range of values of the parameters $\frac{A_c}{A_e}$ and $\frac{r_e}{r_o}$. The results of the experiments indicated that for a given value of $\frac{r_e}{r_o} \leq 0.075$, the valve cutoff quiescent power drain decreased monotonically as $\frac{A_c}{A_e}$ increased while for a given value of $\frac{r_e}{r_o} \geq 0.15$ the valve cutoff quiescent power drain was an absolute minimum at a given value of $\frac{A_c}{A_e}$. The valve turndown ratio increased as $\frac{A_c}{A_e}$ decreased and $\frac{r_e}{r_o}$ increased while the cutoff control pressure ratio increased as both $\frac{A_c}{A_e}$ and $\frac{r_e}{r_o}$ decreased.

As a result of the analytical and experimental studies of valve characteristics, a procedure was developed for designing single exit vortex valves which operate in the incompressible flow regime. The procedure provides a systematic method of progressing from a set of input specifications which include the operating fluid, the maximum supply pressure and flow and the maximum available control pressure and flow to a specification of the values of the valve critical dimensions including control, supply, and exit area as well as valve chamber radius and length. As a part of the procedure the prototype valve characteristic is checked to determine if multiple values of total flow exist in the valve characteristic at the cutoff

value of control flow. The procedure generates sufficient information to obtain a rough sketch of the prototype valve characteristic but does not provide an accurate estimate of valve incremental pressure and flow gains at each point on the characteristic. Finally a method was outlined of analytically determining from a single nondimensional valve characteristic the performance of the vortex valve operating at varying supply and exhaust pressures in fluid circuits.

2.3 Summary of the Studies of the Flow Field in Short Vortex Chambers

In an effort to provide a more complete understanding of vortex valve behavior than can be gained from measurements made only at the valve ports, an experimental and analytical study was conducted of the flow field within the vortex chamber. The study was restricted to chambers operating in the incompressible flow regime. The experimental portion of the study is summarized first.

In the experimental study the flow field in the valve chamber was investigated by flow visualization techniques and by measuring the static pressure distribution on the chamber end wall. Flow visualization photographs were taken for a seven inch diameter chamber operating on water using both a continuous stream of air bubbles and reconstituted powdered milk for visualization. As a result of the flow visualization studies a "picture" of the flow patterns which exist in the vortex valve for various operating points on the valve characteristic was obtained. At very low values of $\frac{v_o}{u_o}$ (ratio of peripheral tangential to radial velocity in the chamber),

the flow procedes from the outer periphery of the chamber to the inlet with radial flow existing at all axial positions in the valve. As the value of $\frac{v_o}{u_o}$ is increased, a major fraction of the flow passing through the chamber is drawn into the end wall boundary layers. At sufficiently high values of $\frac{v_o}{u_o}$, at some point in the chamber all the radial flow is contained in the end wall boundary layers and the radial velocity in the midplane region of the chamber is essentially zero. As $\frac{v_o}{u_o}$ is further increased, the radial flow is drawn into the chamber end wall boundary layers at a larger radius and a "spinning donut" of fluid through which no radial flow passes fills a significant portion of the chamber near the midplane region. At very high values of $\frac{v_o}{u_o}$, this "spinning donut" may extend to a radius beyond 70% of the chamber radius. The "picture" obtained from the flow visualization study provided the insight required to formulate the analytical model of the flow field in the vortex chamber.

Chamber end wall static pressures were measured for a seven inch chamber diameter apparatus operating on air. Profiles were taken of both the radial pressure distribution and the pressure distribution along a constant radius arc extending between two inlet ports. The radial end wall static pressure profiles indicated that at low values of $\frac{v_o}{u_o}$ the pressure gradient in the chamber, excluding the exit region, decreased monotonically with increasing radius. At high values $\frac{v_o}{u_o}$ the pressure gradient in the chamber, excluding the exit region, decreased monotonically only over a part

of the chamber and in a region near the outer periphery of the chamber increased with increasing radius. The profiles also indicated that for sufficiently high values of $\frac{v_o}{u_o}$ subambient pressures existed in the chamber exit region along the chamber centerline. These subambient pressures were accompanied by a reversed axial flow pattern in the chamber exit in which ambient flow was drawn into the vortex chamber exit from atmosphere.

The static end wall profiles measured over a constant radius arc between two inlet port regions in the vortex chamber indicated that almost no measurable variation in pressure occurred along an arc at a radius ratio of 0.75, and that very little variation existed at a radius ratio of 0.96 for a wide range of test conditions.

The radial end wall static pressure distributions were used to determine the effective outer periphery tangential velocity which existed in the chamber. It was found that the effective peripheral tangential velocity differed significantly from the ideal peripheral tangential velocity calculated from a model based upon lossless mixing of the inlet jets with the main chamber vortex flow and conservation of inlet jet angular momentum. The ratio of the effective outer wall tangential velocity to the ideal tangential velocity was defined as a jet recovery factor. It was found that the recovery factor varied from 0.95 to 0.55. The recovery factor was a maximum at low values of $\frac{v_o}{u_o}$ and decreased with increasing $\frac{v_o}{u_o}$. The test data indicated that the value of the recovery factor was relatively independent of the chamber exit size and of whether the chamber

contained a single or a dual exit. The recovery factor appeared to depend primarily upon $\frac{v_o}{u_o}$.

The analytical study was directed to developing a model for the flow in the vortex chamber which considered the effects of the viscous losses that occur in the boundary layers on the chamber end walls. As a result of the analysis it is possible to predict the pressure distribution across the chamber to the chamber exit given the conditions at the chamber outer periphery. The analysis serves as one step toward a complete vortex valve model.

The analysis was developed through a momentum integral formulation of the momentum and continuity equations derived for incompressible flow in a short vortex chamber. In the analysis the flow in the chamber was considered to consist of a boundary layer in which the radial and tangential velocity distributions were assumed to be functions of both radius and axial position and of an inviscid core near the chamber midplane in which the radial and tangential velocity distributions were assumed to be functions only of radius. Two flow regions were considered in the analysis -- a developing flow region and a developed flow region.

The developing flow region extends from the chamber outer periphery to the point in the chamber at which all of the radial flow through the chamber enters the end wall boundary layers. In the developing flow region in which radial flow exists at all axial positions within the region, the midplane circulation (product of midplane tangential velocity and radius) distribution is a constant. At sufficiently low values of $\frac{v_o}{u_o}$ the developing region extends

completely across the chamber and the midplane tangential velocity distribution is similar to that of a potential vortex. At higher values of $\frac{v_o}{u_o}$ the developing flow region of constant circulation extends only over a portion of the chamber and decreases in extent with increasing $\frac{v_o}{u_o}$. At the point in the chamber at which all of the radial flow enters the end wall boundary layers the developing flow region ends and the developed flow region starts and extends through the remainder of the chamber. The basic assumption made in the analysis of the developed flow region is that once all of the flow enters the end wall boundary layer it will remain in the boundary layers until the chamber exit is reached. The developed flow region corresponds to the "spinning donut" region observed in the flow visualization studies. In the developed flow region in the chamber, the midplane circulation distribution is not a constant but is a strong function of the shear stress on the chamber end wall.

Using the results of the analysis, the pressure distribution across the vortex chamber can be predicted for a given chamber geometry and chamber inlet conditions. In the analysis the pressure distribution could be reduced to a function of one parameter for $\frac{y_o}{u_o} > 10$ once the forms of the velocity profiles and shear law were specified. This single parameter could be expressed as a function of vortex valve total and control flows, valve chamber radius, valve maximum flow Reynolds number, inlet jet recovery factor, and a chamber wall friction factor. The parameter, when expressed in terms of these vortex valve quantities, did not depend upon valve chamber length. It is also noted that maximum flow Reynolds number R_w dependence of the

single parameter was weak, i.e. $R_w^{1/4}$. Pressure distributions predicted by the analysis agreed closely with experimental pressure profiles over a wide range of chamber inlet flow conditions and for both single and dual exit vortex chambers.

2.4 Recommendations for Further Research

The investigation of the steady-state characteristics of vortex valves has resulted in a semi-empirical procedure for designing single exit vortex valves which operate in the incompressible flow regime. Further analytical and experimental work is needed to extend the simple design procedure to dual exit valves and to valves which operate in the compressible flow regime. A valuable contribution to the design procedure would also be provided by work which extends the simple design procedure to include detailed information about every point on the prototype valve characteristic and, in particular, the existence of multiple values of valve total flow at any value of control flow. The present investigation has been restricted to valve steady-state behavior; further work is needed to develop design information about valve dynamic behavior.

The studies of the flow field within the valve main chamber have resulted in an analysis which has proved to be successful in predicting the pressure profile across the main chamber to the chamber exit given the conditions at the chamber outer periphery. Basic experimental and analytical work is required to describe adequately the vortex chamber inlet and exit regions. It is noted that the results of basic work concerning these regions would find

application not only to vortex valves but also to the wide variety of other vortex-type devices.

PART II

THE FLUID MODULATOR PORT-CHARACTERISTICS

CHAPTER 3

THE INVISCID VALVE MODEL

3.1 Derivation of the Characteristic Equation

In order to gain some insight into vortex valve behavior it is fruitful to consider an idealized model of the vortex valve. In this investigation the assumptions are utilized that the valve flow rates are steady and incompressible and that the flow field in the valve main chamber is inviscid and one-dimensional. Although the use of these assumptions results in a valve model whose characteristic agrees closely with that of a real valve only over a portion of the valve operating regime, this model provides information which is useful in valve design.

In the analysis three distinct regions of the valve are considered -- the inlet port region which contains the valve supply and control ports, the main chamber region and the exit port region. These three regions are identified in the conceptual vortex valve sketched in Figure 3.1 which is used as a basis for the analysis outlined below.

3.1.1 The Inlet Ports

The inlet port region of the valve is sketched in Figure 3.1. It consists of a number of supply port plenums which feed the valve main chamber region with radial supply flow and a number of identical control ports which supply the valve with tangential control flow. If the valve supply and control ports are assumed to be similar to quadratic orifices, the values of the supply and control flow entering the valve may be expressed as:

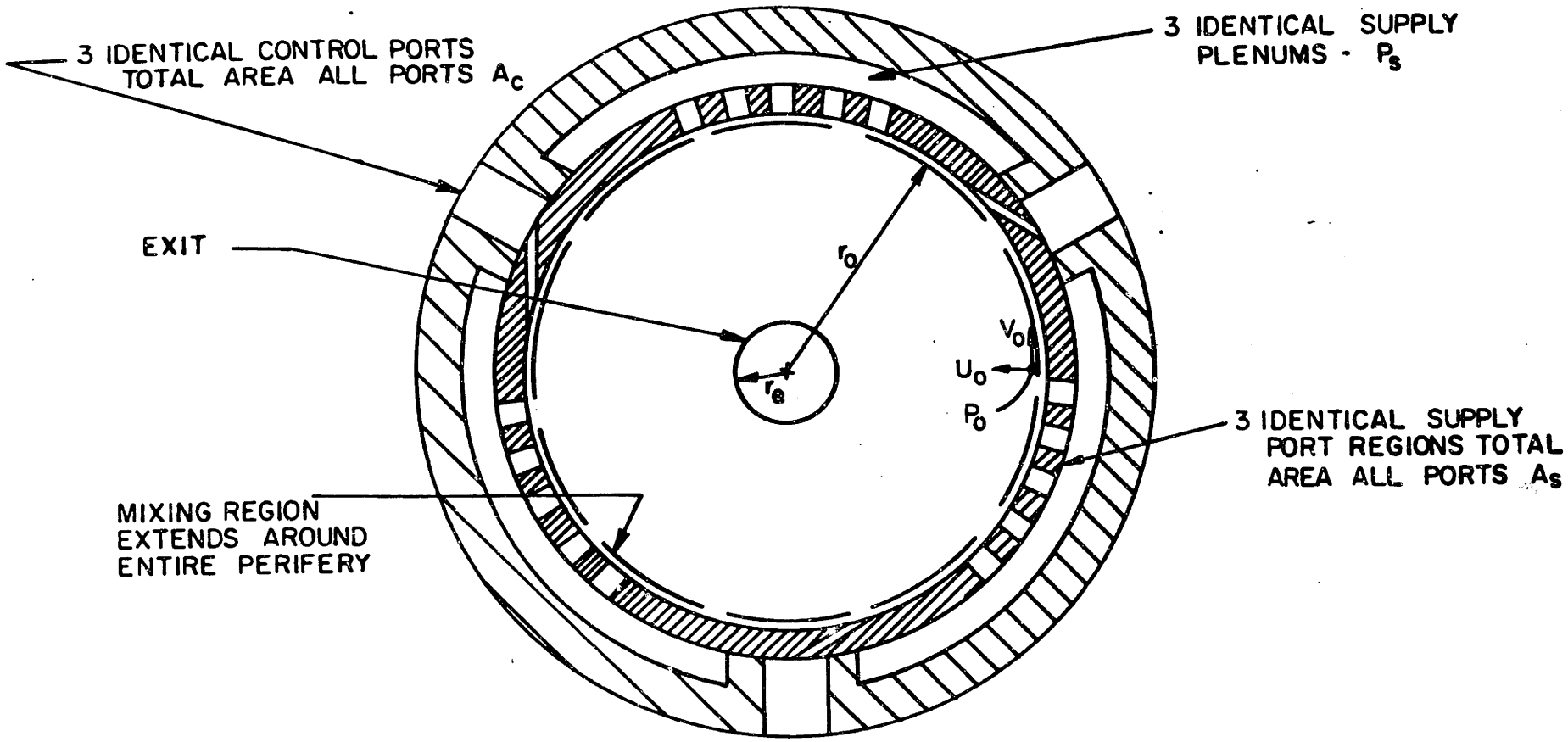

Fig. 3.1. Vortex Valve Inlet, Main Chamber, and Exit Regions.

$$W_s = C_s A_s \sqrt{2\rho\ (P_s - P_o)} \qquad (3.1)$$

$$W_c = C_c A_c \sqrt{2\rho\ (P_c - P_o)} \qquad (3.2)$$

where:

W_s = total mass flow rate entering the valve through the supply ports

W_c = total mass flow rate entering the valve through the control ports

P_s = pressure at the valve supply port plenums measured relative to the exhaust pressure at the valve exit

P_c = pressure at the valve control port (ports) measured relative to the exhaust pressure at the valve exit

P_o = pressure at valve main chamber outer periphery measured relative to the exhaust pressure at the valve exit

A_s = total valve supply port area

A_c = total valve control port area

C_s = discharge coefficient of the supply port

C_c = discharge coefficient of the control port

ρ = operating fluid density

The radial supply flow and the tangential control flow which enter the valve interact in a mixing region at the periphery of the valve main chamber. In the model of this mixing process it is assumed that the velocity profiles across both the supply and control ports are uniform and that the mixing of the two streams is lossless. It is also assumed that the two streams are mixed completely at the radius r_o so that at radius r_o a uniform one-dimensional fluid stream at pressure P_o and with radial and tangential velocity components u_o and v_o is supplied to the valve main chamber. With this model the radial velocity components u_o at the radius r_o may be determined by satisfying continuity

$$u_o = \frac{W_o}{\rho A_o} \tag{3.3}$$

where:

u_o = radial velocity component at r_o, defined positive in the -r direction

$W_o = W_c + W_s$ = total mass flow rate entering the valve

$A_o = 2\, r_o h \pi$ = valve main chamber outer periphery curtain area

h = valve chamber height

r_o = valve main chamber radius

while the tangential velocity component v_o at radius r_o may be determined by satisfying the law of conservation of angular momentum:

$$v_o = \frac{W_c^2}{\rho A_c W_o} \tag{3.4}$$

3.1.2 The Valve Main Chamber

The pressure and velocity components at the outer periphery of the main chamber may be related to those at the inner periphery of the main chamber, the exit radius r_e, by considering the flow in the vortex chamber. The model of the flow field in the main chamber is based upon the assumptions that the flow is steady, one-dimensional, incompressible and inviscid. Under these conditions the flow field is irrotational and consists of the superposition of a potential vortex and a sink flow in which the radial and tangential velocity components at the exit radius r_e are related to the components at radius r_o by equations 3.5 and 3.6:

$$u_e = u_o \frac{r_o}{r_e} \tag{3.5}$$

$$v_e = v_o \frac{r_o}{r_e} \tag{3.6}$$

where: u_e = radial velocity component at radius r_e defined positive in -r direction.

v_e = tangential velocity at radius r_e

r_e = exit radius of the valve

The pressure P_e at radius r_e may be related to the pressure at radius r_o by the Bernoulli equation under the conditions specified above:

$$P_e + \frac{1}{2}\rho\left(u_e^2 + v_e^2\right) = P_o + \frac{1}{2}\rho\left(u_o^2 + v_o^2\right) \qquad (3.7)$$

where:

P_e = pressure at radius r_e measured relative to the exhaust pressure at the valve exit.

By combining equations 3.5, 3.6, and 3.7 the pressure difference across the valve chamber may be determined as a function of the velocity components at radius r_o:

$$P_o - P_e = \frac{1}{2}\rho\left(\frac{r_o^2}{r_e^2} - 1\right)\left(u_o^2 + v_o^2\right) \qquad (3.8)$$

3.1.3 The Exit Port

In considering the calculation of the flow from the valve exit port, the assumptions are made that the pressure P_e acts uniformly over the valve exit and that the flow from the exit may be determined with the quadratic orifice equation:

$$W_o = C_e A_e \sqrt{2\rho P_e} \qquad (3.9)$$

where: A_e = the valve exit area

C_e = the valve exit area discharge coefficient

It is recalled that P_e is measured relative to the exhaust pressure downstream of the valve exit.

3.1.4 The Inviscid Valve Characteristic

The valve characteristic equation which relates total valve flow to control flow for a valve operating at constant supply and exhaust pressures may be derived by combining equations 3.1, 3.2, 3.3, 3.4, 3.8, and 3.9:

$$\frac{W_o^2}{2C_e^2A_e^2\rho} = P_s - \frac{(W_o-W_c)^2}{C_s^2A_s^2 2\rho} + \frac{1}{2\rho}\left[1 - \frac{r_o^2}{r_e^2}\right]\left[\frac{W_o^2}{A_o^2} + \frac{W_c^4}{A_c^2 W_o^2}\right] \qquad (3.10)$$

It is convenient to rewrite equation 3.10 in a nondimensional form in which all the flow rates are normalized with respect to the flow through the valve under the condition of zero control flow. This normalizing flow is the nominal maximum flow through the valve for the given supply pressure and may be determined by setting $W_c = 0$ in equation 3.10

$$W_m = W_o\Big|_{W_c=0} = \gamma C_e A_e \sqrt{2\rho P_s} \qquad (3.11)$$

where: W_m = the valve mass flow rate at zero control flow.

The parameter γ in equation 3.11 is

$$\gamma = \frac{1.0}{\sqrt{1 + \frac{A_e^2 C_e^2}{C_s^2 A_s^2} + \frac{C_e^2 r_e^2}{4h^2}\left(1 - \frac{r_e^2}{r_o^2}\right)}} \qquad (3.12)$$

where it is noted that the substitutions $A_o = 2\pi r_o h$ and $A_e = \pi r_e^2$ have been used in deriving equation 3.12.

When the flow rates in equation 3.10 are normalized with respect to W_m, the resulting nondimensional inviscid valve characteristic equation is:

$$\bar{W}_o^2 = 1 - \gamma^2 \frac{C_e^2 A_e^2}{A_c^2} \left(\frac{r_o^2}{r_e^2} - 1\right) \frac{\bar{W}_c^4}{\bar{W}_o^2} + \gamma^2 \frac{C_e^2 A_e^2}{C_s^2 A_s^2} \left(2 \bar{W}_o \bar{W}_c - \bar{W}_c^2\right) \tag{3.13}$$

where: $\bar{W} = \frac{W}{W_m}$ = nondimensional flow rate

The nondimensional inviscid valve characteristic is a function of the supply and exit area discharge coefficients and the following four geometric parameter ratios:

(1) $\frac{A_s}{A_e}$ - the supply to exit area ratio

(2) $\frac{h}{r_e}$ - the chamber height to exit radius ratio

(3) $\frac{A_c}{A_e}$ - the control to exit area ratio

(4) $\frac{r_e}{r_o}$ - the valve radius ratio

The influence of the ratios $\frac{A_s}{A_e}$ and $\frac{h}{r_e}$ on the nondimensional valve characteristic may be most easily determined by first considering their effect on the flow through the valve at zero control flow, W_m, specified by equations 3.11 and 3.12.

The ratios $\frac{h}{r_e}$ and $\frac{A_s}{A_e}$ influence W_m in equation 3.11 through the parameter γ which effectively represents the contribution of the pressure drops across the valve chamber due to the accelerating radial flow and across the inlet supply port relative to the pressure drop across the valve exit. The value of W_m approaches a maximum for a given valve exit area and given supply pressure as the parameter γ approaches

1.0 and the inlet supply port and main chamber pressure drops become negligible compared to the pressure drop across the valve exit. It is desirable to maximize γ in a valve in order to maximize the valve turndown ratio.

A detailed indication of the effect of $\frac{h}{r_e}$ and $\frac{A_s}{A_o}$ on the value of $\frac{W_m}{C_e A_e \sqrt{2\rho P_s}} = \gamma$ is indicated in Figure 3.2 where lines of constant γ are plotted with $\frac{C_s A_s}{C_e A_e}$ and $\frac{2h}{C_e r_e \sqrt{1 - r_e^2/r_o^2}}$ as parameters. It is noted from the Figure that as $\frac{A_s}{A_e}$ and $\frac{h}{r_e}$ are increased the value of γ increases and at large values of $\frac{A_s}{A_e}$ and $\frac{h}{r_e}$ approaches a maximum value of 1.0. In particular, for all values of A_s/A_e and h/r_e which satisfy equations 3.14 and 3.15, the value of γ may be approximated as 1.0 with no greater than 6% error.

$$\frac{C_s A_s}{C_e A_e} > 4.0 \qquad (3.14)$$

$$\frac{h}{C_e r_e} > 2.0 \qquad (3.15)$$

In the work that follows it will be assumed that the conditions expressed in equations 3.14 and 3.15 are satisfied and the approximation will be made that $\gamma = 1.0$. The restriction of the analysis to valve geometries in which the conditions of equations 3.14 and 3.15 are satisfied does not severely limit the usefulness of the analysis, since these conditions result in the desired maximum value of $\frac{W_m}{C_e A_e \sqrt{2 P_s \rho}}$ and are satisfied in many vortex valve designs. When the assumption is made that equations 3.14 and 3.15 are satisfied and γ is approximated as 1.0,

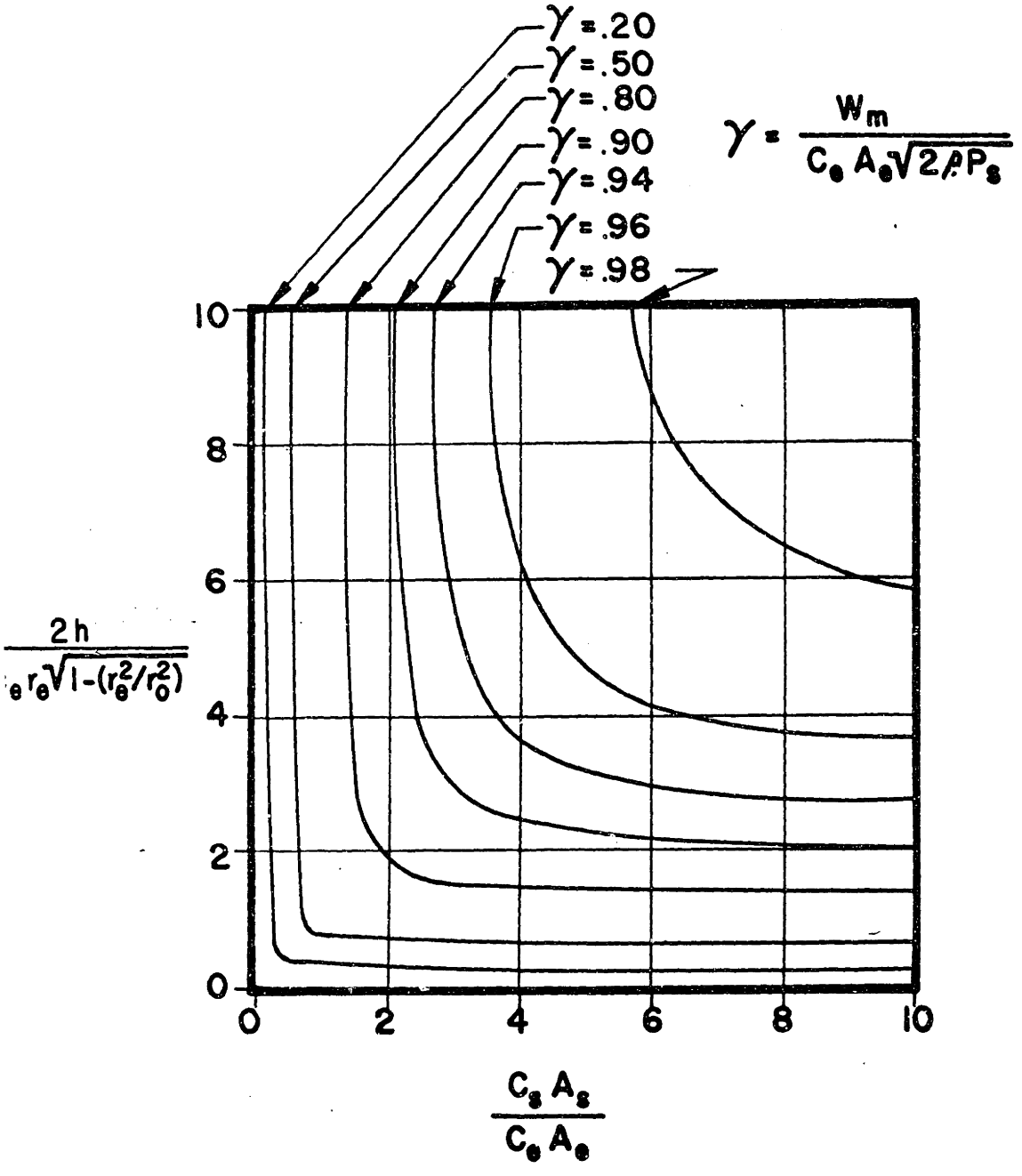

Fig. 3.2. The Influence of h/r_e and A_s/A_e on the Maximum Valve Flow.

considerable simplification is obtained in the valve characteristic equation. When γ is replaced by 1.0 the valve characteristic equation (3.13) becomes independent of the ratio of chamber height to exit radius, $\frac{h}{r_e}$. It is also noted that the condition expressed in equation 3.14 on the parameter $\frac{C_s A_s}{C_e A_e}$ limits the maximum value of the third term on the right-hand side of equation 3.13 to a value less than 0.035 for all reasonable values of $\bar{W}_c$, ie. values of $\bar{W}_c \leq 0.4$ and values of $\bar{W}_o \leq 1.0$. This term in equation 3.13 may be neglected compared with the other terms in equation 3.13 with less than 4% error in the calculated value of $\bar{W}_o$ for any given value of $\bar{W}_c$. When this is set to zero, the valve characteristic equation is

$$\bar{W}_o = 0.707 \sqrt{1 \pm \sqrt{1 - \frac{\bar{W}_c^4}{G^4}}} \tag{3.16}$$

where the geometric parameter G is:

$$G = \sqrt{\frac{\frac{1}{2C_e} \left(\frac{r_e}{r_o}\right) \frac{A_c}{A_e}}{\sqrt{1 - \frac{r_e^2}{r_o^2}}}} \tag{3.17}$$

When the values of A_s/A_e and h/r_e are sufficiently large so that equations 3.14 and 3.15 are satisfied, the nondimensional valve characteristic of equation 3.13 reduces to a function of only one geometric parameter G as noted in equation 3.16. The parameter G contains the exit area discharge coefficient and the ratios r_e/r_o and A_c/A_e.

The normalized valve characteristic of equation 3.16 is plotted in Figure 3.3 for two values of G. As the value of G, or more specifically

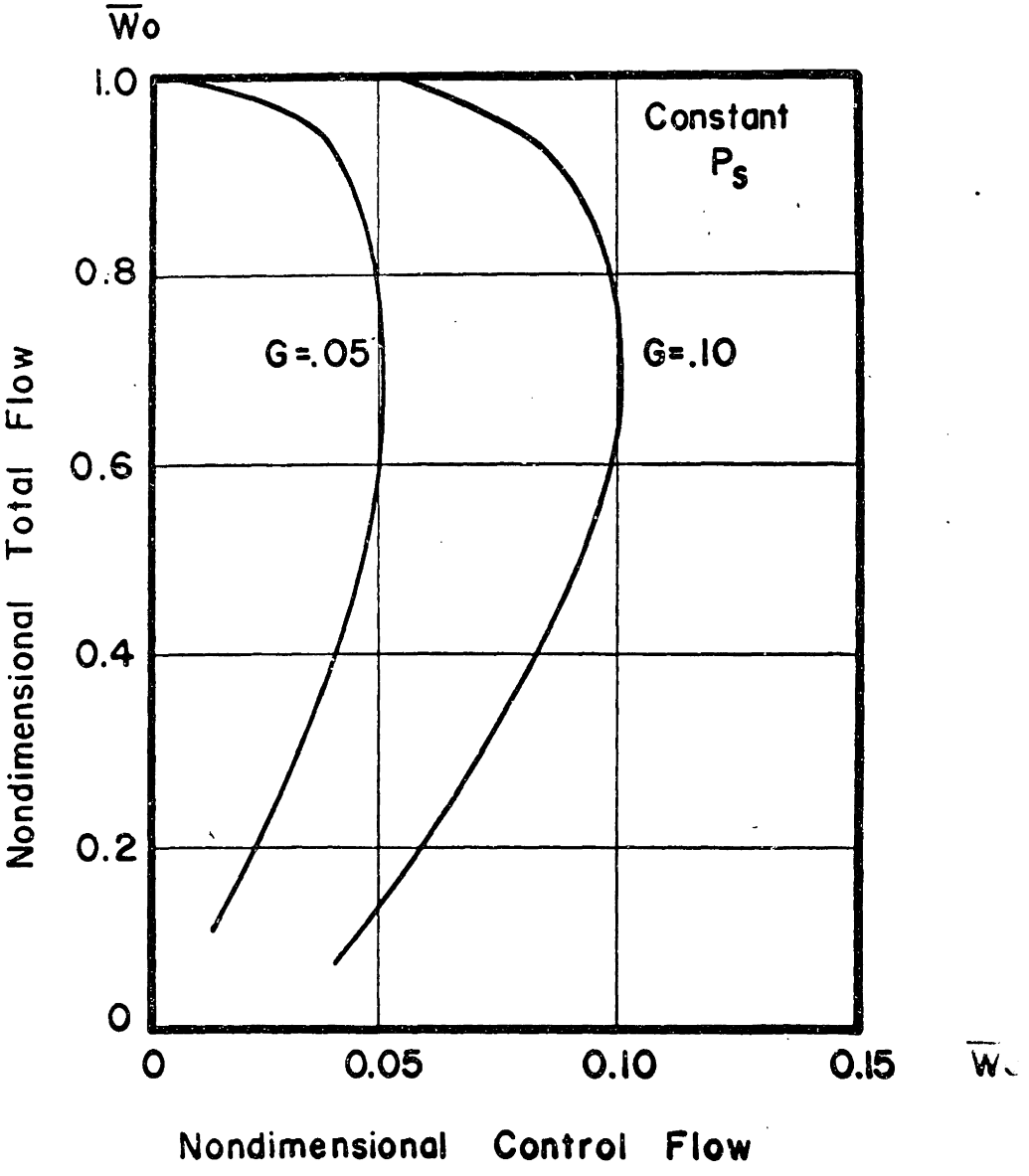

Fig. 3.3. The Inviscid Valve Characteristics.

the values of the parameters A_c/A_e and r_e/r_o are increased, the amount of control flow required at each point on the characteristic is increased. The inviscid analysis then indicates that in order to minimize valve control flow requirements the values of the parameters r_e/r_o and A_c/A_e should be small. It is also noted from Figure 3.3 that the inviscid valve characteristics are multivalued, i.e. two values of total flow exist for a given value of control flow. A real valve with a characteristic similar to the inviscid valve characteristic would not be a very useful flow control valve and could tend to oscillate between the two values of total flow which exist for a given value of control flow.

A point of interest on each of the valve characteristics is the unique point at which the maximum control flow is required. This point, as may be determined from equation 3.16, always occurs at a value of total flow equal to 0.707. The value of control flow required at $\bar{W}_o = 0.707$ is:

$$\bar{W}_c^+ \equiv \bar{W}_c\Big|_{\bar{W}_o = .707} = \sqrt{\frac{\frac{1}{2C_e}\left(\frac{r_e}{r_o}\right)\frac{A_c}{A_e}}{1 - \frac{r_e^2}{r_o^2}}} \qquad (3.18)$$

The value of nondimensional control pressure required at the point $\bar{W}_o = 0.707$ is also of interest and may be derived directly from equation 3.18 with the aid of equation 3.2:

$$\bar{P}_c^{+} \equiv \left.\frac{P_c}{P_s}\right|_{W_o = .707} = 1.0 + \frac{\frac{C_e}{C_e^2}\left(\frac{A_e}{A_c}\right)\left(\frac{r_e}{r_o}\right)^{1/2}}{\sqrt{1 - \frac{r_e^2}{r_o^2}}} \qquad (3.19)$$

It is interesting to compare equations 3.19 and 3.18 for the case in which A_e is replaced by πr_e^2 to determine the values of r_e, r_o, and A_c which minimize the valve requirements of both nondimensional control flow and pressure. When this comparison is made, the analysis indicates that as r_o is increased both $\bar{P}_c^{+}$ and $\bar{W}_c^{+}$ decrease while as A_c is increased and r_e decreased the value of $\bar{W}_c^{+}$ increases. To keep the values of both $\bar{P}_c^{+}$ and $\bar{W}_c^{+}$ required in a valve small, the inviscid analysis indicates that r_o should be large and that a compromise must be reached in the selection of the values of A_c and r_e.

The inviscid valve characteristic of equation 3.16 and the values of $\bar{W}_c^{+}$ and $\bar{P}_c^{+}$ of equations 3.18 and 3.19 are compared with the results of experimental measurements in Section 4.4.

CHAPTER 4

EXPERIMENTAL VALVE CHARACTERISTICS

4.1 Introduction

An experimental investigation was conducted to determine the influence of fluid properties and geometry on vortex valve characteristics. In the test series valves were tested on both air and water at pressure levels which were sufficiently low so that the flow in the valve was incompressible. The geometric variables studied in the tests included the control, the supply and the exit port areas, as well as the valve main chamber height and diameter. Data generated by the tests serves as a basis for the valve design procedure outlined in Chapter 5 and provides a catalog of valve characteristics which can be used with the methods described in Chapter 5 to design fluidic circuits.

4.2 The Experimental Apparatus

Two test valves were used in the experimental investigation -- a seven inch chamber diameter valve and a four inch chamber diameter valve. The four inch valve was tested only on air while the seven inch valve was tested on both air and water. In the design of both test valves an effort was made to obtain an axisymmetric flow pattern in the valve main chamber. The two valves are similar in construction and only the four inch valve shown in Figure 4.1 is described in detail.

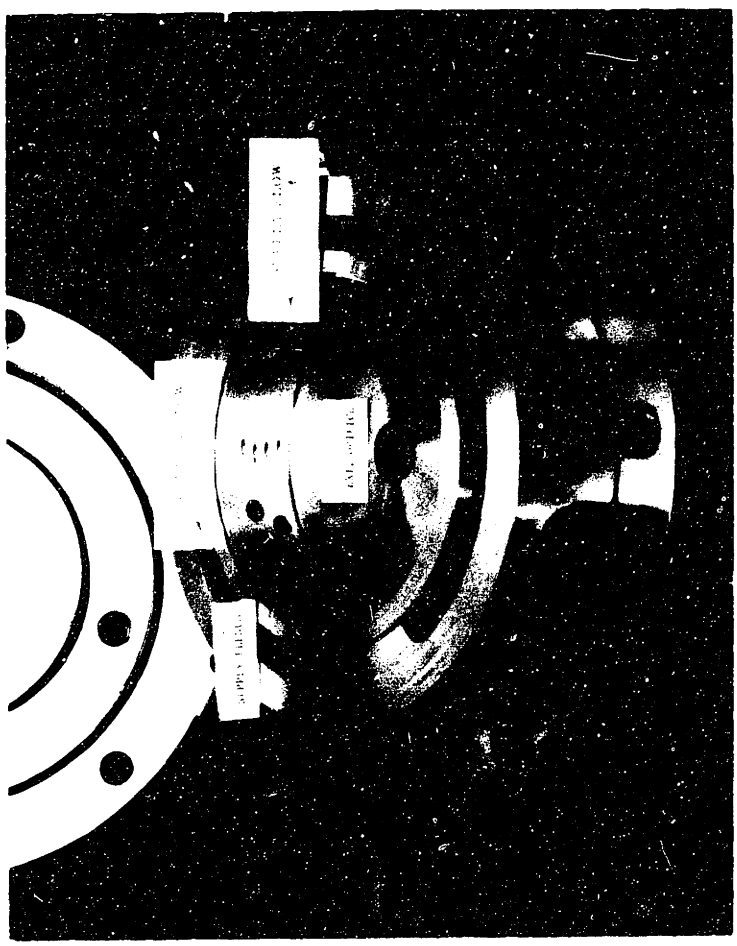

Fig. 4.1 Photograph of the Four Inch Test Valve

The four inch valve consists of a four inch diameter porous ring which contains three identical supply port regions spaced at 120°, a top plate, a bottom plate, and a retaining ring which isolates the supply port plenums from the control port plenums. Each control port region consists of four 0.082 inch diameter holes drilled tangent to a radius of 1.92 inches, while each supply port region consists of eleven 0.30 inch diameter holes. The control and supply port areas to the valve may be varied by selectively closing off a number of the inlet holes or by inserting stainless steel needle tubing of various internal diameters into the holes. The exit port of the valve consists of a sharp edged tapered hole machined into a removable bottom plate which can be changed to vary the valve exit area. A detailed sketch of the exit orifice is included in Figure 4.7. The bottom plate of the valve may be placed in different positions relative to the top plate to vary the valve chamber length. Sealing between the various members of the valve assembly is accomplished with the aid of O-rings.

The four and seven inch valve chambers were tested on air in the flow loop shown schematically in Figure 4.2. The valve supply flow is measured with a set of standard ASME orifice plates that are accurate to better than 2%. The control flow is measured with a critical-flow orifice set which has been calibrated with a gasometer and should be accurate to 2%. The control and supply port pressures are measured in the respective port plenum chambers with either mercury manometers or 0.25% Helicoid test gauges which have been calibrated on a dead weight tester. The source of control

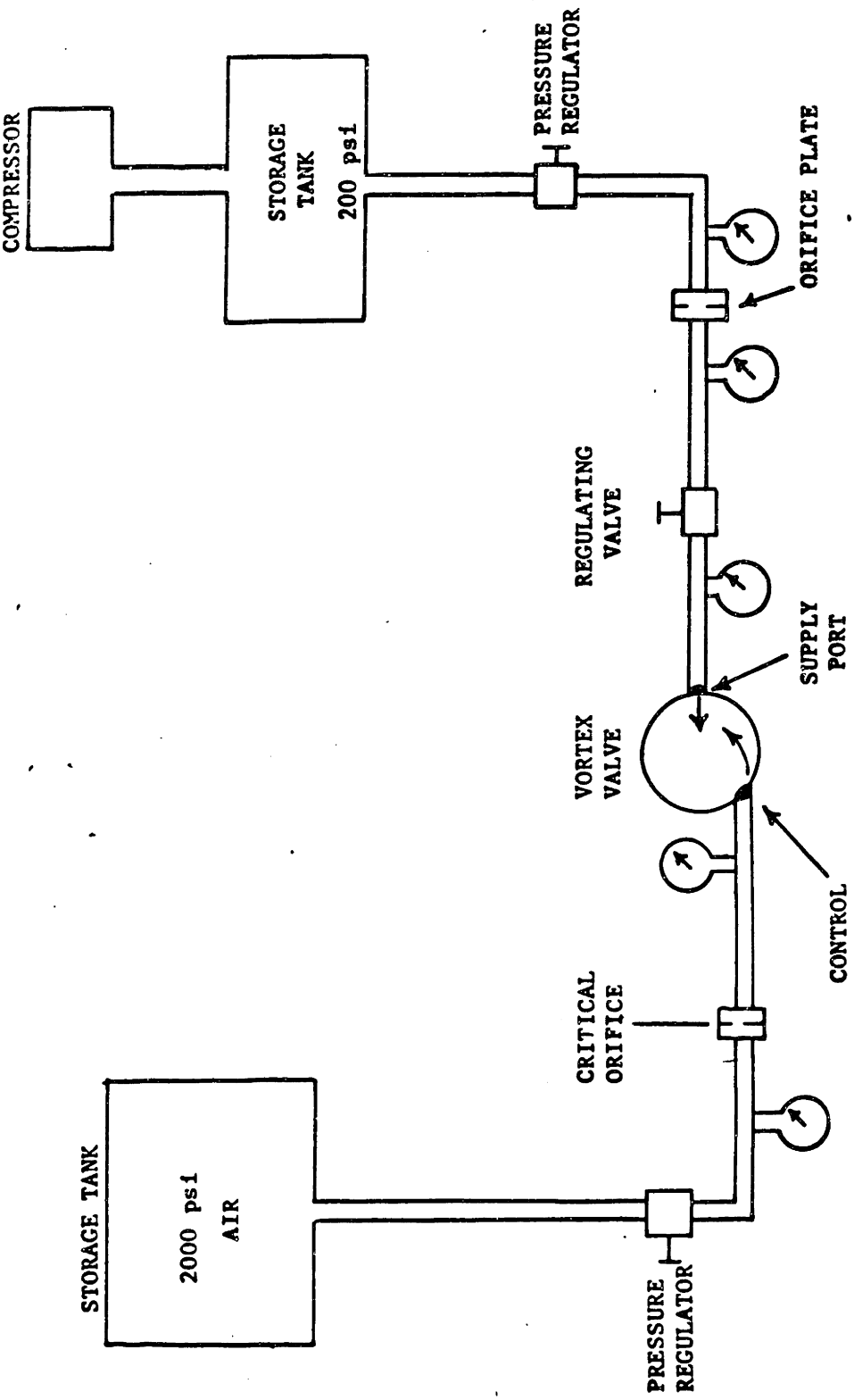

Fig. 4.2. Vortex Valve Test Flow Loop.

flow is a 1500-2000 psi storage tank of compressed air, while the supply flow is obtained from a storage tank maintained at 200 psi by a compressor running continuously. Although the maximum pressure required at the valve is low, i.e. a maximum supply pressure of 5 psi, the high pressure air supplies are used to obtain choked flow in the critical orifice measuring the control flow and across the metering valve to the vortex test valve supply plenum. The choked flow sources provide the constant flow rates, independent of downstream pressure which are required to measure a vortex valve characteristic in its multivalued region.

In tests run on water, valve supply and control flows are measured with a set of rotameters which can be calibrated in place on a day-to-day basis with a weigh tank and which should be accurate to within 4%. The supply and control port plenum pressures are measured with 0.25% Helicoid test gauges.

4.3 The Experimental Results

The results of the tests conducted to determine the influence of fluid properties and geometry on valve characteristics are presented in this section. In each of the characteristics presented, the valve was tested with the supply port plenum pressure held constant and with the valve exhausting to atmosphere. The valve characteristics are plotted as nondimensional total flow versus nondimensional control flow where the nondimensional flow rates are obtained by dividing the measured flows at each point on the

characteristic by the flow measured at zero control flow. It is noted that this method of normalizing the valve characteristic is identical to the method described in Chapter 3. For each test described in this section the values of the supply pressure, the flow measured at zero control flow, and the test apparatus pertinent geometric parameters are tabulated in Appendix A.

4.3.1 The Influence of Reynolds Number

A series of tests were conducted to determine the influence of the maximum flow Reynolds number on the valve characteristic where the maximum flow Reynolds number is defined as:

$$R_w = \frac{W_m}{2\pi r_o \mu} \tag{4.1}$$

where μ = fluid viscosity

The maximum flow Reynolds number is a constant for a given valve characteristic and varies only as the valve supply pressure varies for a fixed valve geometry operating on a constant temperature fluid.

The results of a typical test series conducted on the seven inch valve using both air and water to determine the influence of variations in R_w on the valve characteristic are presented in Figure 4.3. The three characteristics determined at R_w = 940 (water), 1340 (air) and 1910 (air) are almost identical while the characteristic at R_w = 390 (water) differs significantly from the other three.

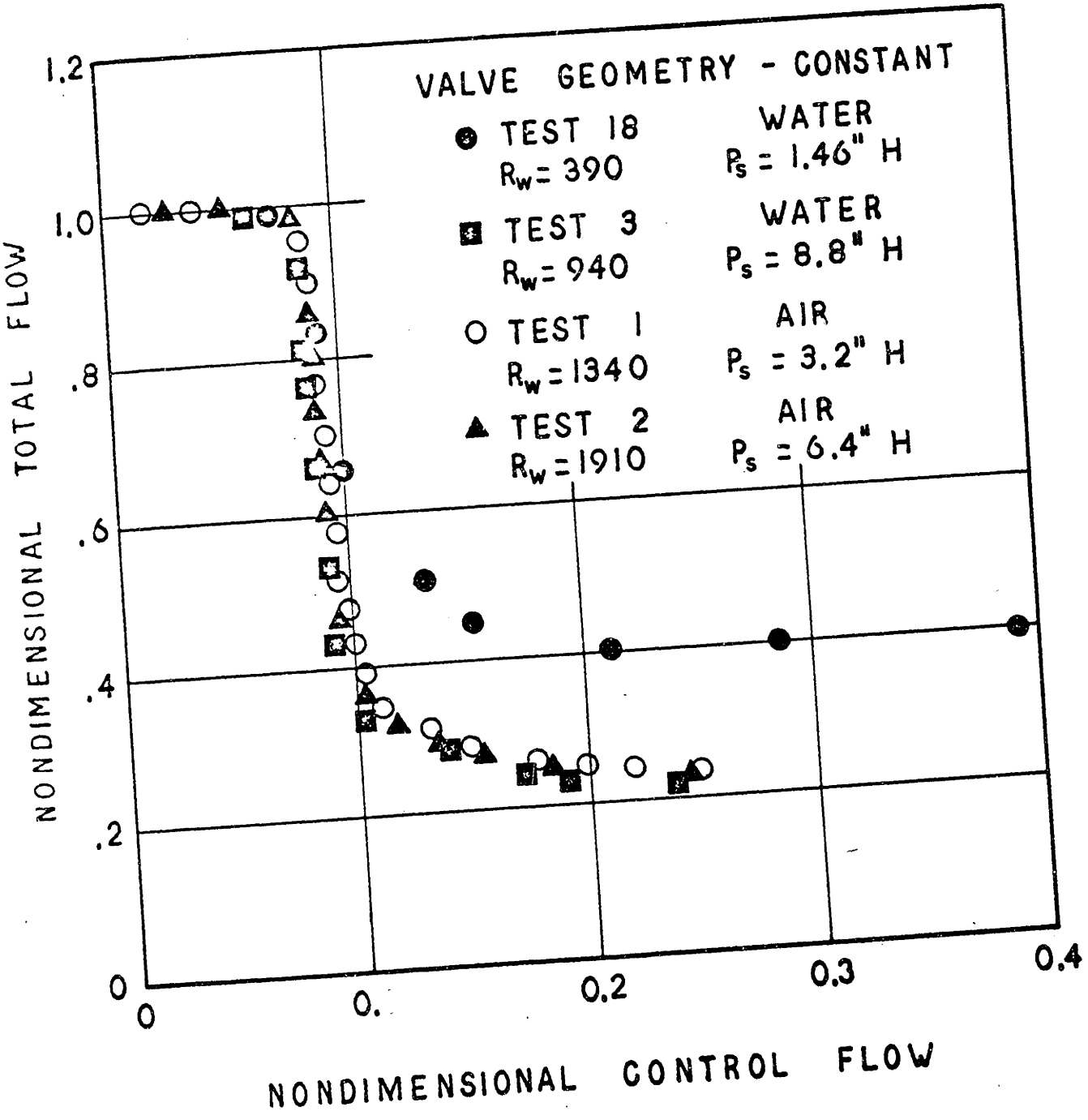

Fig. 4.3. The Influence of Reynolds Number on the Valve Characteristics.

These test results indicate that at low values of R_w near 400 the valve characteristic is strongly dependent upon the value of R_w while at higher values of R_w the nondimensional valve characteristic is independent of the value of R_w. Tests run on other configurations of the seven inch valve and tests run on the four inch valve indicated that in general for tests conducted in which $R_w > 750$, the nondimensional valve characteristic is essentially independent of the value of the maximum flow Reynolds number. Although the largest Reynolds number of the test series was 3300, data is available in the literature for incompressible flow in vortex valves (4) and vortex tubes (33) which suggests that the nondimensional vortex valve characteristic is essentially independent of R_w or weakly dependent on R_w for maximum flow Reynolds numbers 3-4 times the value of 3300.

In this investigation in which valves are operated in the incompressible flow regime, the finding that the nondimensional valve characteristic is independent of R_w for $R_w \geq 750$ indicates that the nondimensional characteristic is also pressure level independent for $R_w \geq 750$. This result implies that a valve characteristic measured at one value of supply pressure with a given fluid may be simply scaled to determine the characteristic at another value of supply pressure (for a different operating fluid) if both characteristics correspond to conditions in which $R_w > 750$ and in which the flow is incompressible. This result provides the basis for the valve design procedure outlined in Chapter 5 and for the design of vortex valve circuitry in which the valve is operating with neither a constant supply nor a constant exhaust pressure as outlined in Chapter 5.

It is finally noted that data exists in the literature (10) for valves operated on air at supply to exhaust pressure ratios varying from 5 to 50 which indicates that the nondimensional characteristics of valves operated in the compressible flow regime are also essentially independent of the maximum flow Reynolds number.

4.3.2 The Influence of Geometry

In this section the results of tests are reported which indicate the influence of geometry on the vortex valve characteristic. All of the results presented were taken within a range of maximum flow Reynolds numbers and valve supply pressures in which the nondimensional valve characteristic is Reynolds number independent and in which the flow in the valve is incompressible.

4.3.2.1 The Control Port Area

The influence on the nondimensional valve characteristic of changes in control port area was determined by operating the four inch valve on air. In the test series the control port area was changed by selectively plugging the control port holes or by inserting stainless steel needle tubing of various internal diameters into the holes while all other geometric parameters were held constant. The results of the test series are presented in Figure 4.4 in which characteristics are plotted for values of the ratio of control to exit port area ranging from 0.042 to 0.322. The result of the tests indicates that a decrease in control port

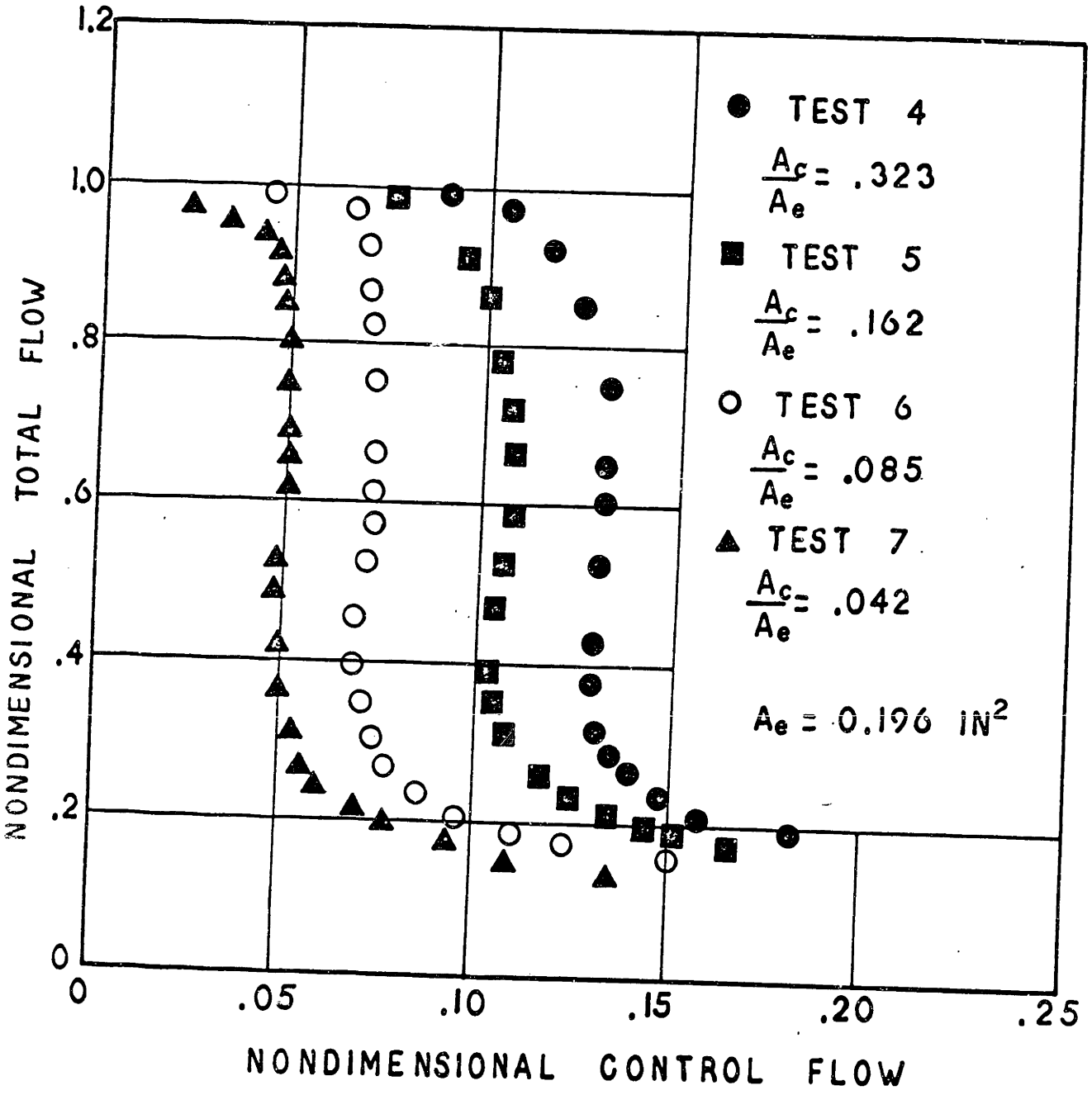

Fig. 4.4. The Influence of Control Port Area on the Valve Characteristic.

area reduces the nondimensional control flow required at each point on the characteristic. This result is identical to the result indicated by the inviscid analysis and stems from the fact that for a given control flow as the control port area is decreased the tangential velocity generated at the chamber outer wall is increased. It should be noted that a consequence of a decrease in control port area is to increase the nondimensional control port pressure, $\bar{P}_c = \frac{P_c}{P_s}$, required at each point on the characteristic. A plot of $\bar{W}_o$ versus $\bar{P}_c$ may be constructed using the data of Figure 4.4 and the data in Appendix B of Figure B.1 which contains a plot of the pressure flow characteristics for each of the control port areas listed in Figure 4.4.

The basic shape of each valve characteristic in Figure 4.3 is quite similar. In each characteristic a region of nearly infinite incremental flow gain exists near $\bar{W}_o = 0.707$ and a multivalued region of flow exists between $\bar{W}_o = 0.6$ and $\bar{W}_o = 0.3$. This similarity in shape of the characteristics indicates that it should be possible to correlate the effects of changes in control port area for the various curves. The inviscid analysis indicates that the effects of changes in control port area on the valve characteristic can be correlated by the parameter $\bar{W}_c/\sqrt{A_c/A_e}$. The data for the four values of control port area in Figure 4.4 are plotted as nondimensional total flow versus the parameter $\bar{W}_c/\sqrt{A_c/A_e}$ in Figure 4.5. It is noted from the Figure that the characteristics of the valves with the three smaller ratios of $\frac{A_c}{A_e}$ (0.042, 0.085 and

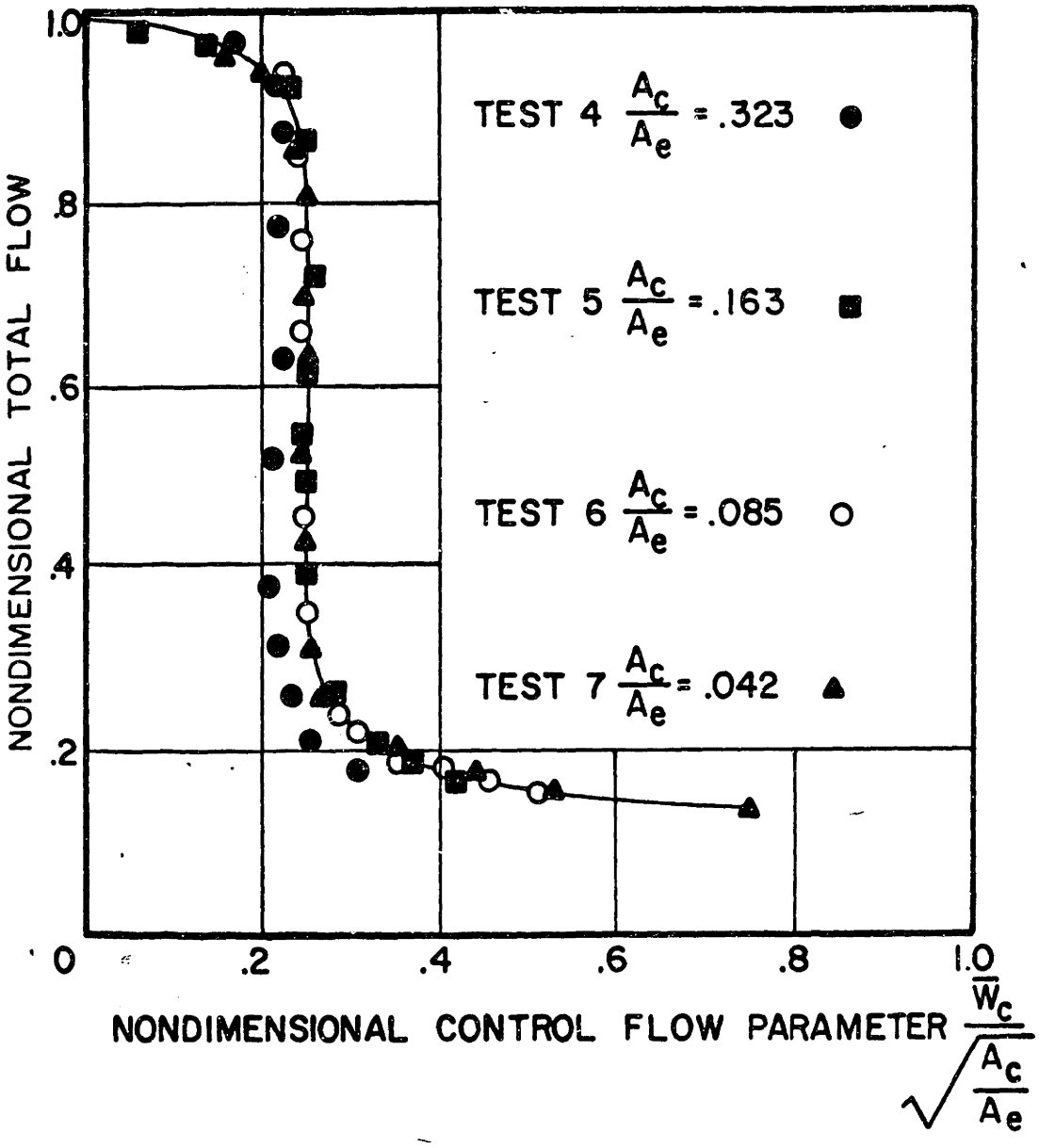

Fig. 4.5. Correlation of Valve Characteristics for Various Control Port Areas.

0.102) correlate very well while the curve for the largest ratio of $\frac{A_c}{A_e}$ (0.323) does not correlate quite as well. The correlation of characteristic curves with the parameter $\bar{W}_c/\sqrt{A_c/A_e}$ works well over a range of values of $\frac{A_c}{A_e}$ and may be used to scale valve characteristics with respect to changes in control port area if the control port area variation is not large, i.e. is within a factor of two of the value for the prototype characteristic.

4.3.2.2 The Supply Port Area

A test series was conducted with the four inch valve operating on air to determine the influence of variations in supply port area on the valve characteristic. The results of these tests in which the valve supply port area was changed by selectively closing off the supply inlet holes or by inserting stainless steel needle tubing of various internal diameters into the holes are presented in Figure 4.6. The data of Figure 4.6 indicates that as the valve supply port area ratio, $\frac{A_s}{A_e}$, is decreased from 2.0 to 0.5 the value of nondimensional control flow required at each point on the valve characteristic is increased. For values of $\frac{A_s}{A_c}$ greater than 3.0 no change in the valve characteristic was observed as the supply port area was increased. This result is in accord with the result of the inviscid analysis which indicated that at large values of $\frac{A_s}{A_e}$ the inviscid valve characteristic is essentially independent of the value of the supply port area. The effect of a change in supply port area is easily understood if it is recalled from Chapter 3 that the supply port area is effectively a resistance in series with the

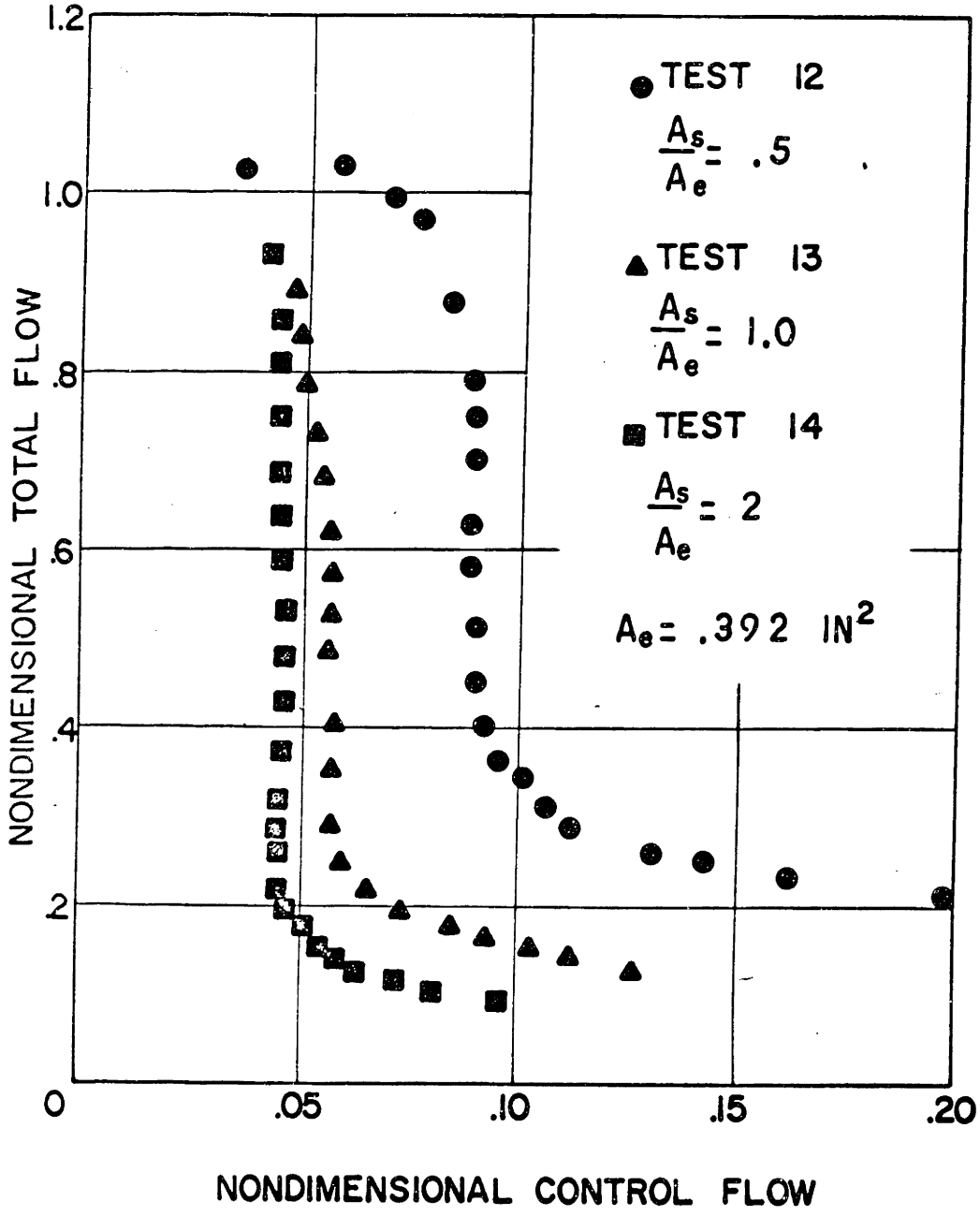

Fig. 4.6. The Influence of Supply Port Area on the Valve Characteristic.

exit port area resistance. A reduction in supply port area to a value where the supply port area resistance is significant compared with the exit port resistance, i.e. $A_s \leq 3A_e$, decreases the value of the maximum valve flow and does not effectively change the value of control flow and pressure required to cutoff the valve supply flow. A consequence of the decrease in the valve maximum flow while the cutoff flow remains constant is a decrease in valve turndown ratio. In order to build a valve with a large turndown ratio, the valve supply port area should be large compared to the exit area, i.e. $A_s \geq 3\ A_e$.

4.3.2.3 The Exit Port Area

The influence of the exit port area on the valve characteristic was evaluated using a single exit four inch chamber diameter valve operating on air. The exit areas used in the test consisted of sharp edge tapered holes as shown in Figure 4.7. For the valves considered in the test a change in valve exit area may be considered as equivalent to a change in the valve radius ratio, $\frac{r_e}{r_o}$. The results of the test series are presented in Figure 4.7 in which characteristics have been presented for radius ratios varying from 0.089 to 0.25. The results indicate that as the valve radius ratio, or exit area, is increased the value of nondimensional control flow required at each point on the characteristic is reduced. This trend corresponds closely with the results of the inviscid analysis which indicates that $\bar{W}_c$ decreases as $\frac{r_e}{r_o}$ increases. It is also noted that as the valve radius ratio is increased the valve characteristic tends to change in shape. The characteristic of the

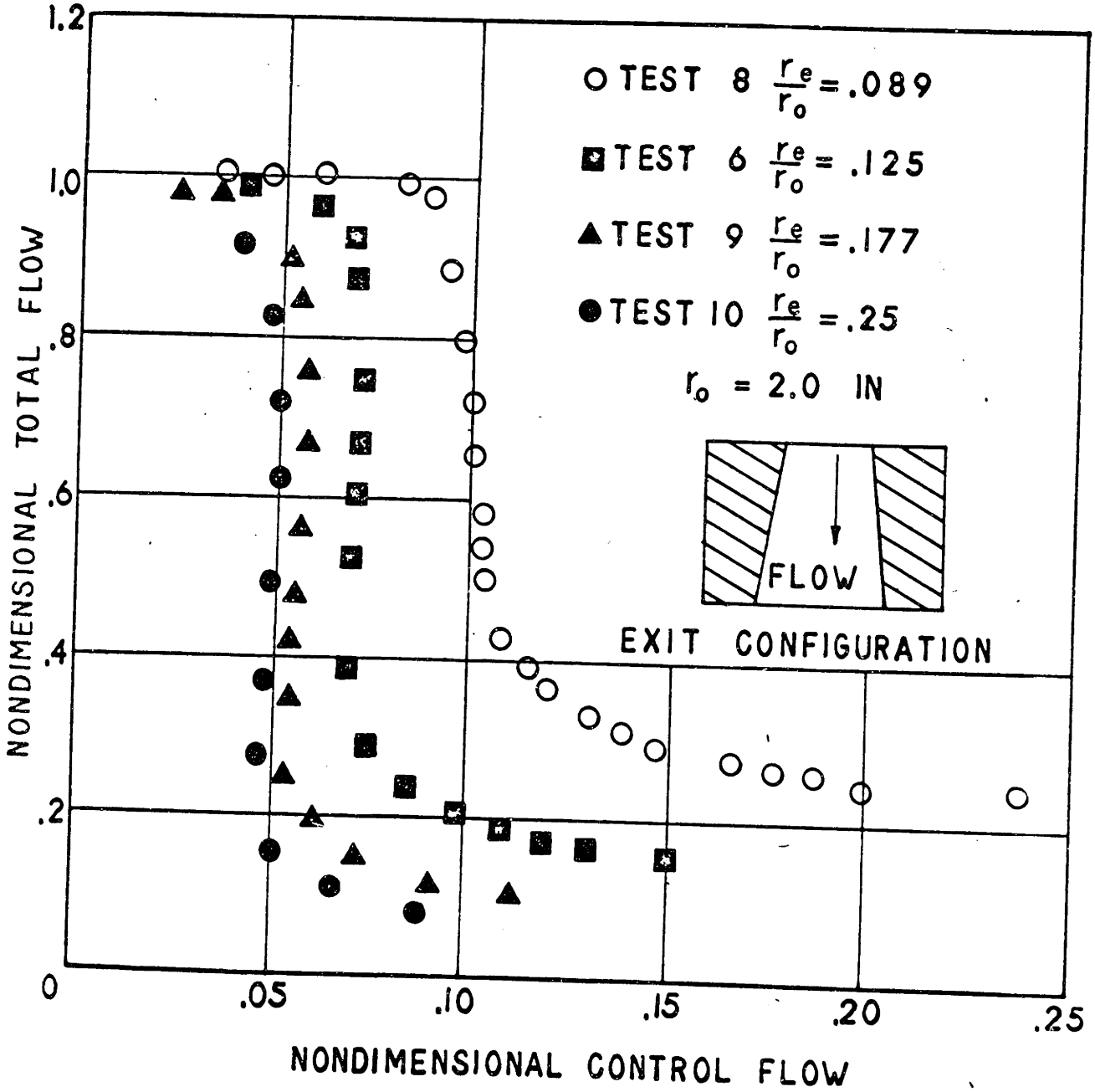

Fig. 4.7. The Influence of Exit Radius on the Valve Characteristic.

valve with $\frac{r_e}{r_o} = 0.089$ might be called a proportional characteristic since the incremental flow gain is finite ($\frac{\Delta W_o}{\Delta W_c} \simeq -15$) and fairly constant over a range of total flows from $\bar{W}_o = 0.9$ to $\bar{W}_o = 0.45$. As the radius ratio increases the maximum valve incremental flow gain tends to become infinite and the characteristic tends to be virtually that of a bistable valve. It is also noted that the larger radius ratio valves with high flow gain characteristics have larger turndown ratios than the valves with smaller radius ratios and lower flow gains. The effect of the valve radius ratio on the values of valve turndown ratio, cutoff control pressure ratio, and quiescent power drain are discussed in more detail in Section 4.3.

In some applications of vortex valves it is desirable to maximize the value of flow at zero control flow while maintaining a small exit radius valve. One method for increasing the flow through the valve while keeping the exit radius of the valve small is to use a dual exit valve. An exploratory test was carried out using a dual exit valve which had identical exits in both the top and bottom plates of the valve. The result of the test is presented in Figure 4.8. The test data indicates that the dual exit valve requires less nondimensional control flow at each point on the characteristic than a single exit valve with the same exit area. At the cutoff point, the dual exit valve requires a value of nondimensional cutoff control pressure of 3.2 and has a turndown ratio of 8.9 while the single exit valve of the same exit area requires a nondimensional cutoff control pressure of 5.5 and has a turndown ratio of 6.7. The dual exit valve then has a higher turndown ratio and a lower cutoff control pressure ratio than a single exit valve of the same exit

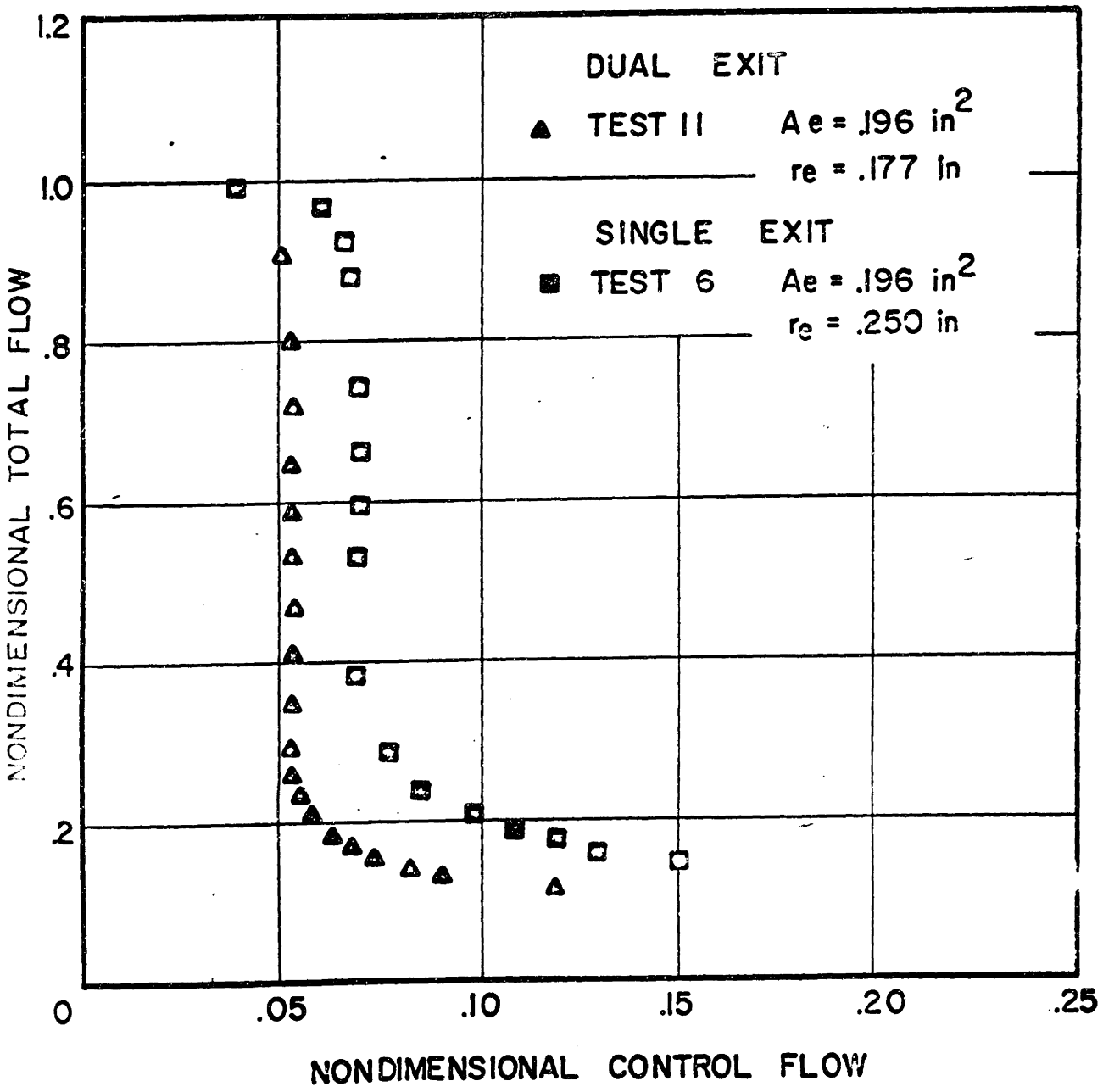

Fig. 4.8. The Dual Exit Valve Characteristic.

area. The dual exit valve can pass the same maximum flow at zero control flow as the single exit valve of the same total exit area, but has a smaller radius ratio and therefore requires less control flow at cutoff. In applications where packaging requirements permit the use of double exit valves, their superior characteristics at cutoff can be used to advantage.

4.3.2.4 The Chamber Length

The influence of chamber length on the vortex valve characteristic was determined with the seven inch valve operating on air. In the test the valve chamber length was altered by moving the valve bottom plate with respect to the top plate while the valve supply, control, and exit port areas were all maintained at constant values. The results of the test, which are presented in Figure 4.9, indicate that the valve characteristic is independent of the value of chamber length for the complete range of $\frac{h}{r_o}$ covered in the tests, i.e. $\frac{h}{r_o}$ varying from 0.144 to 0.64. This range of values of $\frac{h}{r_o}$ corresponds to a range of values of $\frac{h}{r_e}$ in the valve tested from 2.1 to 8.65. It is noted that the range over which a valve characteristic is chamber length independent depends on both the parameters $\frac{h}{r_o}$ and $\frac{h}{r_e}$. If a valve were tested in the same range of $\frac{h}{r_o}$ as specified above but had a value of $\frac{h}{r_e} < 0.25$, the valve characteristic would be strongly dependent upon the value of chamber length, for the valve exit area would be effectively the curtain area $2\pi r_e h$ rather than the cross section area πr_e^2.

As a result of this study, it is concluded that for valve chambers in which $0.144 < \frac{h}{r_o} < 0.64$ and in which $\frac{h}{r_e} > 2$ the valve

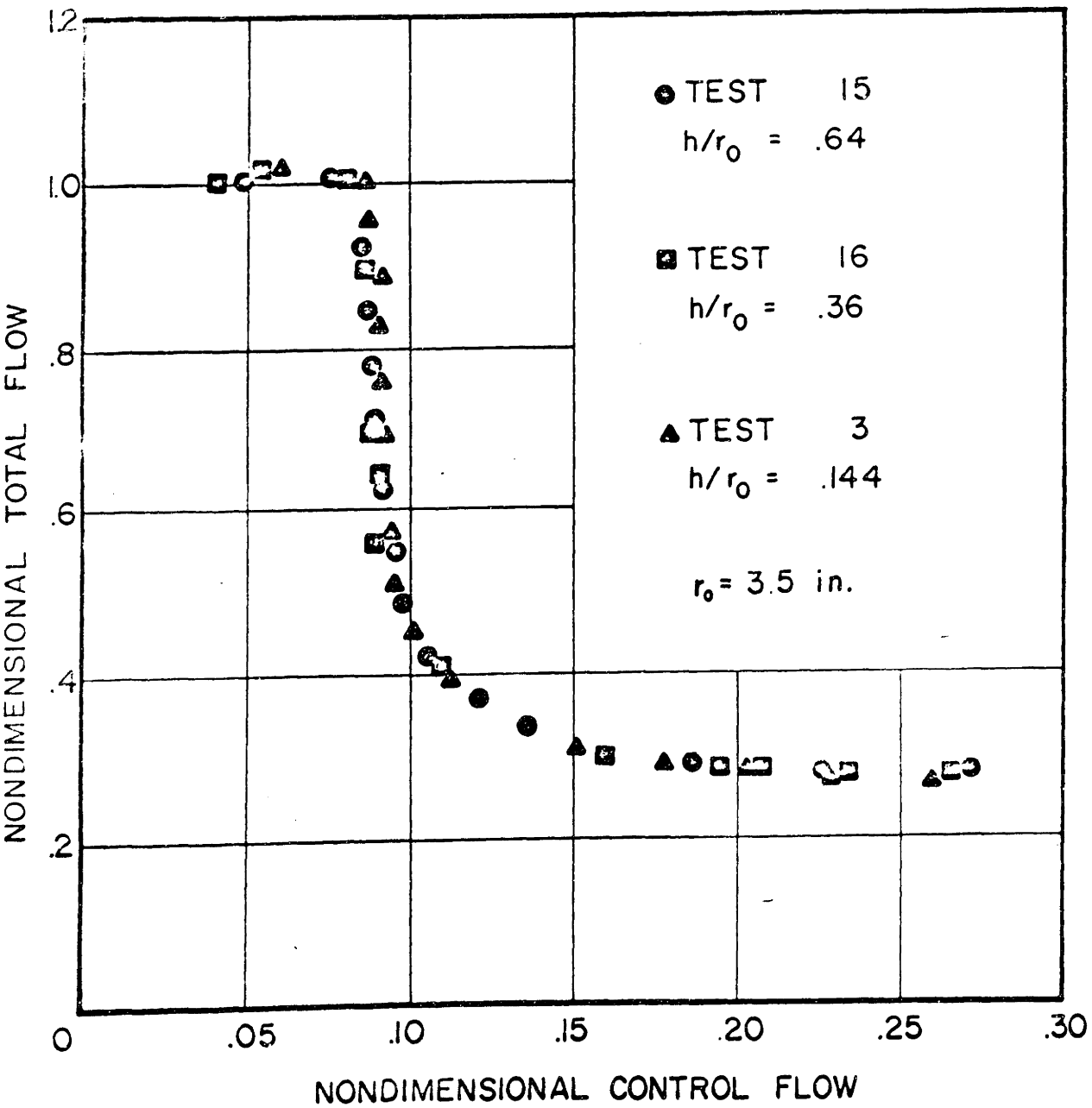

Fig. 4.9. The Influence of Chamber Length on the Valve Characteristic.

characteristic is independent of the value of chamber length. It is recalled that the inviscid analysis indicated that the inviscid valve characteristic was also independent of chamber length if $\frac{h}{r_c} > 2$.

4.3.2.5 The Chamber Radius

A test was conducted with the four and seven inch valve chambers to determine the influence of valve chamber radius on the valve characteristic. In the test, the exit areas, control port areas, and chamber lengths of the four and seven inch valves were identical in value and the supply port areas of both valves were greater than three times the exit areas. The result of the test is presented in Figure 4.10 in which it is noted that the characteristic curves for the two valves cross each other indicating that the effect of chamber radius on the valve characteristic depends upon the particular flow conditions in the valve. At large values of total flow, or for relatively weak vortex strengths, the seven inch valve requires less control flow than the four inch valve. This behavior is in agreement with the results of the inviscid analysis which indicates that as the valve chamber radius is increased, the valve control flow and pressure requirements at each point on the characteristic are reduced. At low values of total flow in the high vortex strength region of the characteristic the seven inch valve requires more control flow than the four inch valve. This result for the high vortex strength regions of the characteristic is opposite to the result of the inviscid theory. In particular, at the cutoff point, the four

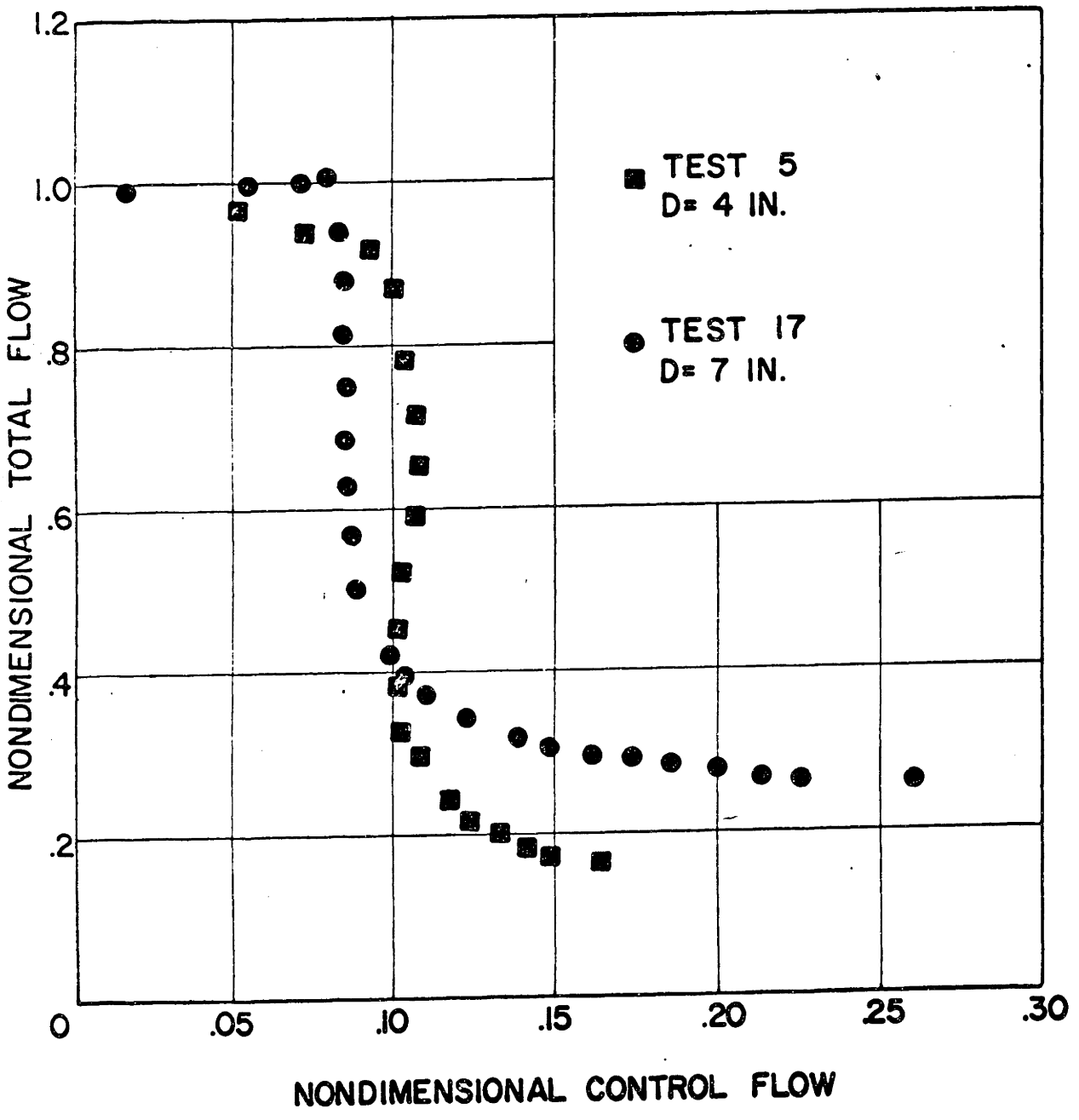

Fig. 4.10. The Influence of Chamber Radius on the Valve Characteristic.

inch valve turndown ratio is higher than the seven inch valve turndown ratio and the four inch valve cutoff control pressure ratio is lower than the seven inch valve cutoff control pressure ratio. It is apparent that in order to model adequately the influence of chamber radius on the complete valve characteristic, a model must be formulated which includes the effects of viscous losses in the chamber. Such a model is discussed in Chapter 7.

4.4 Determination of Vortex Valve Maximum and Minimum Flow Properties

The experimental data presented in the preceeding sections has indicated that the valve characteristic and, in particular, the non-dimensional cutoff quantities -- turndown ratio, cutoff control pressure ratio, and normalized quiescent power drain -- are dependent only upon the ratios A_c/A_e and r_e/r_o if (1) the valve is tested in the incompressible flow regime with a maximum flow Reynolds number between 750 and 3300, (2) the valve supply port area is three times greater than the exit area, (3) the chamber length satisfies the conditions that $.144 < h/r_o < .64$ and $h/r_e > 2$. An experimental apparatus ($r_o = 1.0"$, $h = 0.625"$) that meets these specifications was designed to determine the maximum and minimum flow properties of a valve over a range of r_e/r_o varying from 0.075 to 0.35 and a range of A_c/A_e varying from 0.03 to greater than 1.0 (It is noted that for the test with $r_e/r_o = 0.35$, $h/r_e \approx 1.8$ rather than $h/r_e > 2.0$ as specified. This violation of the specifications is not critical as indicated in the data of Section 5.5.) A photograph of the apparatus is shown in Figure 4.11. The apparatus consists of a top plate, a bottom plate, a retaining

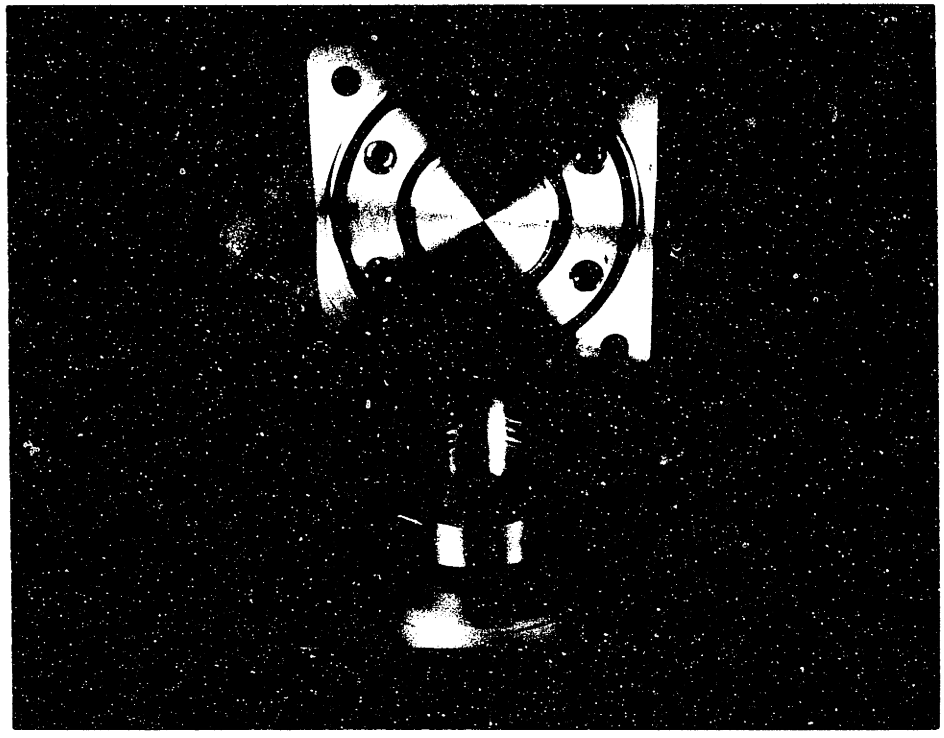

Fig. 4.11 Photograph of the Maximum and Minimum Flow Test Apparatus

ring and an inlet port ring. The apparatus exit port which is of the same shape as the exit port shown in Figure 4.7 is contained in the bottom plate. Four bottom plates were used with the apparatus, each with respective exit port radii of 0.075, 0.15, 0.25, and 0.35 inches. The top plate contains a 0.020 inch pressure tap which is used to measure the pressure at the periphery of the valve chamber. Three inlet port rings were used with the apparatus. For measurement of the maximum flow properties inlet port ring #1 which contains forty 0.125 inch radial holes was used. For measurement of the minimum flow properties inlet port ring #2 or inlet port ring #3 were used. Each of these rings contains 18 holes drilled tangent to the ring inside radius. In ring #2 the holes are 0.0995 inches in diameter while in ring #3 they are 0.032 inches in diameter. The valve was tested in the flow loop described in Section 4.2 using air as the test fluid. The maximum and the minimum flow properties were determined by the following procedure:

1) With a given outlet orifice, inlet ring #1 with radial inlet holes was installed and the flow rate through the valve W and the pressure tap pressure P_t were measured as a function of the pressure P_p in the plenum between the retaining ring and the inlet ring. The conditions measured in this test correspond to the maximum flow conditions in a valve, i.e. $W = W_m$ and $P_p = P_s$. The pressure tap pressure P_t was found in all cases to be essentially identical to the supply plenum pressure, i.e. negligible pressure drop occurred across the supply inlet ring.

2) Inlet ring #1 was replaced with a tangential hole inlet ring (ring #2 or ring #3) and the flow rate through the valve W and the pressure tap pressure P_t were measured as a function of the pressure P_p in the plenum between the retaining and inlet rings. The conditions of this test correspond to the minimum flow or cutoff conditions in a vortex valve. The measured flow corresponds to the cutoff control flow, $W = W_{cc}$, the pressure tap pressure corresponds to the valve supply pressure $P_t = P_s$, i.e. pressure required to cutoff the supply flow, and the plenum pressure corresponds to the cutoff control port pressure $P_p = P_{cc}$.

3) The quantities of interest -- the turndown ratio, TR, the normalized cutoff control flow, $\bar{P}_{cc}$, and the normalized cutoff power drain, $\overline{QP}$, -- were determined by forming the following ratios between the maximum and the minimum flow quantities:

$$\bar{P}_{cc} = \frac{P_{cc}}{P_s} \qquad TR = \frac{W_m}{W_{cc}} \qquad \overline{QP} = \frac{P_{cc} W_{cc}}{P_s W_m}$$

under the constraint that P_s of the maximum flow test condition was equal to the pressure tap pressure ($P_t = P_s$) of the minimum flow test condition. These conditions correspond to the maximum and minimum flow states of a valve operated at constant supply pressure.

Experimental data was taken for each of the four outlet ports described above and for a number of control port areas. The discharge coefficients for each of the exit orifices over the range of flow conditions studied in the test series were: $r_e = 0.075"$, $C_e = .77$; $r_e = 0.15"$, $C_e = .74$; $r_e = 0.25"$, $C_e = .75$;

$r_e = 0.35"$, $C_e = .72$. The results of the test series are summarized in Figures 4.12, 4.13, and 4.14. The data in Figure 4.12 and 4.13 indicate that as the ratio $\frac{A_c}{A_e}$ is decreased; the turndown ratio and the cutoff control pressure ratio of a valve increase monotonically, while as $\frac{r_e}{r_o}$ increases the valve turndown ratio increases and the cutoff control pressure ratio decreases. If a valve with a large turndown ratio is desired $\frac{r_e}{r_o}$ should be large and $\frac{A_c}{A_e}$ should be small. A valve with a large turndown ratio also has a large cutoff control pressure ratio. A balance must then be obtained in the values of $\frac{A_c}{A_e}$ and $\frac{r_e}{r_o}$ for a valve so that both a satisfactory turndown ratio and cutoff control pressure ratio are obtained.

A measure of the relative magnitudes of both $\bar{P}_{cc}$ and TR is the normalized power drain at cutoff, $\overline{QP}$, which relates the valve power consumption at cutoff to the maximum flow power consumption. The value of $\overline{QP}$ is plotted in Figure 4.14 versus $\frac{A_c}{A_e}$ for several values of $\frac{r_e}{r_o}$. The data indicates that for $\frac{r_e}{r_o} = 0.35$, 0.25, and 0.15, the curves for the cutoff power drain ratios possess a minimum at a given value of $\frac{A_c}{A_e}$. If for example in the case $\frac{r_e}{r_o} = 0.35$, the ratio of $\frac{A_c}{A_e}$ is either increased or decreased from the value $\frac{A_c}{A_e} = 0.16$, the cutoff power drain ratio increases. For values of $\frac{r_e}{r_o} = 0.25$ and $\frac{r_e}{r_o} = 0.15$ the minimum values of quiescent power drain occur respectively at $\frac{A_c}{A_e} = 0.175$ and $\frac{A_c}{A_e} = 0.32$. In the curve for $\frac{r_e}{r_o} = 0.075$ the normalized quiescent power drain decreases monotonically with decreasing $\frac{A_c}{A_e}$ for the range of $\frac{A_c}{A_e}$ covered in the test. The increase in the value of $\overline{QP}$ with decreasing values of $\frac{A_c}{A_e}$ at small values of $\frac{A_c}{A_e}$ is largely due to the rapid increase in $\bar{P}_{cc}$ as $\frac{A_c}{A_e}$ is decreased, while the

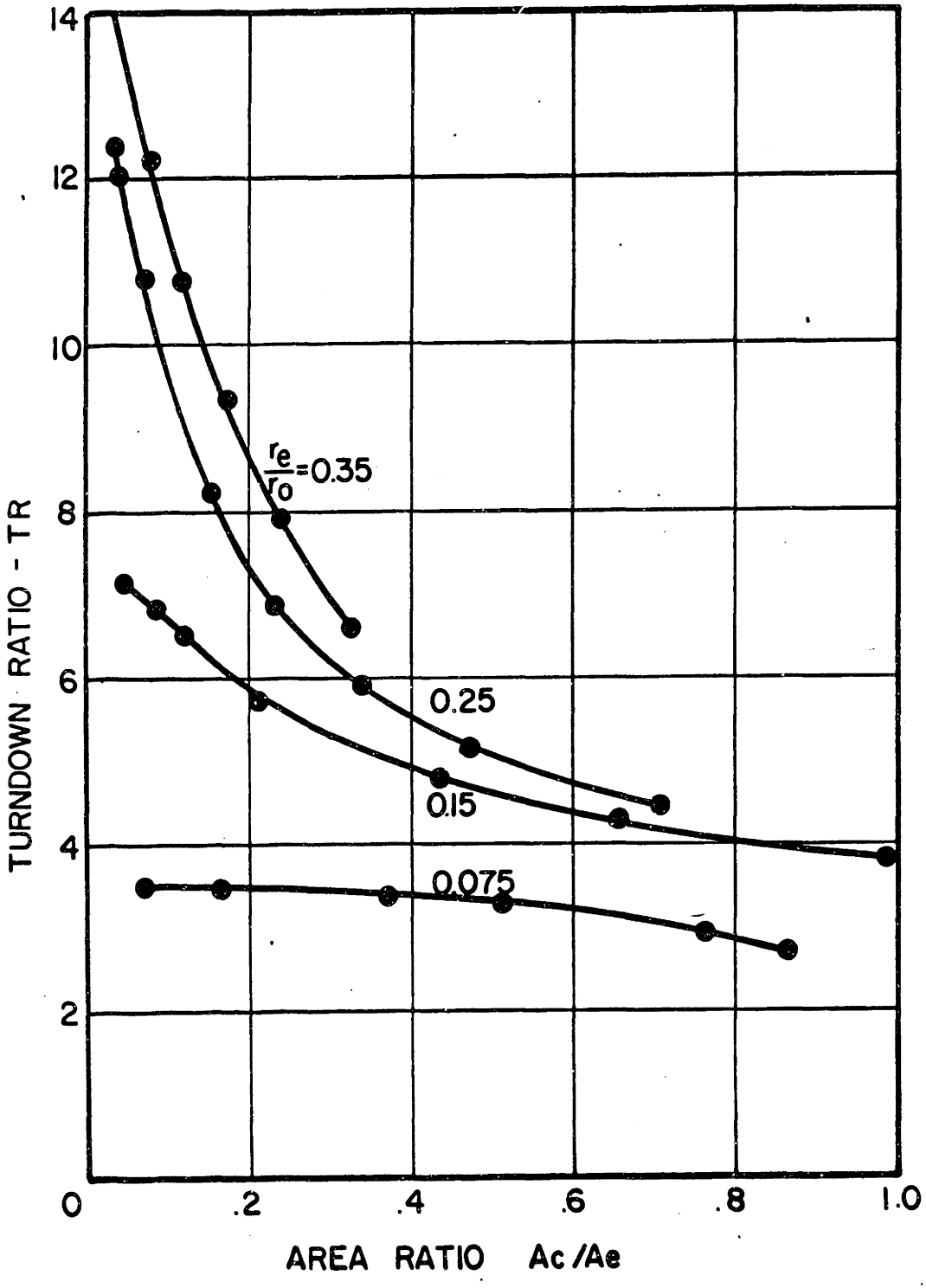

Fig. 4.12. Vortex Valve Turndown Ratio.

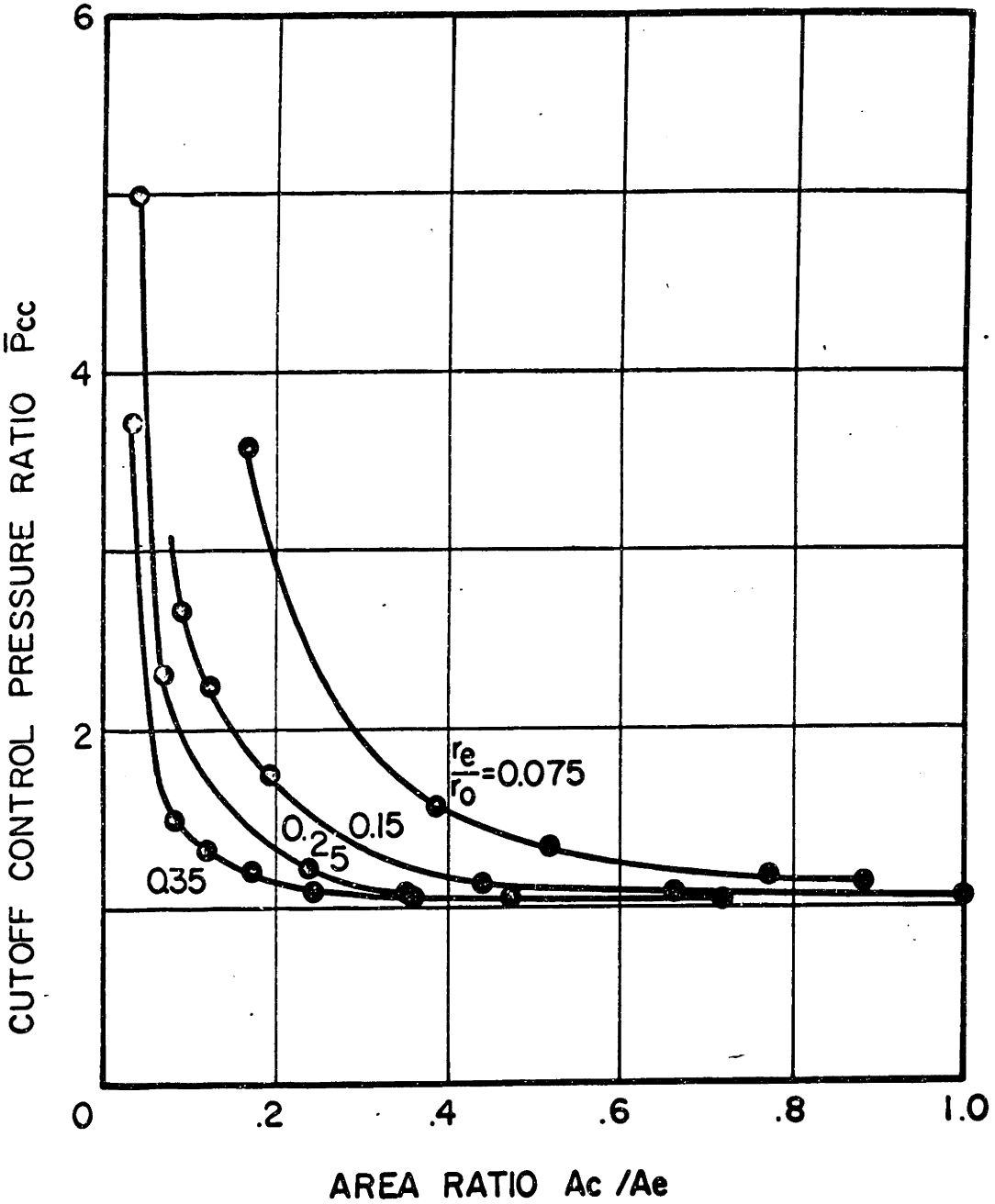

Fig. 4.13. Vortex Valve Cutoff Control Pressure Ratio.

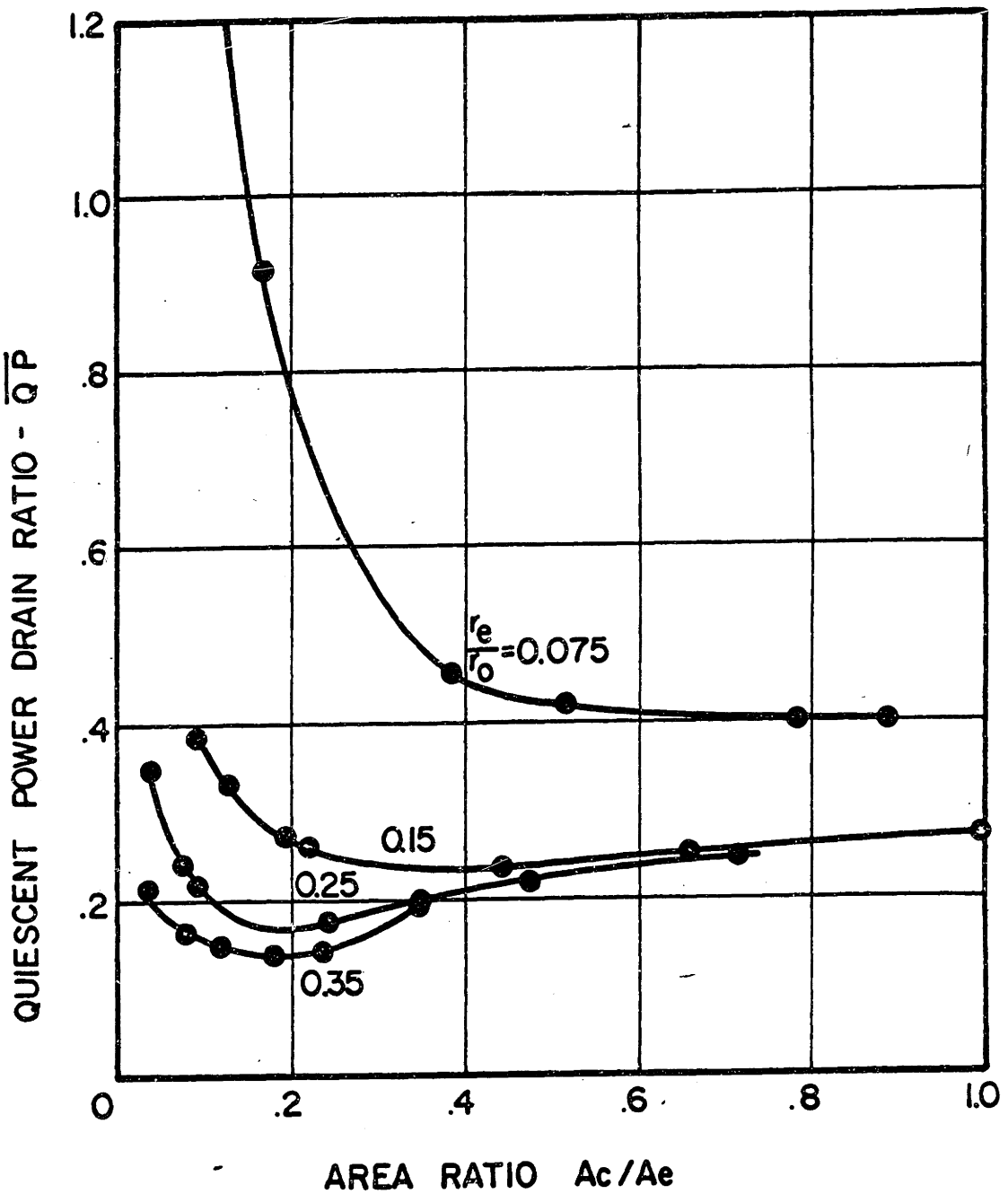

Fig. 4.14. Valve Quiescent Power Drain Ratio.

increase in the value of $\overline{QP}$ at large values of $\frac{A_c}{A_e}$ for valves with large radius ratios is largely due to the decrease in turndown ratio as $\frac{A_c}{A_e}$ increases.

The test data of Figures 4.12, 4.13, and 4.14 is used as a basis for the valve design procedure developed in Chapter 5.

4.5 Comparison of Experimental Data with the Results of the Inviscid Theory

It is meaningful to compare some of the experimentally measured valve characteristics directly with the characteristics predicted by the inviscid valve model. In Figure 4.15 experimental data for the valve characteristics measured in test runs 5 and 7 are compared with corresponding inviscid valve characteristics determined from equation 3.16. The values of the valve geometrical parameters for test numbers 5 and 7 are tabulated in Appendix A. It is noted that in both tests $\frac{C_s}{C_e}\frac{A_s}{A_e} > 4.0$ and $\frac{h}{C_e r_e} > 2.0$. The value of the exit area discharge coefficient used in equation 3.16 was 0.8 for both test runs.

The comparison between the inviscid characteristics and the experimental characteristics in Figure 4.15 indicates that the inviscid characteristics are almost identical to the experimental characteristics for large values of total flow, i.e. for relatively weak vortex strengths; while, at low values of total flow and correspondingly greater vortex strengths, the ideal characteristic differs significantly from the experimental characteristic. The poor agreement between the predicted and experimental characteristics

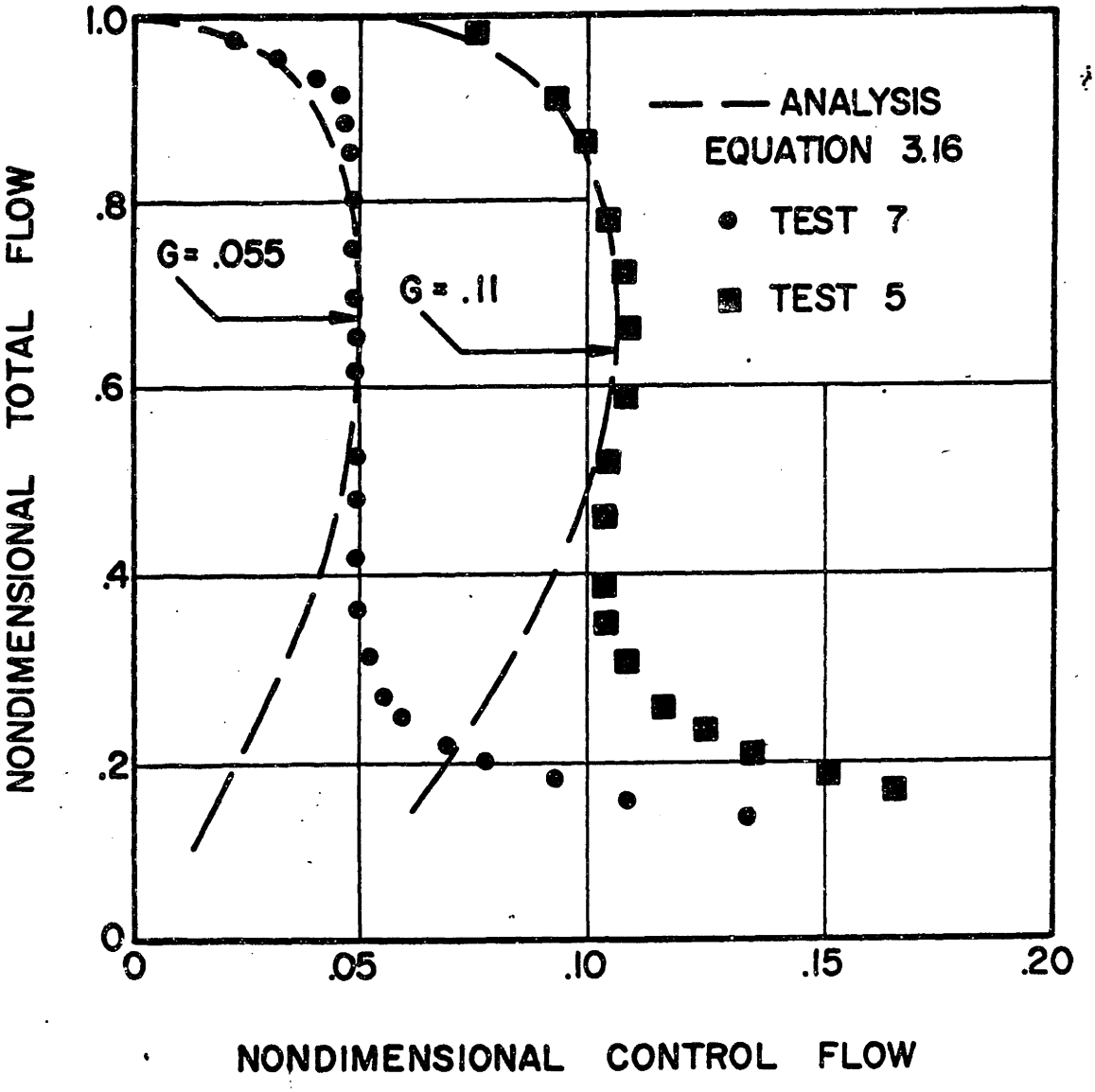

Fig. 4.15. Comparison of Inviscid and Experimental Valve Characteristics.

at low values of total flow is a result of the assumptions to neglect the effects of mixing losses at the valve inlet, the effects of chamber wall viscous boundary layers and the effects of highly swirling flow in the valve exit which all become important at high vortex strengths. A more detailed discussion of these effects is included in Chapter 7.

The inviscid valve characteristic agrees so poorly with the experimental characteristics at low values of total flow that its results cannot be used to gain information about a real valve operating at the cutoff point; however, the fact that the inviscid valve characteristic agrees closely with experimental characteristics at large values of total flow and, in particular, at $\bar{W}_o = 0.707$ deserves further investigation.

The valve normalized control flow $\bar{W}_c^+$ and control pressure $\bar{P}_c^+$ requirements at $\bar{W}_o = 0.707$ as predicted by the inviscid analysis are given in equations 3.18 and 3.19. These values of $\bar{W}_c^+$ and $\bar{P}_c^+$ are compared in Table 4.1 with experimentally measured values obtained on the test valves described in preceding sections. In the comparison the values of the exit port discharge coefficient C_e and the control port discharge coefficient C_c used to compute $\bar{P}_c^+$ and $\bar{W}_c^+$ were 0.8 and 0.75 respectively. The data of Table 4.1 indicates that the values of $\bar{W}_c^+$ predicted by equation 3.18 were within 15% of the experimental values and that the values of $\bar{P}_c^+$ predicted by equation 3.19 were within 15% of the experimental values. The fact that the values of $\bar{P}_c^+$ and $\bar{W}_c^+$ predicted by equations 3.18 and 3.19 have been found to agree closely with experimentally measured values for a broad range of values of $\frac{A_c}{A_e}$ and $\frac{r_e}{r_o}$ including

TABLE 4.1

COMPARISON OF PREDICTED* VALUES OF $\bar{W}_c^+$ AND $\bar{P}_c^+$ WITH EXPERIMENTAL DATA

TEST	r_o IN.	$\frac{r_e}{r_o}$	$\frac{A_c}{A_e}$	W_c^+ EQUATION 3.18	$\frac{\bar{W}_c^+(\text{EXP.})}{\bar{W}_c^+(\text{EQ3.18})}$	P_c^+ EQUATION 3.19	$\frac{\bar{P}_c^+(\text{EXP.})}{\bar{P}_c^+(\text{EQ3.19})}$
1	3.5	.071	.162	.085	1.0	1.35	1.03
4	2.0	.125	.324	.159	1.15	1.31	1.05
5	2.0	.125	.162	.112	1.04	1.62	0.99
6	2.0	.125	.085	.079	1.10	2.24	0.97
7	2.0	.125	.042	.056	1.12	3.48	1.02
8	2.0	.089	.170	.094	0.94	1.42	0.89
9	2.0	.177	.042	.067	1.15	4.30	1.03
10	2.0	.250	.021	.056	1.12	10.5	1.02

*$C_c = 0.7$, $C_e = 0.8$

values of $\frac{A_c}{A_e}$ varying from 0.021 to 0.324 and $\frac{r_e}{r_o}$ varying from 0.071 and 0.25 is used as a basis for the design method described in Chapter 5.

CHAPTER 5

VORTEX VALVE DESIGN

5.1 Introduction

In this chapter a procedure for designing vortex valves which operate in the incompressible flow regime is developed. The procedure provides a systematic method for progressing from a set of performance specifications which include the maximum available supply pressure and flow and the maximum available control pressure and flow to the establishment of the critical dimensions--r_e, r_o, A_c, A_s, h -- of a single-exit prototype valve if it is possible to build a valve which can meet the performance specifications. As an integral part of the procedure the valve characteristic is checked to determine if multiple values of total flow exist at the cutoff value of control flow. Finally the procedure provides a method by which a rough sketch of the valve characteristic is obtained.

The design procedure provides sufficiently detailed information so that for a prototype valve which is to be operated in a bi-stable or on-off mode, the control pressure and flow required to switch the valve from a flow level near maximum flow to a flow level near minimum flow is indicated. The procedure does not, however, provide a precise prediction of the entire valve characteristic and is not useful for determining the incremental flow and pressure gain of a prototype valve. The requirements of a design method which will precisely predict the complete valve characteristic are discussed in Chapter 7. At the

present time the best method available for determining the details of a valve characteristic after the general shape is determined by the design procedure developed in this chapter is to determine it experimentally. Work is included in this chapter which outlines analytical methods of deriving from a single valve characteristic measured at constant supply pressure all the information required, i.e., inlet and exit port impedances, to determine steady-state valve performance in fluid circuits employing valves which operate at varying supply and exhaust presusres.

5.2 The Design Procedure

The design procedure consists of six steps:

Step 1: Specification of operating fluid, maximum supply pressure and flow and maximum control pressure and flow.

Step 2: Translation of dimensional input specifications to the nondimensional performance paramters -- cutoff control pressure ratios and cutoff control flow ratios.

Step 3: Selection of the dimensionless valve parameters -- A_c/A_e, r_e/r_o, A_s/A_e, h/r_o -- to meet the performance specifications.

Step 4: Calculation to determine if multiple values of total flow exist in the valve characteristic at the cutoff value of control flow.

Step 5: Translation of the nondimensional geometry parameters into values of the valve critical dimensions r_e, r_o, A_c, A_s, h and calculation of the maximum flow Reynolds number.

Step 6: Determination of values of W_c^+ and P_c^+ required to sketch the prototype valve characteristic curve.

The design procedure is developed with the aid of the analytical and experimental results reported in Chapters 3 and 4. In particular, the experimental result of Chapter 4 is utilized which indicates that the nondimensional valve characteristic is a function of only two variables A_c/A_e and r_e/r_o when the selection of appropriate values for A_s/A_e, h/r_o and maximum flow Reynolds number is made. Without the simplification afforded by this result, a design procedure which requires only simple paper and pencil calculations in its implementation would not be feasible.

Each of the steps of the design procedure is described in detail in the paragraphs that follow.

5.2.1 Input Specifications

The first step in the design procedure requires the specification of the valve operating fluid, maximum valve supply pressure P_s and flow W_m and the maximum valve control pressure P_{cc} and flow W_{cc}. In the specification of the operating fluid both the fluid density ρ and viscosity μ are required. It is recalled from Chapter 3 that the pressures, P_s and P_{cc} are measured relative to the pressure downstream of the valve exit for the incompressible flow case considered in this investigation.

The maximum pressure and flow quantities which require specification are the typical quantities required in a conventional valve design

(for example the second stage spool of a two stage servovalve) and represent simply the maximum output flow and pressure required at the valve and the maximum pressure and flow available for actuating the valve. It is noted that in the case of the vortex valve the quantity $P_{cc}\ W_{cc}$ is proportional to the power drain of the valve operating at cutoff.

5.2.2 Nondimensional Performance Parameters

Using the input quantities specified in 5.21, the cutoff control pressure ratio and the cutoff control flow ratio, or equivalently the turndown ratio, required by the prototype valve can be determined from equations 5.1 and 5.2:

$$\overline{P}_{cc} = \frac{P_{cc}}{P_s} \tag{5.1}$$

$$\overline{W}_{cc} = \frac{W_{cc}}{W_m} \tag{5.2}$$

It is noted that these two ratios simply relate the valve maximum flow state to the valve minimum flow state and that their product $\overline{P}_{cc}\overline{W}_{cc}$ represents the ratio of cutoff power drain to valve maximum power consumption.

5.2.3 Selection of Prototype Valve Dimensionless Geometric Parameter Values

The values for the prototype valve dimensionless geometric parameters - A_c/A_e, r_e/r_o, A_s/A_e and h/r_o required to meet the specified values of $\overline{P}_{cc}$ and $\overline{W}_{cc}$ (if it is possible to build a valve which meets the input specifications) may be determined by utilizing the experimental

results reported in Chapter 4. These results indicate that when the following two conditions are satisfied:

$$\frac{A_s}{A_e} \geq 3 \tag{5.3}$$

$$0.144 \leq \frac{h}{r_o} \leq 0.64 \text{ and } \quad 2 \leq \frac{h}{r_e} \tag{5.4}$$

the ratios $\bar{P}_{cc}$ and $\bar{W}_{cc}$ are functions of only A_c/A_e and r_e/r_o if the maximum flow Reynolds number lies between 750 and 3300. If it is assumed that $750 \leq R_w \leq 3300$ (the validity of this assumption is checked in Step 5) and if the values of A_s/A_e and h/r_o (and h/r_e) are selected as specified in equations 5.3 and 5.4, then the experimental data presented in Figures 4.12 and 4.13 may be used to determine the values of A_c/A_e and r_e/r_o required in the prototype valve. The data of Figures 4.12 and 4.13 are reproduced and combined as shown in Figure 5.1. From Figure 5.1 the values of A_c/A_e and r_e/r_o corresponding to a given pair of values of $\bar{P}_{cc}$ and $\bar{W}_{cc}$ may be readily found. For example, the values of A_c/A_e and r_e/r_o required to meet the cutoff specification $\bar{P}_{cc} = 3.0$ and $\bar{W}_{cc} = 0.15$ are indicated in Figure 5.1 as $r_e/r_o = 0.15$ and $A_c/A_e = 0.1$. Thus as a result of the experimental investigation, the values of the geometric parameters required to meet the performance specifications $\bar{P}_{cc}$ and $\bar{W}_{cc}$ are determined from Figure 5.1 for r_e/r_o and A_c/A_e and from equations 5.3 and 5.4 for A_s/A_e and h/r_o (h/r_e). It is recalled that from the discussion of Chapters 3 and 4 that the specification of A_s/A_e and h/r_o (h/r_e) as indicated in equations 5.3 and 5.4 leads to valves with maximum turndown ratios.

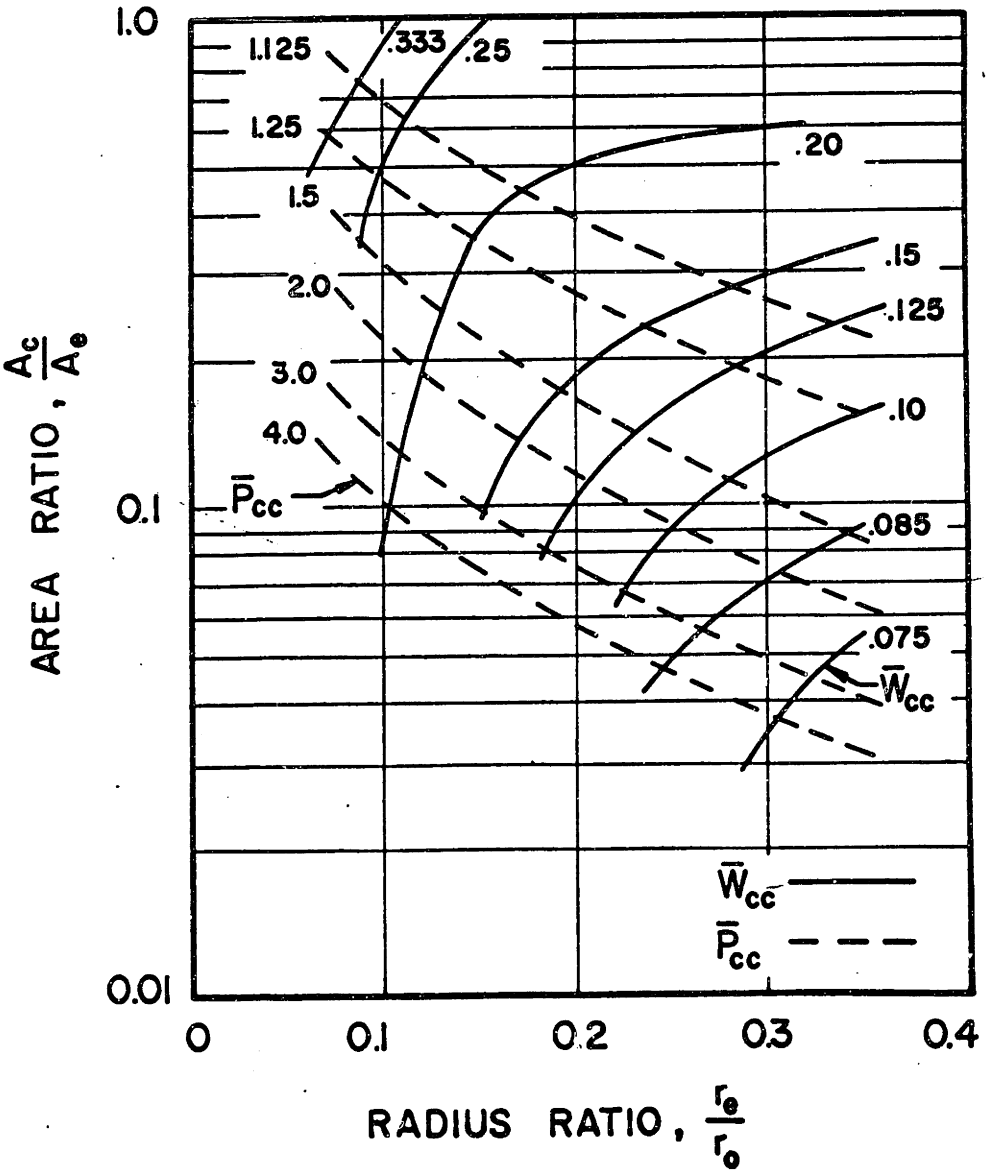

Fig. 5.1. Vortex Valve Cutoff Flow Characteristics.

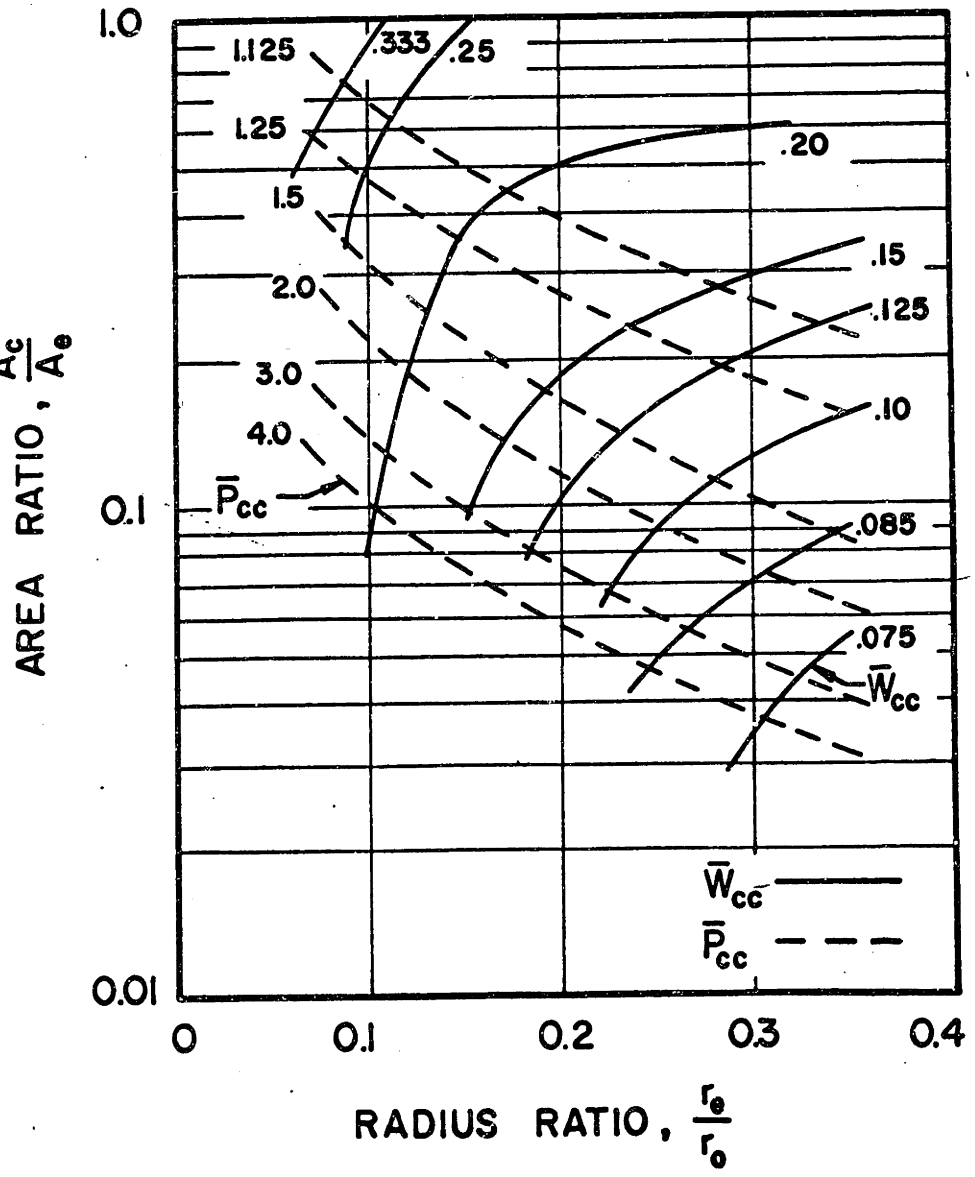

Fig. 5.1. Vortex Valve Cutoff Flow Characteristics.

5.2.4 Existence of Multiple Values of Total Flow at the Cutoff Value of Control Flow

The procedure outlined in Section 5.2.3 may result in a prototype valve whose characteristic has a single value of total flow or multiple values of total flow which exist at the cutoff value of control flow. The two possibilities may be illustrated by an example. Consider a case in which the input specifications for the application reduce to the requirement that $\bar{W}_{cc} = 0.1$ and that $\bar{P}_{cc} \leq 4.0$. As may be determined from Figure 5.1, a number of valve geometries may be constructed to meet these specifications. Two of the possible ones are designated as prototype Valve A with $\bar{W}_{cc} = 0.1$, $\bar{P}_{cc} = 4.0$, $\frac{r_e}{r_o} = 0.215$ and $\frac{A_c}{A_e} = 0.05$, and prototype Valve B with $\bar{W}_{cc} = 0.1$, $\bar{P}_{cc} = 2.0$, $\frac{r_e}{r_o} = 0.25$, and $\frac{A_c}{A_e} = 0.09$. The nondimensional characteristics of these two valves are sketched in Figure 5.2 in which it is noted that Valve A has a single possible value of total flow, $\bar{W}_o = 0.1$, at the cutoff value of control flow, $\bar{W}_c = 0.1$. Valve B has a multivalued characteristic and three values of total flow, $\bar{W}_o = 0.1$, $\bar{W}_o = 0.36$ and $\bar{W}_o = 0.9$, which are possible at the cutoff value of control flow, $\bar{W}_c = 0.1$. Valve B in which multiple values of total flow exist at the cutoff value of control flow is not a very useful valve for most applications because when the valve is supplied with a constant pressure supply source and the control flow is set to its cutoff value the valve may tend to oscillate, hunting from one value of total flow to another. The cutoff operating point for Valve B may be an unstable operating point while the cutoff operating point for Valve A is stable. It is important to determine for any given application whether a prototype

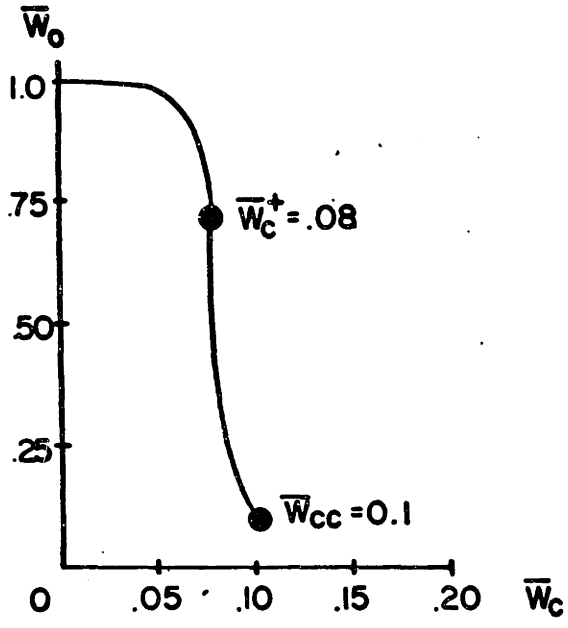

VALVE A

$\frac{r_e}{r_o} = .215$, $\frac{A_c}{A_e} = .05$, $\overline{P}_{cc} = 4.0$

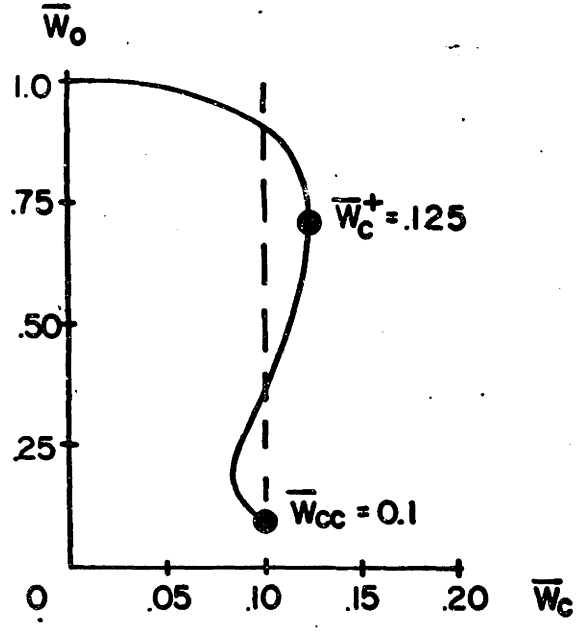

VALVE B

$\frac{r_e}{r_o} = .25$, $\frac{A_c}{A_e} = .09$, $\overline{P}_{cc} = 2.0$

Fig. 5.2. Characteristics of Prototype Valve A and Valve B.

valve has single or multiple possible values of total flow which exist at the cutoff value of control flow.

In order to determine if multiple values of total flow exist at the cutoff value of control flow, it is necessary to determine at least one point on the valve characteristic in addition to the maximum flow and cutoff flow points. A point which will yield the necessary information is the point at which $\bar{W}_o = 0.707$ and $\bar{W}_c = \bar{W}_c^+$. It is recalled from the discussion of Sections 3.1.4 and 4.4 that the point $\bar{W}_o = 0.707$ is the point of theoretical maximum required control flow in an inviscid valve model and that the control flow requirements of a real valve at $\bar{W}_o = 0.707$ may be accurately predicted with the aid of equation 3.18 which is reproduced as:

$$\bar{W}_c^+ = \frac{\sqrt{\left(\frac{1}{2C_e}\right)\left(\frac{r_e}{r_o}\right)\frac{A_c}{A_e}}}{\sqrt{1 - \frac{r_e^2}{r_o^2}}} \tag{5.5}$$

The condition which is sufficient to insure that multiple values of total flow exist at the cutoff value of control flow may be determined from Figure 5.2 to be:

$$\bar{W}_c^+ \geq \bar{W}_{cc} \tag{5.6}$$

The locus of values of the geometric parameters $\frac{r_e}{r_o}$ and $\frac{A_c}{A_e}$ for which equation 5.6 is satisfied may be determined by using the results of Figure 5.1 in which $\bar{W}_{cc}$ is plotted as a function of

$\frac{A_c}{A_e}$ and $\frac{r_e}{r_o}$ and by using equation 5.5 in which $\bar{W}_c^+$ is expressed as a function of $\frac{A_c}{A_e}$ and $\frac{r_e}{r_o}$. A convenient method to determine the locus is shown in Figure 5.3 in which lines of constant $\bar{W}_{cc}$ determined from Figure 5.1 and lines of constant $\bar{W}_c^+$ as determined from equation 5.5 are plotted with $\frac{A_c}{A_e}$ and $\frac{r_e}{r_o}$ as parameters. The value of the exit orifice discharge coefficient used in calculating $\bar{W}_c^+$ was 0.75 since the experimental data of Figure 5.1 was obtained on an apparatus in which the exit orifice discharge coefficient was within 4% of 0.75 for all test conditions. The locus of points for which $\bar{W}_{cc} = \bar{W}_c^+$ is indicated by the dashed line in Figure 5.3. For values of $\frac{A_c}{A_e}$ and $\frac{r_e}{r_o}$ which result in a point that lies to the right of the line $\bar{W}_{cc} = \bar{W}_c^+$ the value of $\bar{W}_c^+$ is greater than $\bar{W}_{cc}$ and multiple values of total flow exist at the cutoff value of control flow. For values of $\frac{A_c}{A_e}$ and $\frac{r_e}{r_o}$ which result in a point to the left of the dashed line, the value of $\bar{W}_c^+$ is less than $\bar{W}_{cc}$ and it might be concluded that a single value of total flow would tend to exist at the cutoff valve of control flow. Although this conclusion cannot be proved in the general case since, conceivably, a value of control flow may exist at some other point on the characteristic which is greater than either $\bar{W}_c^+$ or $\bar{W}_{cc}$, it is noted that in the experiments described in this investigation and in the literature referenced in the bibliography, no case has been observed in which multiple values of total flow exist at the cutoff value of control flow when $\bar{W}_c^+ < \bar{W}_{cc}$. It is concluded that for values of $\frac{A_c}{A_e}$ and $\frac{r_e}{r_o}$ which result in $\bar{W}_c^+ < \bar{W}_{cc}$ a single value of total flow will "tend" to exist at the cutoff value of control flow. It is finally noted that a valve which has a single possible value of

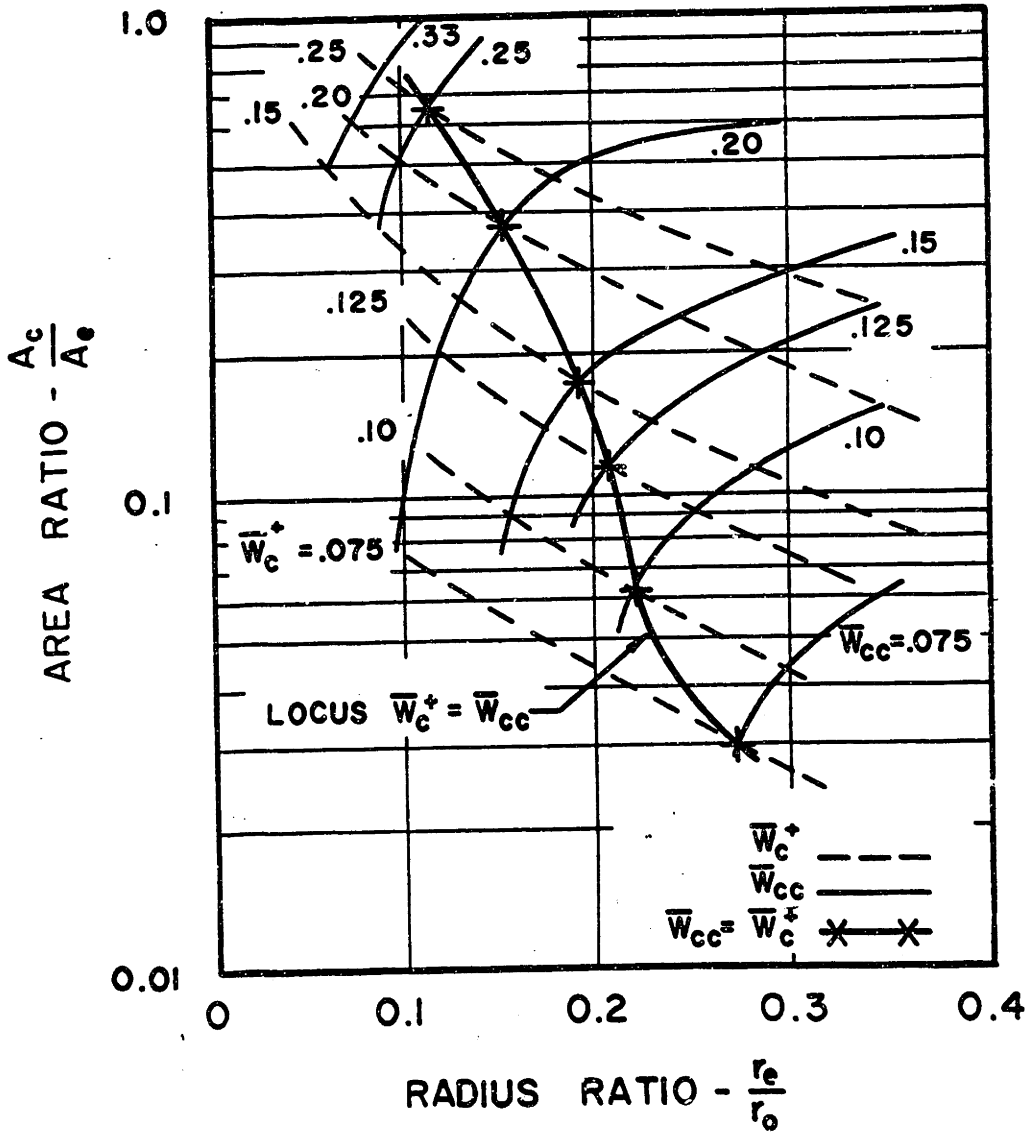

Fig. 5.3. Determination of the Existence of Multiple Values of Total Flow at the Cutoff Control Flow.

total flow at the cutoff value of control flow may still have a multivalued characteristic as demonstrated by the characteristics of Chapter 4. In bistable valves a small multivalued region in the characteristic, if it does not include the cutoff value of control flow, may be desirable.

The results of the investigation to determine the existence of multiple values of total flow at the cutoff value of control flow may be added to Figure 5.1 as shown in Figure 5.4. Several conclusions may be drawn from the results presented in Figure 5.4. As the value of the nondimensional cutoff control flow $\bar{W}_{cc}$ decreases, i.e. as the valve turndown ratio increases, the value of the nondimensional cutoff control pressure $\bar{P}_{cc}$ required to prohibit the existence of multiple values of total flow at the cutoff value of control flow increases. For example, a valve with a turndown ratio of 5 will have multiple values of total flow at the cutoff value of control flow if $\bar{P}_{cc} < 1.25$ while for a valve with a turndown ratio of 10 multiple values of total flow will exist at the cutoff value of total flow if $\bar{P}_{cc} < 3.0$. A second result of interest indicates that as the valve radius ratio increases, the value of $\bar{P}_{cc}$ must increase to guarantee a single possible value of total flow at cutoff control flow. In valves with radius ratios of 0.15 if $\bar{P}_{cc} < 1.3$ multiple values of total flow exist at the cutoff control flow while in valves with radius ratios of 0.3 if $\bar{P}_{cc} < 4.0$ multiple values of total flow exist at the cutoff control flow. The results of Figure 5.4 clearly indicate the tradeoff which exists between valves with high turndown ratios and valves with low cutoff control pressure ratios in order to prevent the existence of multiple values of total flow at the cutoff

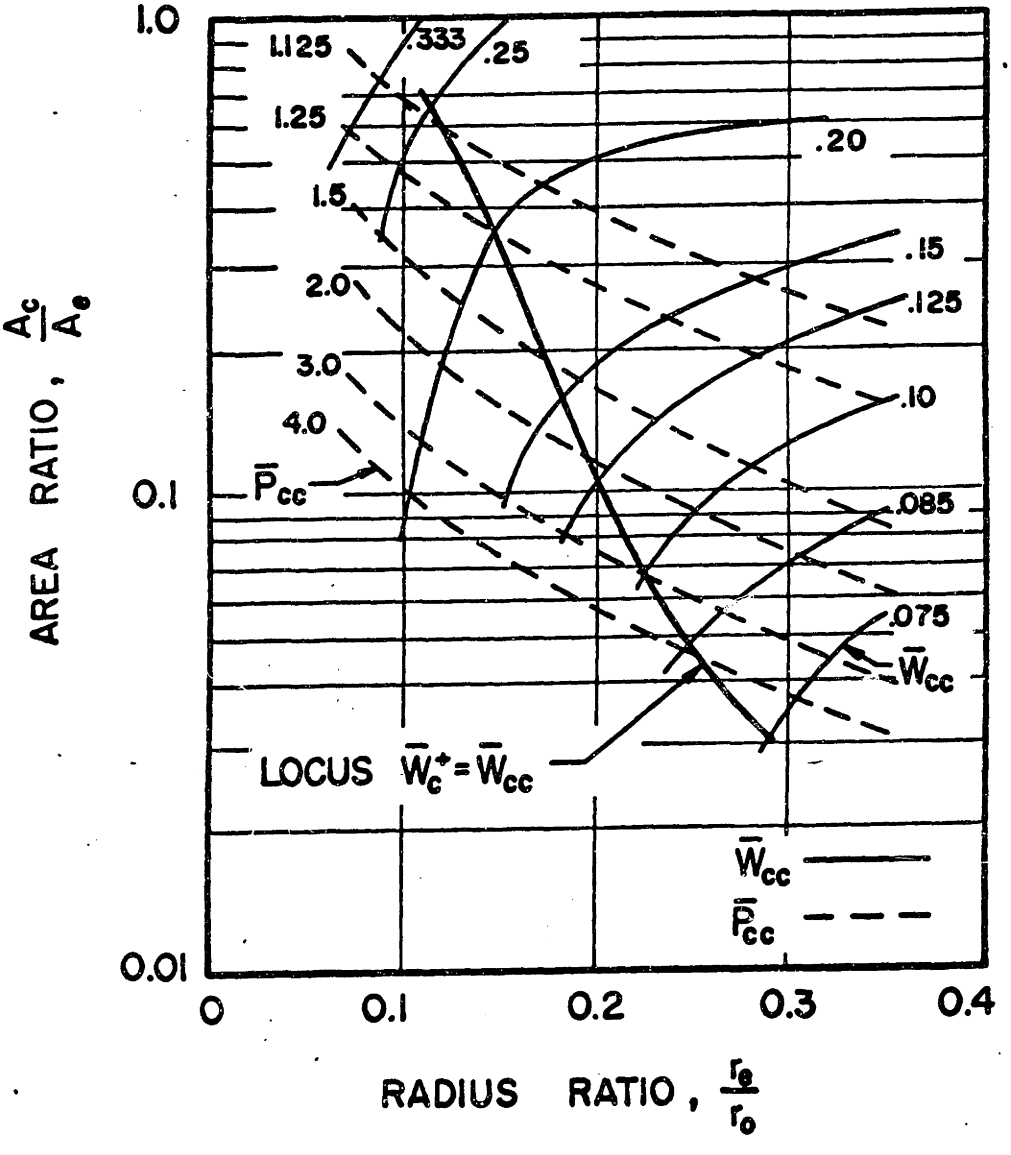

Fig. 5.4. Vortex Valve Cutoff Flow Characteristics.

value of control flow.

5.2.5 The Values of the Valve Critical Dimensions

The work described in the previous sections representing steps 1-4 in the design procedure has resulted in the determination of the values of the nondimensional geometric ratios which are required to meet the input specifications. The values of the valve critical dimensions may be determined from these ratios and from the valve maximum flow requirements. The maximum flow rate through the valve for the case considered in the design procedure has been derived in Chapter 3 as:

$$W_m = C_e A_e \sqrt{2\rho P_s} \tag{5.7}$$

Equation 5.7 may be rewritten to demonstrate that the valve exit area and consequently the exit radius, is uniquely determined by the maximum pressure P_s and flow W_m required at the valve, the operating fluid density ρ and the exit area discharge coefficient C_e:

$$A_e = \frac{W_m}{C_e \sqrt{2\rho P_s}} = \pi r_e^2 \tag{5.8}$$

The values of P_s, W_m and ρ are specified in Step 1. The discharge coefficient in equation 5.8 is in general a function of both valve and exit orifice geometry and the flow conditions. The values of the discharge coefficient for the exit orifice configurations and flow conditions which exist in short vortex valves are not available in the literature. The work described in this investigation for sharp edged orifices of the shape shown in Figure 4.7 indicates that for a

variety of flow conditions and valve geometries, the exit area discharge coefficient lies between 0.7 and 0.8.

With the determination of A_e, and subsequently r_e, from equation 5.8, the values of A_c, A_s, r_o and h are readily determined for the prototype valve:

$$A_c = \left(\frac{A_c}{A_e}\right) \cdot A_e \tag{5.9}$$

$$A_s = \left(\frac{A_s}{A_e}\right) \cdot A_e \tag{5.10}$$

$$r_o = \left(\frac{r_o}{r_e}\right) \cdot r_e \tag{5.11}$$

$$h = \left(\frac{h}{r_e}\right) \cdot r_e \tag{5.12}$$

The final task required in Step 5 is to determine if the maximum flow Reynolds number required in the application is within the bounds:

$$750 < R_w = \frac{W_m}{2\pi r_o \mu} < 3300 \tag{5.13}$$

If the Reynolds number is less than 750 the data of Figure 5.4 in which lines of constant $\bar{W}_{cc}$ and $\bar{P}_{cc}$ are plotted versus the parameters A_c/A_e and r_e/r_o is no longer independent of Reynolds number and the values of $\bar{P}_{cc}$ and $\bar{W}_{cc}$ specified in Figure 5.4 cannot be used to design a prototype valve operating with $R_w < 750$. If the procedure is used to design valves which operate at a maximum flow Reynolds number above 3300, it is not known how successful the procedure would be.

However, as a result of the discussion in Chapter 4, it is anticipated that the procedure is valid for a valve operated at maximum flow Reynolds number approaching 3-4 times the value of 3300.

5.2.6 Sketch of the Prototype Valve Characteristic

As the final step in the design procedure, the characteristic curve for the prototype valve is sketched. Two points on the curve are specified in Step 1, the maximum ($\bar{W}_o = 1.0$, $\bar{W}_c = \bar{P}_c = 0.0$) and the minimum ($\bar{W}_o = \bar{W}_{cc}$, $\bar{W}_c = \bar{W}_{cc}$, $\bar{P}_c = \bar{P}_{cc}$) flow points. The control flow $\bar{W}_c^+$ and pressure $\bar{P}_c^+$ requirements at a third point ($\bar{W}_o = 0.707$, $\bar{W}_c = \bar{W}_c^+$, $\bar{P}_c = \bar{P}_c^+$) may be determined from equations 5.5 and 3.19. It is noted that the values of $\bar{W}_c^+$ and $\bar{P}_c^+$ essentially represent the switching values of control flow and pressure required in a bistable valve to switch the valve from a flow level near maximum flow to a flow level near minimum flow. Using the values of these three points a rough sketch for the prototype valve characteristic may be obtained in terms of either control flow or control pressure. The procedure is illustrated in Section 5.3.

5.2.7 Summary of the Design Procedure

The design procedure outlined in Sections 5.2.1 - 5.2.6 may be summarized as shown in Figure 5.5.

5.3 Design Example

As an example in the use of the design procedure let us consider the design of a vortex valve for a hydraulic system application. The specifications for the application are:

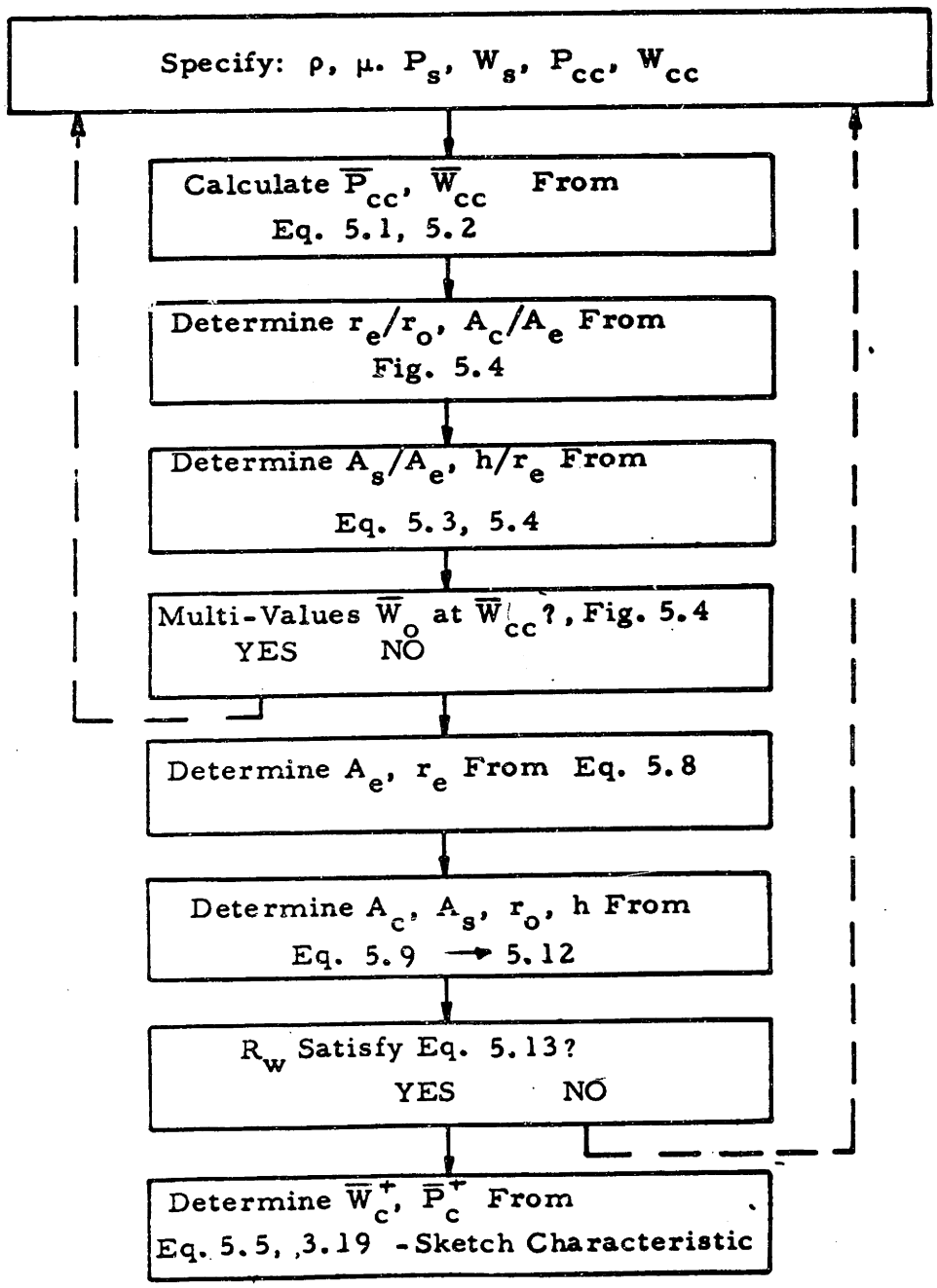

Fig. 5.5. Summary of the Design Procedure.

(1) Operating fluid: MIL - 0 - 5606 hydraulic fluid operating at 200°F: density = 58 lb/ft^3 - viscosity = $3.2 \cdot 10^{-4}$ lb/in.sec.

(2) Maximum available control port pressure 975 psi.

(3) Maximum available supply pressure 600 psi.

(4) Exhaust pressure at valve exit 100 psi.

(5) Flow through valve in maximum flow state must excede 60 in^3/sec.

(6) Flow through valve in minimum flow state must be less than 10 in^3/sec.

The work entailed in the six steps of the design procedure is outlined below:

Step 1

From the data specified for the application, the maximum weight flow is

$$W_m = 2.02 \text{ lb/sec.}$$

and the minimum weight flow is

$$W_{cc} = 0.34 \text{ lb/sec.}$$

The value of the valve supply pressure is

$$P_s = 600 - 100 = 500 \text{ psi.}$$

while the value of the cutoff control pressure is

$$P_{cc} = 975 - 100 = 875 \text{ psi.}$$

where it is recalled that both P_s and P_{cc} are measured relative to valve exhaust pressure.

Step 2

From equations 5.1 and 5.2:

$$\bar{W}_{cc} = \frac{0.34}{2.02} = 0.166 \; ; \quad \bar{P}_{cc} = \frac{875}{500} = 1.75$$

Step 3

The values of A_c/A_e and r_e/r_o required to meet the specifications of Step 2 are determined from Figure 5.4 as:

$$\frac{r_e}{r_o} = 0.175 \; ; \quad \frac{A_c}{A_e} = 0.165$$

The values of A_s/A_e and h/r_e may be determined by satisfying the conditions expressed in equations 5.3 and 5.4

$$\frac{A_s}{A_e} = 3.0 \; ; \quad \frac{h}{r_e} = 2.0$$

Step 4

For the values of $\frac{r_e}{r_o}$ and $\frac{A_c}{A_e}$ specified in Step 3, Figure 5.4 indicates that a single value of total flow will tend to exist at the cutoff value of control flow.

Step 5

From equation 5.8, the value of exit area required to pass the 60 $in^3/sec.$ flow at the valve of supply pressure of 500 psi is determined to be:

$$A_e = \frac{2.02 \cdot 1728}{(.75)\sqrt{2(58)500\ 32.2 \cdot 144}} \text{ in}^2 = 0.024 \text{ in}^2$$

if the exit area discharge coefficient is assumed to be 0.75. The exit radius corresponding to the area is:

$$r_e = 0.087 \text{ in.}$$

and the value of valve critical dimensions are determined from equations 5.9 - 5.12 as:

$$A_c = 0.004 \text{ in}^2 \qquad A_s = 0.072 \text{ in}^2$$

$$r_o = 0.5 \text{ in} \qquad h = 0.174 \text{ in}$$

The value of the valve maximum flow Reynolds number may be calculated from equation 5.13;

$$R_w = \frac{W_m}{2\pi r_o \mu} = \frac{2.02}{2\pi(.5)\ 3.2 \times 10^{-4}} \simeq 2000$$

the value of R_w is within the limits specified in equation 5.14.

Step 6

From equation 5.5 and 3.19 the values of $\bar{W}_c^+$ and $\bar{P}_c^+$ for the values of r_e/r_o and A_c/A_e specified in Step 3 are:

$$\bar{W}_c^+ = 0.13 \qquad \bar{P}_c^+ = 1.65$$

where it has been assumed that $C_e = C_c = 0.75$.

The sketch of the valve characteristic for the application in terms of the volume flows is shown in Figure 5.6.

5.4 The Influence of Vortex Valve Dynamic Behavior on Valve Design

In the preceding sections of this chapter discussion has been

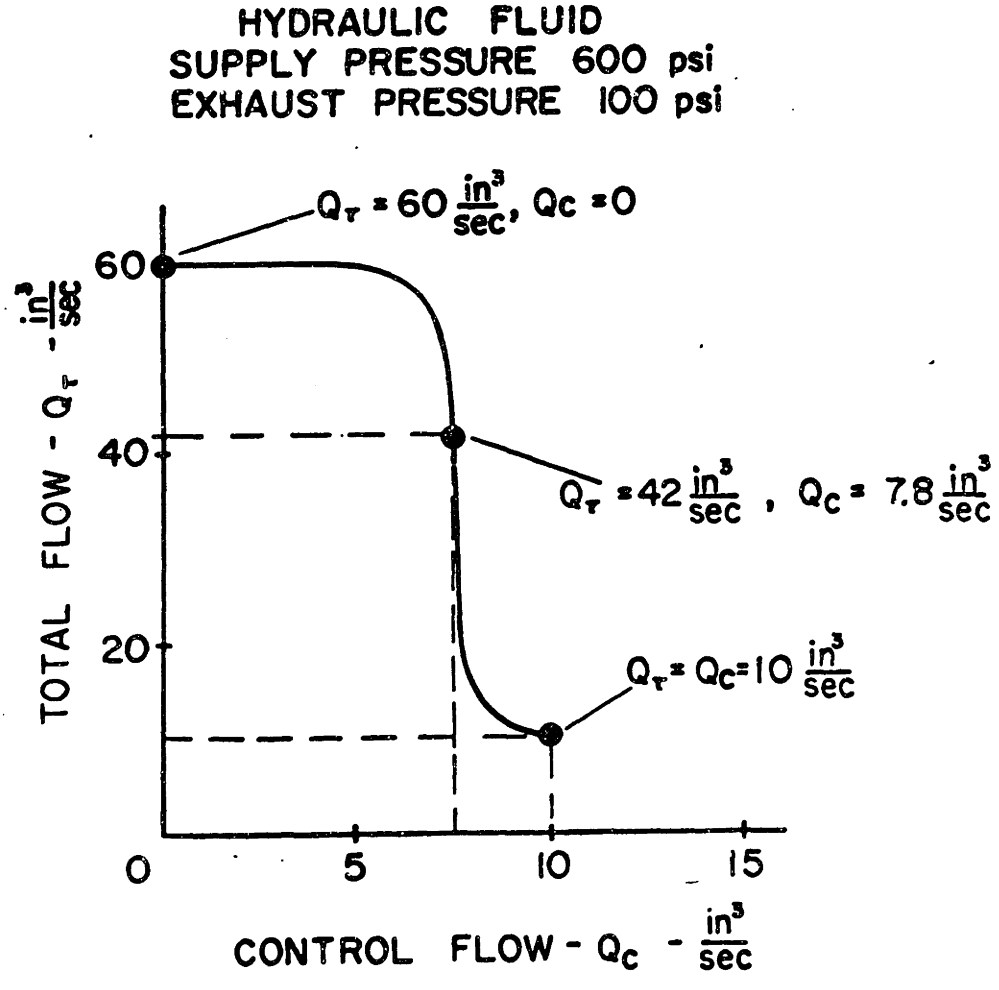

Fig. 5.6. Sketch of Prototype Hydraulic Valve Characteristic.

limited to steady-state valve performance. In many applications the time required for a valve to switch from a given operating point to a new one and even the detailed time history of the response are important factors in valve design. Although no original work is reported in this investigation concerning valve dynamic behavior, References 11, 12, and 13 contain some experimental measurements of valve dynamic behavior.

A.C. Bell has reported (11) that the time required to switch an essentially bistable vortex valve from an operating point near cutoff to one near maximum flow is four valve fill times where the valve fill time T is

$$T = \frac{(r_o^2 - r_e^2)h}{Q_{av}} \tag{5.14}$$

and where Q_{av} is the average volume flow rate through the valve. Bell characterized the detailed time response by modeling it as a pure time delay of delay time equal to T/2 in cascade with a first order lag which has a time constant equal to 1.3T.

L.B. Taplin has reported (12) that frequency response measurements made for small signal responses of vortex valves indicate that the valve response can be modeled as a pure delay with a delay time equal to T/4 cascaded with a first order lag with a time constant of T/4. In other work (13) Taplin has developed a more detailed linearized dynamic model of a vortex valve which includes the effects of both fluid capacitance and inertance in the model.

The work reported in the studies of Bell and Taplin tends to emphasize the differences which result in the value of vortex valve response time depending upon whether the input signal is large or small.

It is noted that the dependence of response time upon input signal level is a common characteristic of nonlinear devices.

The fact that the valve response time is related to the fill time may be interpreted as indicating that the larger the valve annular volume $(r_o^2 - r_e^2)h$ and the smaller the average flow rate through the valve, the longer the response time. In designing a valve to meet the steady-state performance requirements the values of r_o, r_e and Q are usually specified and the only parameter which may be varied to influence the valve response time without significantly influencing the valve steady-state performance is the valve chamber length h. As the value of valve chamber length is decreased, the data of References 11 and 12 indicates that the valve time response becomes faster. In order to obtain a valve with a minimum time response which will meet the steady-state specifications for the application, the valve chamber length should be made as small as possible without adversely affecting the steady-state performance.

5.5 Construction of a Prototype Valve

The design procedure outlined in the preceding sections has been based upon experimental data and upon analytical results which were confirmed with experimental tests. All of these tests were conducted on valve geometries similar to the one of Figure 4.1 in which the valve control and supply port regions consisted of a number of drilled holes. These valves were designed to achieve an axisymmetric flow pattern in the valve main chamber and to allow easy variation of the valve

geometric parameters. In an exploratory effort to determine if the design procedure could be extended to the design of valve configurations which are more easily manufactured than valves of the type photographed in Figure 4.1 and which could be packaged in a modular fashion, a valve was built in which the geometry was essentially planar as shown in Figure 5.7. In the valve construction all machining operations except for the machining of the valve exit were performed with a vertical mill. It is noted that they could also have been performed by etching, molding, or casting. The critical dimensions of the valve which was built are:

$$r_e = 0.087 \text{ in} \qquad r_o = 0.5 \text{ in}$$

$$A_c = 0.004 \text{ in}^2 \qquad A_s = 0.075 \text{ in}^2$$

$$h = 0.063 \text{ in}$$

The dimensions of this planar valve are identical to those of the valve in the design example of Section 5.3 except for the valve chamber height which in the planar valve is 37% of the value specified in the design example. The characteristic of the planar valve was measured by testing the valve on air with a maximum flow rate of 0.0067 lb/sec. and supply pressure of 4.5 psi. These test conditions result in a maximum flow Reynolds number of 2000 which is identical to the Reynolds number specified in the design example. The nondimensional characteristic of the planar valve is presented in Figure 5.8. Also presented in Figure 5.8 is the nondimensional sketch of the predicted characteristic of the prototype valve designed in Section 5.3. The measured

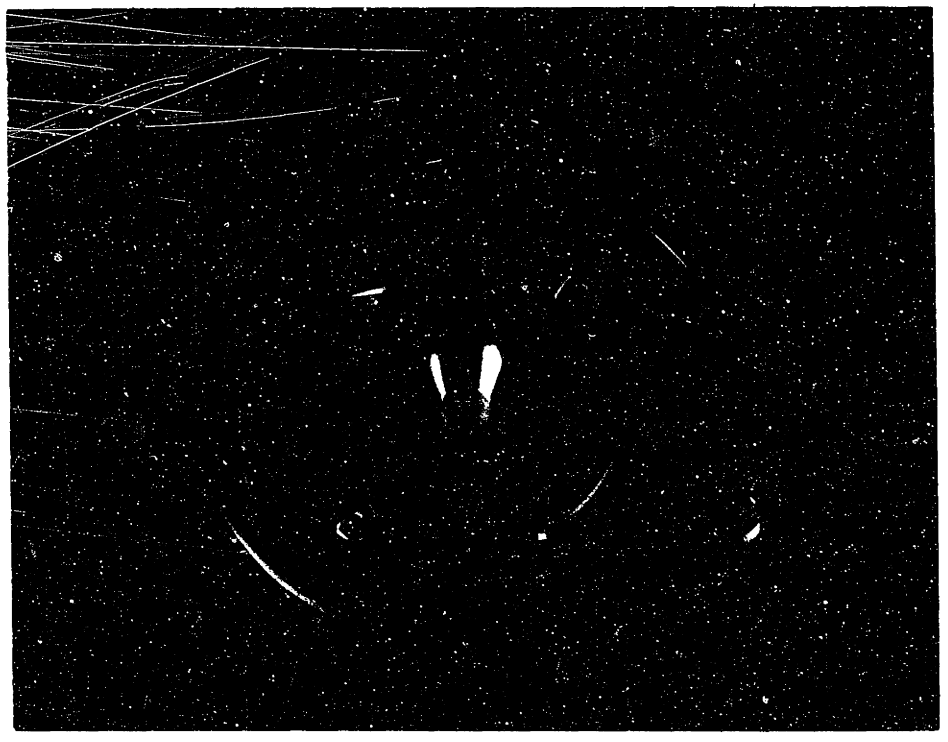

Fig. 5.7 Photograph of the One Inch Chamber Diameter Planar Valve

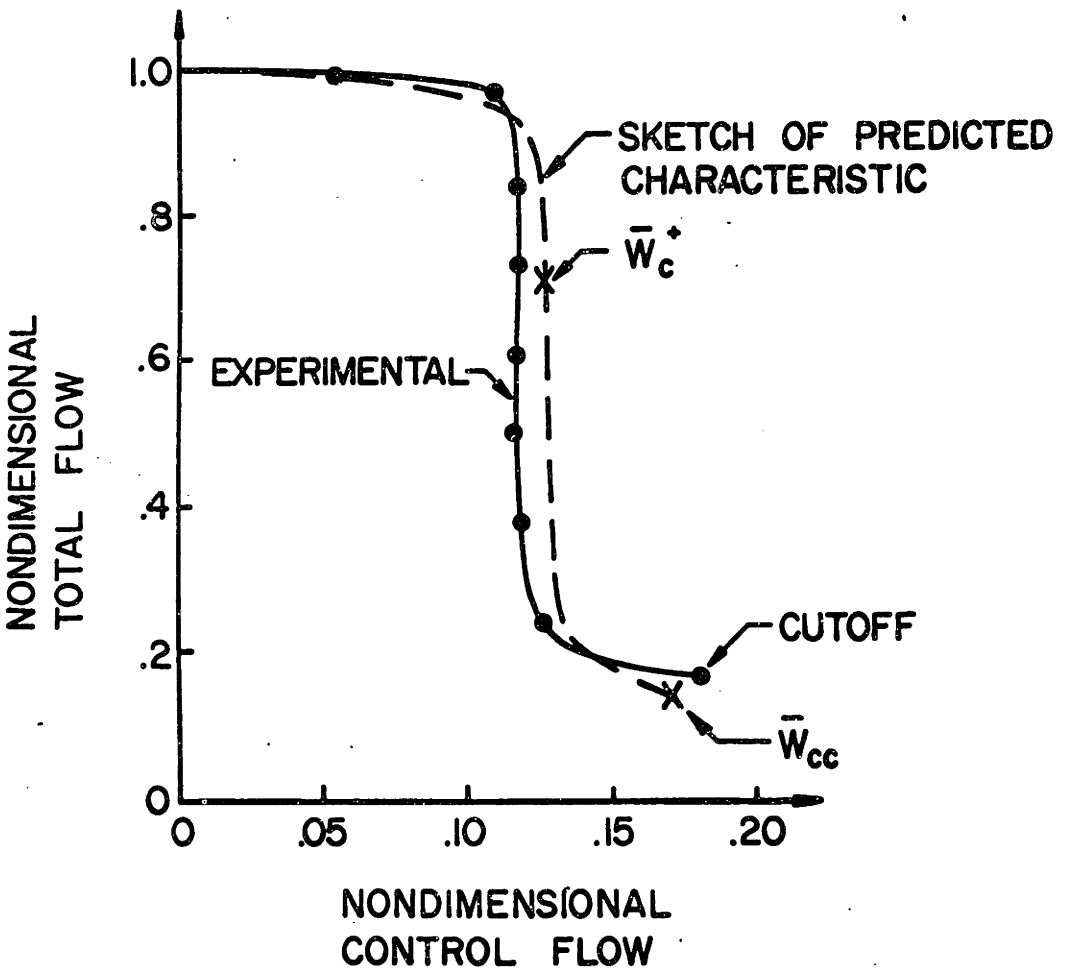

Fig. 5.8. Characteristic of the Planar Valve.

characteristic of the planar valve and the predicted characteristic are very similar. The values of nondimensional control flow required in the planar valve at cutoff and at 70.7% of maximum flow are within 10% of the values specified in the design procedure. As a result of the construction and testing of the planar valve, it has been found that the design procedure can be used successfully to design vortex valves whose inlet port geometries are not similar to those of the valve shown in Figure 4.1. A valve designer then has some flexibility in the detailed design and placement of the valve inlet ports so that a particular valve geometry may be tailored to meet specific manufacturing and packaging requirements. It is noted, however, that some care must be used in inlet port design in order to achieve an axisymmetric flow pattern in the valve main chamber.

As a second result of the tests conducted on the planar valve, it has been found that the valve chamber length can be reduced to a value of 0.74 r_e, which is 37% of the value specified in the design procedure, without significantly influencing the valve steady-state characteristic. In applications in which valve response time is an important consideration in valve design, it is possible to reduce the valve chamber length to a value approaching .75 r_e and decrease valve response time without strongly influencing the valve steady-state performance characteristics.

5.6 The Vortex Valve as a Circuit Component

In the preceding sections of this chapter, the vortex valve has been represented by a characteristic plot of total flow versus control flow for the valve operating at constant supply and exhaust pressures. In fluid circuits vortex valves are rarely operated under conditions in which both the supply and exhaust pressures are held constant. For example, consider the bridge circuits in Figure 5.9 in which none of the valves operate at both constant supply and exhaust pressures. In designing vortex valve circuitry containing valves that operate under varying supply or exhaust port pressures such as shown in Figure 5.9, it is convenient to use plots of the valve supply port input impedance and exit port output impedance. The supply port input impedance is represented as a plot of supply flow versus supply pressure for selected values of control flow and constant exhaust pressure, while the exit port output impedance is represented as a plot of valve exit flow versus exhaust pressure for selected values of control flow with valve supply pressure held constant. For the incompressible flow case considered in this investigation both of these representations of vortex valve characteristics may be derived from the single nondimensional vortex valve characteristic measured at constant supply and exhaust pressure for the range of supply and exhaust pressures in which the nondimensional valve characteristic is maximum flow Reynolds number independent. As an example in this derivation, the inlet and outlet impedances for the valve designed to operate in the hydraulic

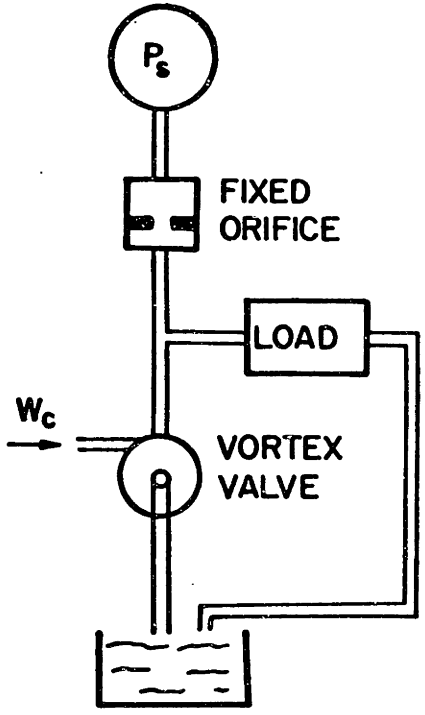

CIRCUIT A
HALF BRIDGE — FIXED UPSTREAM VARIABLE DOWNSTREAM ORIFICE

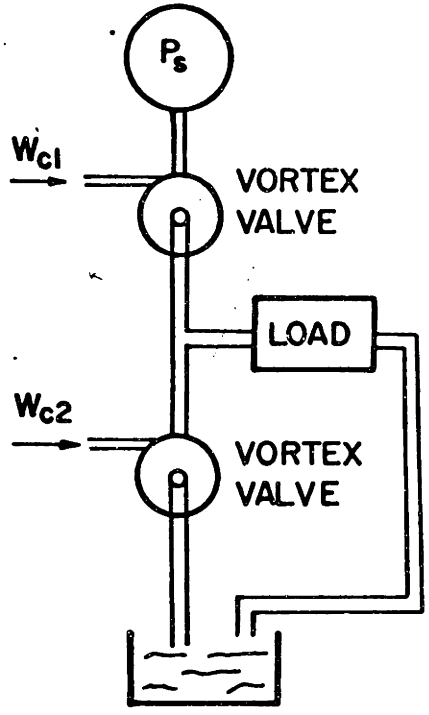

CIRCUIT B
HALF BRIDGE — TWO VARIABLE ARMS

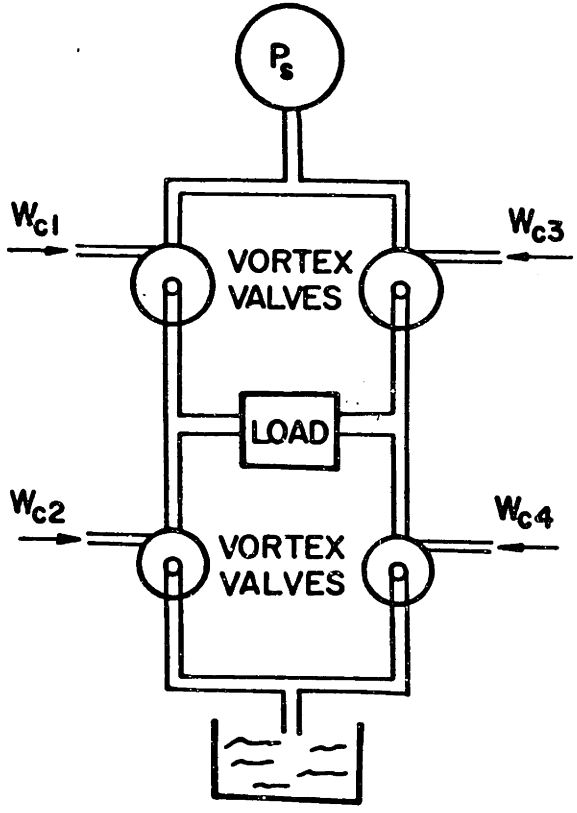

CIRCUIT C
FULL BRIDGE — FOUR VARIABLE ARMS

Fig. 5.9. Vortex Valve Bridge Circuits.

system application of Section 5.3 are derived.

The first step in the derivation is illustrated in Figure 5.10 in which a family of dimensional plots of total flow versus control flow is obtained for selected values of $P_s = P_{sg} - P_{dg}$* from the single nondimensional valve characteristic. The family of curves has been constructed for values of P_s from 125 psi to 1000 psi. These values of supply pressure are within the range in which the nondimensional valve characteristic is supply pressure or maximum flow Reynolds number independent.

The supply port input impedance may be determined directly from the family of curves in Figure 5.10 by the graphical method illustrated in Figure 5.11. The resultant plot of supply port input impedance is presented in Figure 5.12 in which it is noted that the curve for $Q_c = 0$ is simply the pressure flow relationship of the valve exit orifice under zero control flow. Each of the curves for finite values of Q_c in Figure 5.12 contain a given supply pressure at which a step-wise increase in valve supply flow of almost a factor of 5 occurs. It is noted that curves at finite values of Q_c are not plotted for negative values of Q_s which represent flow out of the valve supply port into the supply line. The region of valve operation for negative supply flow is not considered in this section.

The valve exit port output impedance may be determined from

---

* P_{sg} = gage supply pressure
  P_{dg} = gage exhaust pressure

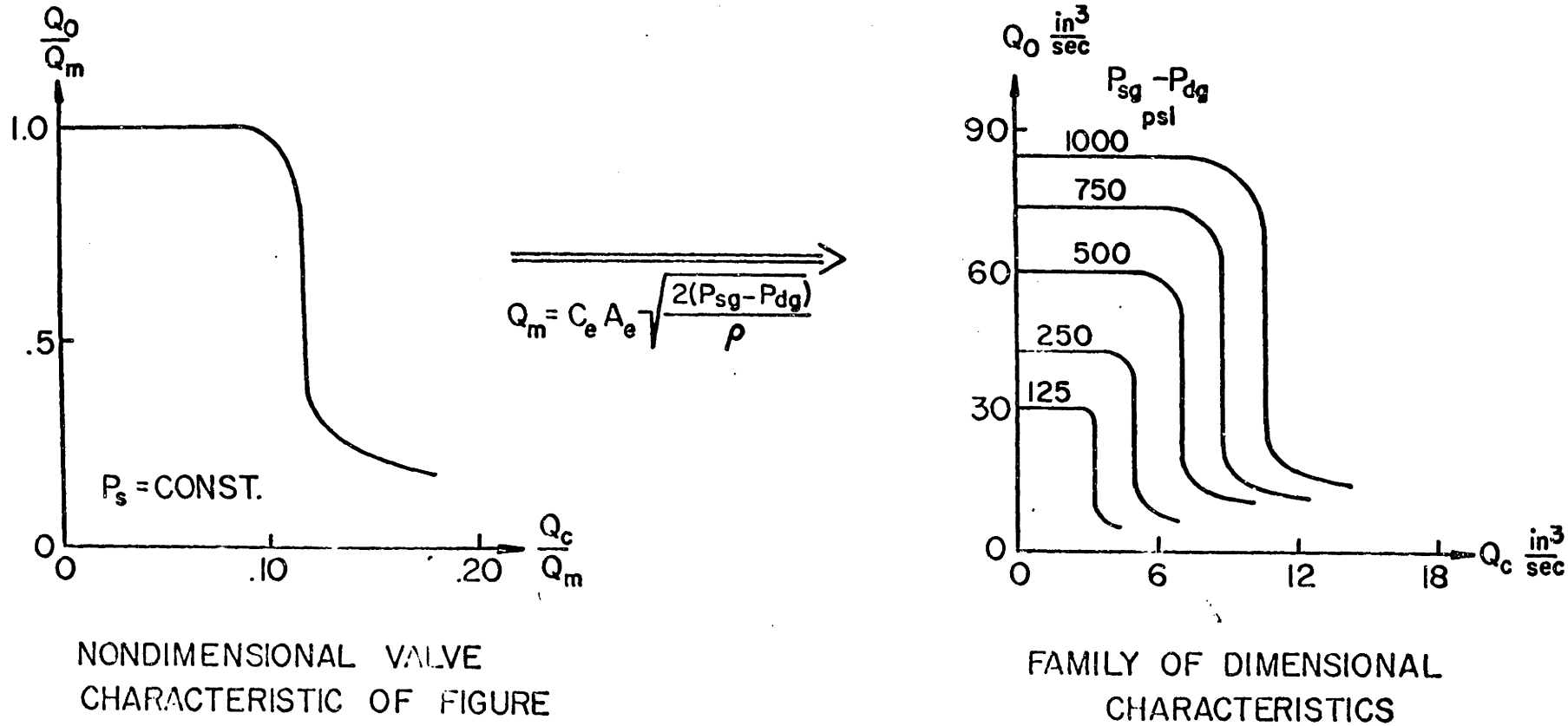

NONDIMENSIONAL VALVE CHARACTERISTIC OF FIGURE

FAMILY OF DIMENSIONAL CHARACTERISTICS

Fig. 5.10. Determination of the Family Valve Characteristics.

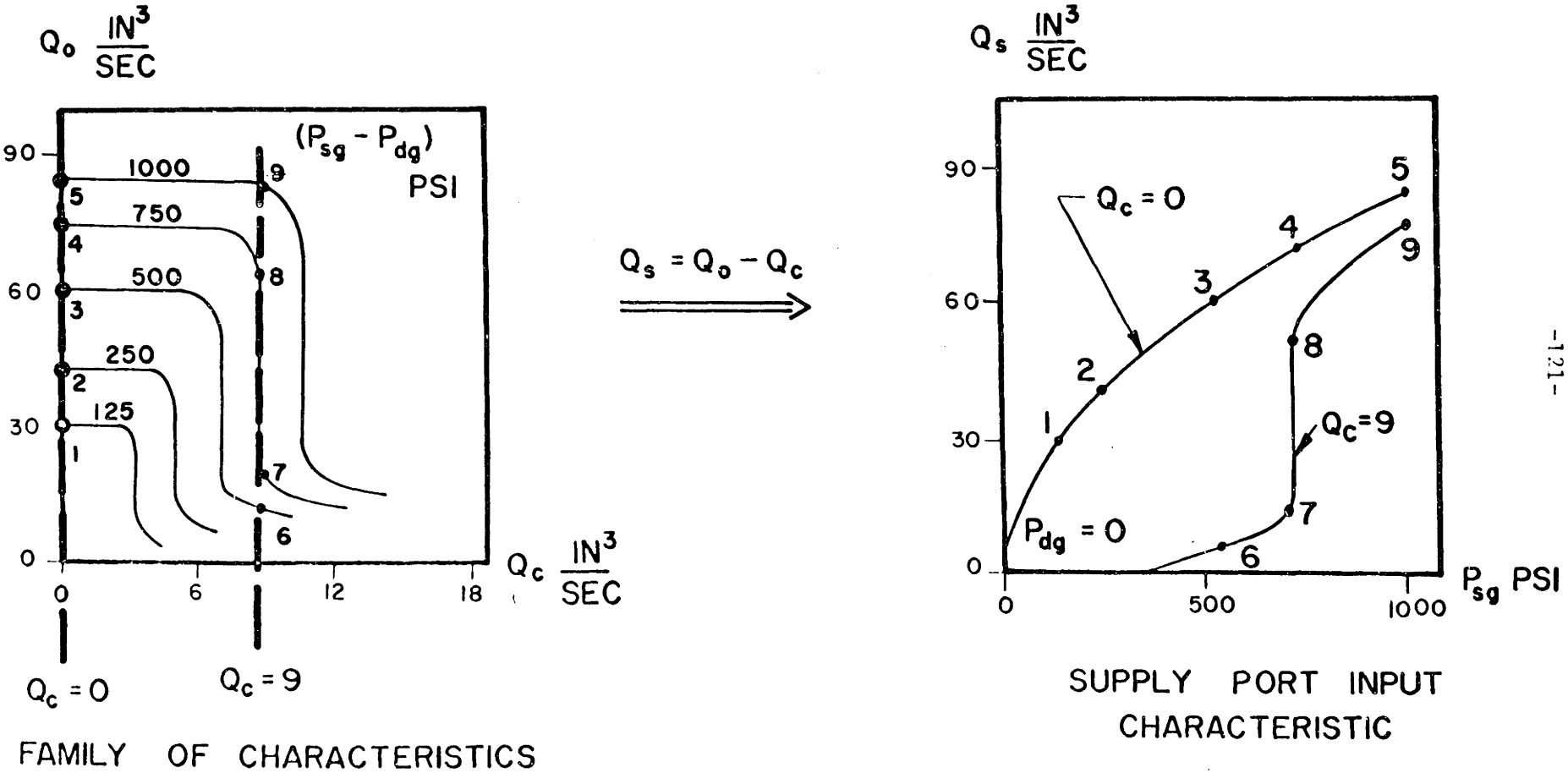

Fig. 5.11. Derviation of Supply Port Input Characteristics.

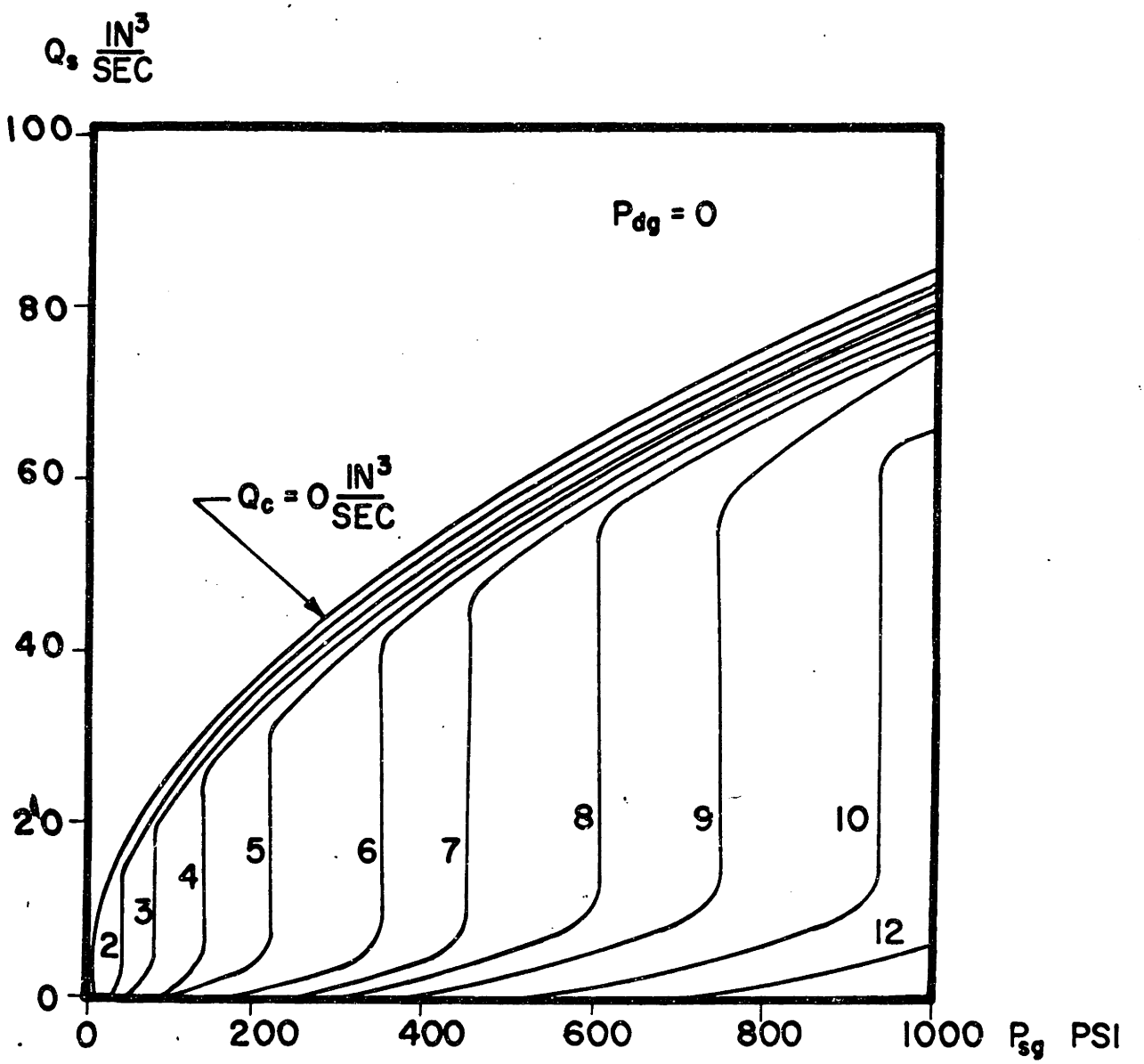

Fig. 5.12. The Supply Port Input Characteristics.

the family of curves in Figure 5.10 as illustrated in Figure 5.13. In the resultant plot of exit port impedance presented in Figure 5.14, it is noted that the curve of $Q_c = 0$ represents the pressure flow characteristic of the valve exit orifice under the condition of zero control flow. It is also noted that each of the curves of exit flow plotted for finite values of Q_c decrease in a step-wise manner by a factor of almost five at a given value of exhaust pressure. The curves for each value of Q_c are defined only for exit flows greater than or equal to the control flow since negative supply flows are not considered.

The plots of valve input and output impedance may be used with standard graphical circuit design techniques such as described in Reference 14 to determine the characteristics of circuits containing vortex valves which operate under varying supply and exhaust pressures. To provide an example in the use of these techniques, the characteristics of circuit A the half bridge circuit consisting of a fixed upstream orifice and a vortex valve are derived. The derivation is illustrated graphically in Figure 5.15 in which the characteristic of a fixed orifice whose area is half the area of the valve exit orifice has been superimposed upon the valve supply port input impedance characteristics. The resultant plot of the load pressure and flow as a function of valve control flow is presented in Figure 5.16. The circuit characteristics of Figure 5.16 indicate that for a given value of valve control flow the load pressure is constant over a range of load flows. The circuit then acts over some

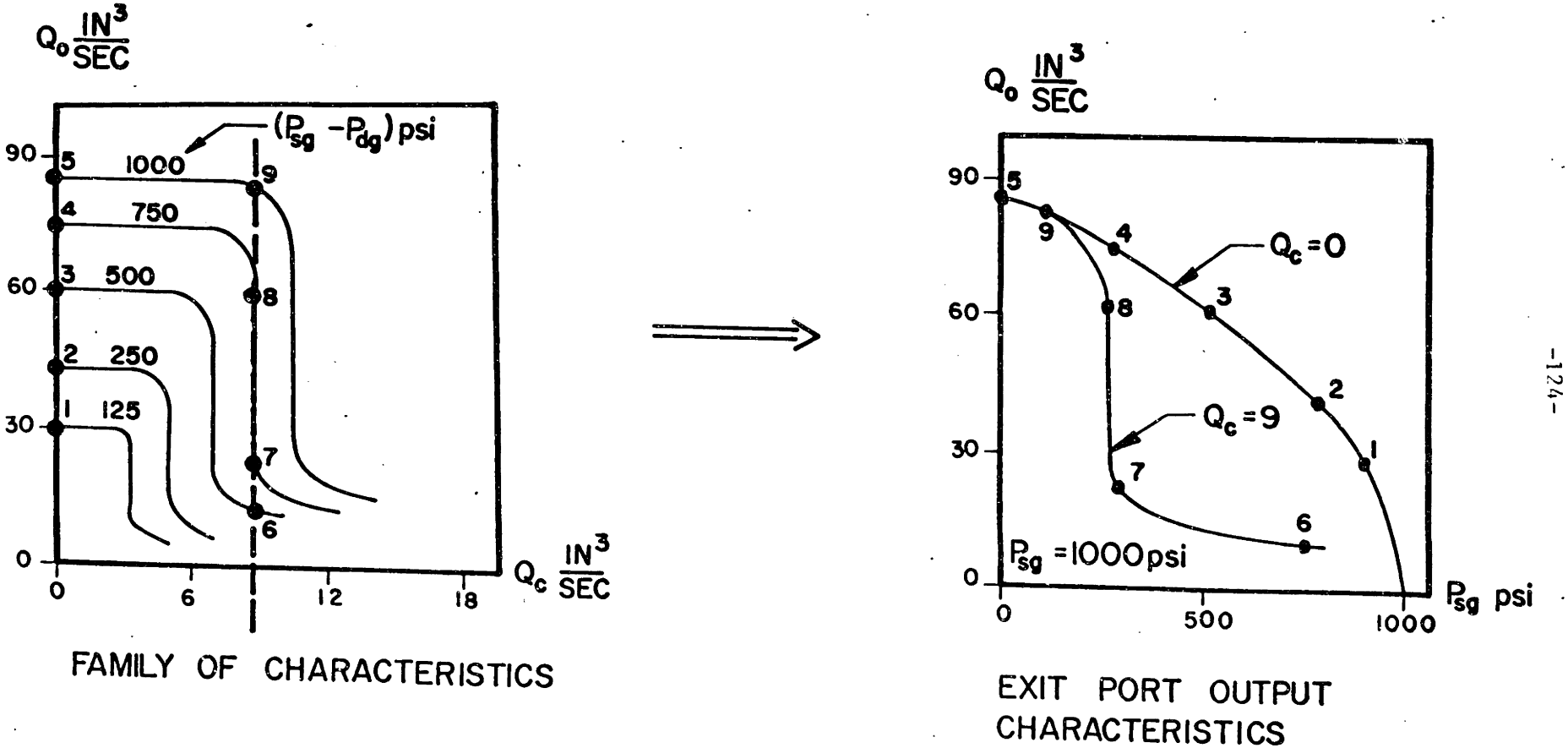

Fig. 5.13. Derivation of Exit Port Output Characteristics.

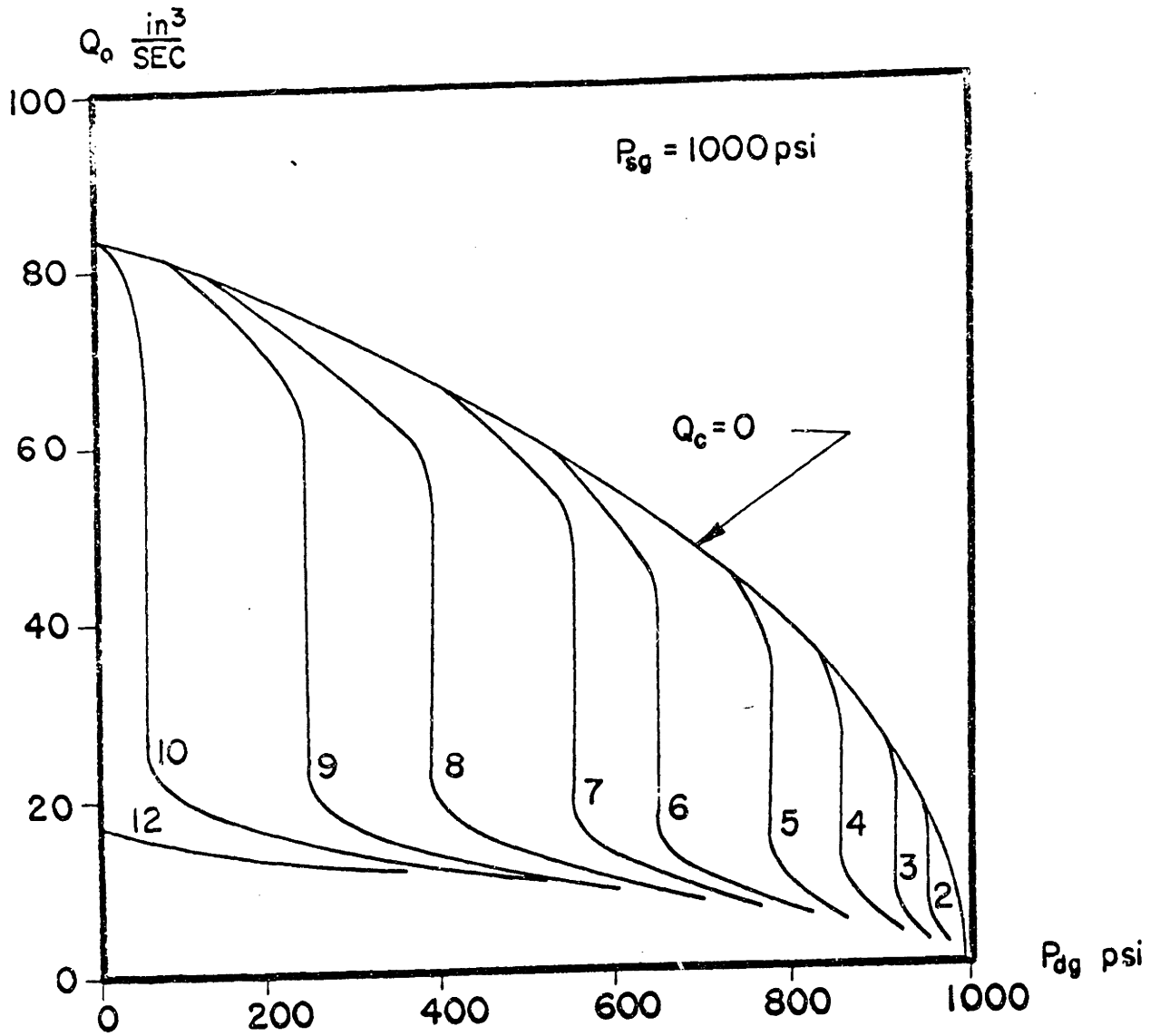

Fig. 5.14. The Exit Port Output Characteristics.

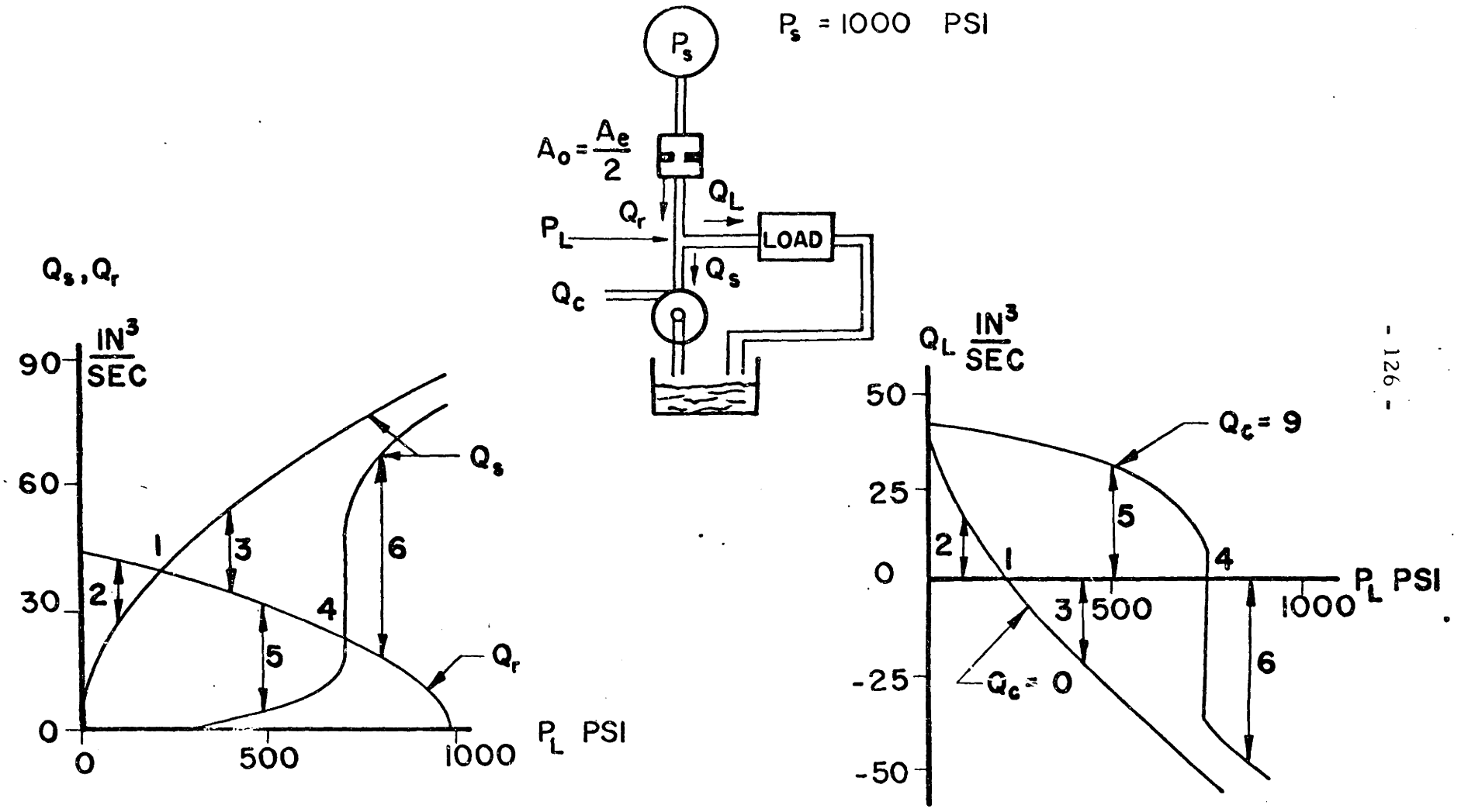

Fig. 5.15. Derivation of Half Bridge Characteristics.

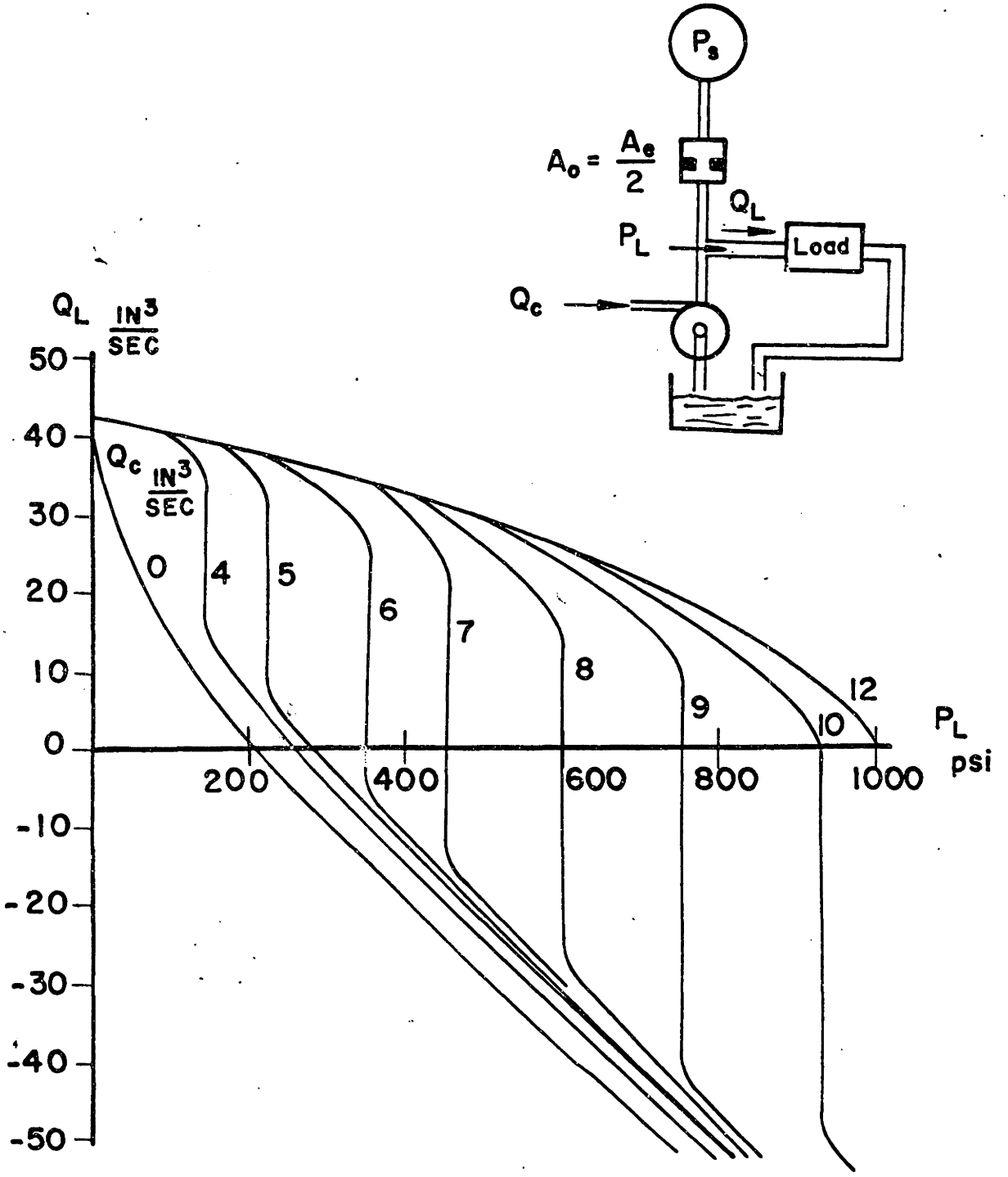

Fig. 5.16. The Half Bridge Circuit Characteristics.

regions of operation as a constant load pressure source in which the value of load pressure may be selected by setting the value of control flow.

It is noted that if valve control port pressure rather than control flow were considered as the input to the vortex valve, a procedure analogous to the one described above could be used to determine circuit behavior starting from a single nondimensional valve characteristic plot of total flow versus control pressure, rathen than total flow versus control flow.

PART III

STUDIES OF THE FLOW FIELD IN THE VORTEX CHAMBER

CHAPTER 6

EXPERIMENTAL STUDIES OF THE FLOW FIELD IN SHORT VORTEX CHAMBERS

6.1 Introduction

The experimental studies described in the preceding chapters of this thesis have been limited mainly to measurements made at the valve ports and have not been concerned with the flow field inside the valve main chamber. In order to gain a more complete understanding of valve behavior it is necessary to study in some detail the flow field in the valve. In this chapter results of experimental studies are reported in which the valve chamber flow field was investigated by flow visualization techniques and by measuring the static end wall pressure distribution across the vortex chamber. These studies have served as a basis for the analytical model of the vortex chamber flow field formulated in Chapter 7.

A number of previous experimental studies have been conducted on vortex chambers. Many of these studies (26, 32, 33, 34, 35) have been concerned with long vortex chambers in which $\frac{h}{r_o} > 1$, while other studies (19, 27, 28, 37, 38) have been concerned with short vortex chambers, $\frac{h}{r_o} < 1$ which are of interest in this investigation. The most detailed study has been completed by Savino and Keshock (28) who measured the radial and tangential velocity distribution in a short vortex chamber ($\frac{h}{r_o} = 0.17$) for one flow condition in which the ratio of tangential to radial velocity at the chamber outer wall was about 15. The data of Savino and Keshock is discussed in further detail in

Chapter 7. While the present study has not studied the vortex flow field in such painstaking detail as Savino and Keshock, it has attempted to provide limited data regarding the flow field for a broad range of flow conditions.

6.2 Flow Visualization Studies

A series of flow visualization studies were conducted with the seven inch vortex valve which was fitted with a plexiglass top plate to allow visualization of the flow. In these studies the valve was operated on water. Two means were used to visualize the flow in the chamber. A steady stream of air bubbles were injected into the flow at the outer periphery of the valve near the valve top plate. The bubbles proceeded through the chamber traveling along the top plate. The second means of visualizing the flow was to inject a given quantity of reconstituted powdered milk at the chamber outer periphery near the chamber midplane region and observe the resulting redistribution of the milk in the chamber.

The pertinent geometric parameters for the valve configuration used in the test series were:

$r_o = 3.5$ in. $\qquad r_e = 0.707$ in.

$h = 1.75$ in. $\qquad A_c = 0.095$ in^2

$A_s = 3.73$ in^2

A photograph of the test valve assembly is shown in Figure 6.1 while the characteristic of the test valve is shown in Figure 6.2. The points on the characteristic which represent the conditions for which flow visualization photographs were taken are also indicated in the Figure; at each of these points on the

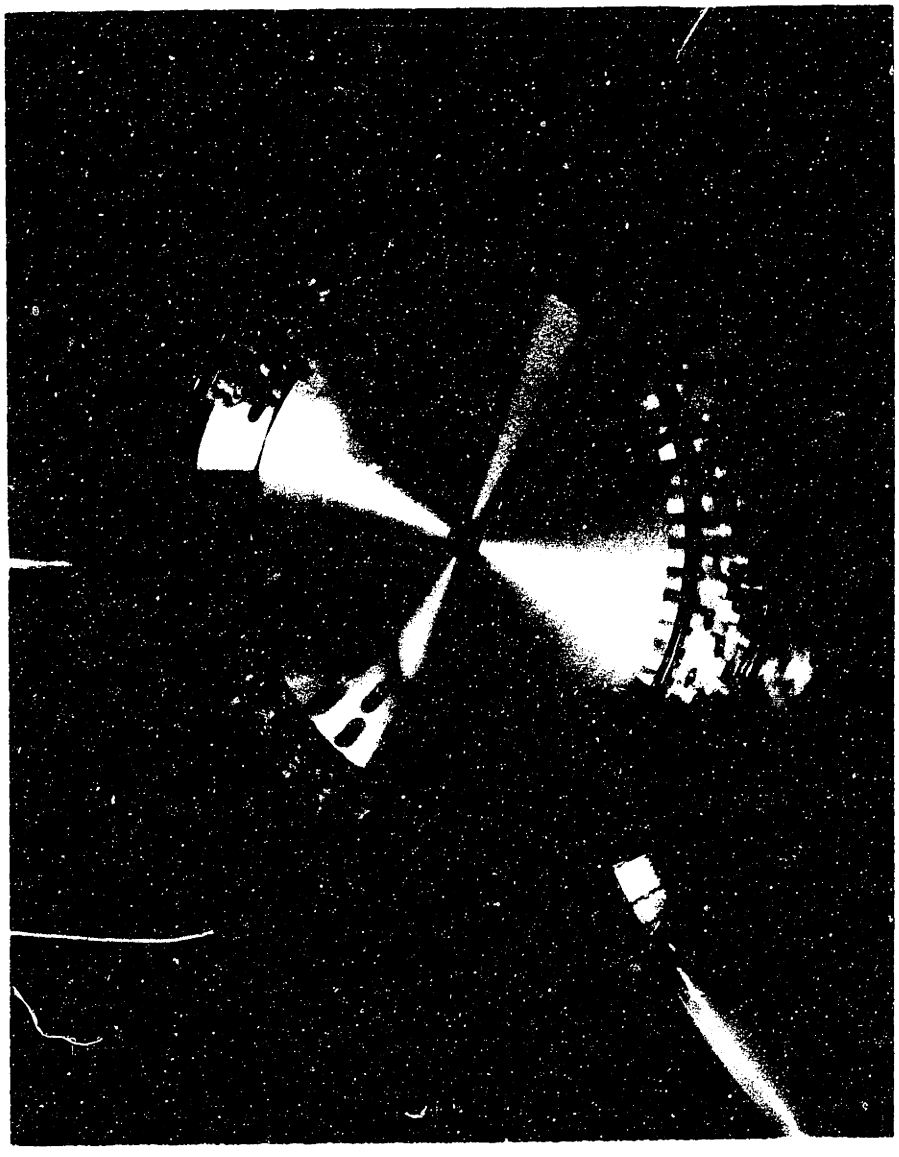

Fig. 6.1 Photograph of the Seven Inch Chamber Diameter Valve

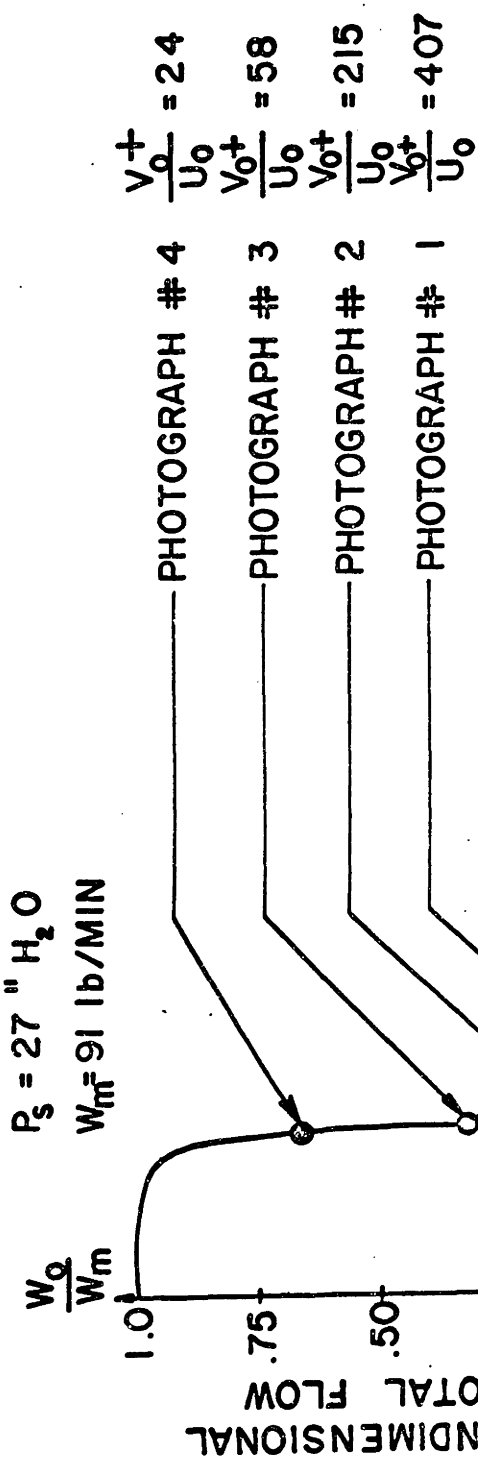

Fig. 6.2. Flow Conditions for the Flow Visualization Photographs.

characteristic, the ideal ratio of the tangential to radial velocity, $\frac{v_o^+}{u_o}$, at the chamber outer periphery is indicated. The ratio $\frac{v_o^+}{u_o}$ was calculated from the measured supply and control flow rates using equations 3.3 and 3.4 from Chapter 3 which indicated that under ideal conditions, i.e. lossless mixing, the ideal ratio of $\frac{v_o}{u_o}$ is:

$$\left.\frac{v_o}{u_o}\right|_{ideal} = \frac{v_o^+}{u_o} = \frac{A_c \quad \bar{W}_c^{\,2}}{2\pi r_o h \quad \bar{W}_o^{\,2}} \tag{6.1}$$

It is noted that the ideal ratio of $\frac{v_o}{u_o}$ may differ considerably from the actual ratio achieved in a vortex chamber, as demonstrated in section 6.4 of this chapter.

The results of the flow visualization study are presented in the photographs of Figures 6.3, 6.4, 6.5, and 6.6. Let us first consider the photograph in Figure 6.3. This photograph was taken for flow conditions in which the valve was operating at cutoff with $\frac{v_o^+}{u_o} = 407$. The spiral path traced out by the air bubbles traveling along the valve top plate is clearly visible. The air bubbles give some indication of the flow field in the top plate boundary layer but not an exact indication because their density is so different from the operating fluid density and because they are large enough so that they extend across a region of flow in which a large axial velocity gradient exists. The bubble streaks do serve as a convenient visual reference of the relative swirl strengths in the chamber which correspond to various inlet conditions. The relative magnitudes of $\frac{v_o^+}{u_o}$ for the various inlet flow conditions represented in each of the photographs are reflected in the bubble streaks visible in the photographs. It is noted that

Fig. 6.3 Flow Visualization Photograph No. 1, $\frac{v_o^+}{u_o} = 407$

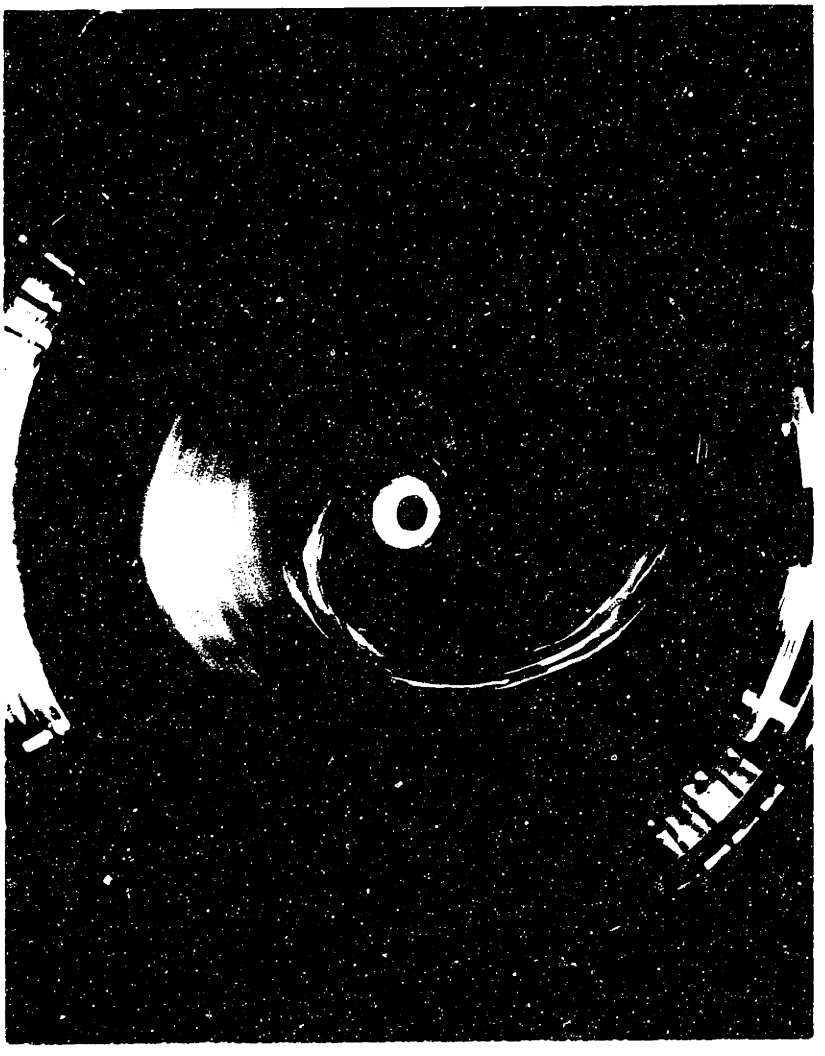

Fig. 6.4 Flow Visualization Photograph No. 2, $\frac{v_o^+}{u_o} = 215$

Fig. 6.5 Flow Visualization Photograph No. 3, $\frac{v_o^+}{u_o} = 58$

Fig. 6.6 Flow Visualization Photograph No. 4, $\frac{v_o^+}{u_o} = 24$

as the ratio of $\frac{v_o^+}{u_o}$ is decreased the length of the spiral path and total included angle of the path change noticeably.

Qualitative information about the flow in the midplane region of the chamber is provided by the milk injection visualization. When a sufficient quantity of powdered milk was injected into the chamber at the chamber outer perifery near the midplane region, the milk would completely fill the chamber, and after a time period of about 5-10 chamber fill times (chamber fill time ≈ chamber volume divided by volume flow rate) the complete chamber was milky in appearance. After another short period of time which lasted from 5-20 chamber fill times, the milk would no longer fill the chamber and a region near the outer wall and near the valve exit would appear clear and be free from milk. After these regions became clear, a "milky donut" of fluid remained in the chamber as shown in Figure 6.3. (The dark portions of the photograph represent clear fluid while the light portions represent milky regions.) The donut would remain as represented in the photograph for a period of time which in many cases exceeded 100 chamber fill times. The long life of the milky donut indicates that essentially no radial flow passes through the region of the chamber filled by the donut to clear the region of milky fluid. All of the radial flow passing through the chamber in this region must be contained in the end wall boundary layers leaving a sizable portion of the chamber near the chamber midplane region with no radial flow. The alternate clear and milky rings of fluid within the donut were observed to exist in an essentially stable pattern for the life of the donut. These rings suggest that a nested series of

axial cells exist within the milky donut of fluid in which a small but finite axial velocity exists. An interpretation of the flow pattern which was observed is sketched in Figure 6.7 in which the "radial" flow stream lines are sketched for a cross section of the chamber.

In the flow visualization photographs of Figures 6.4 and 6.5 for $\frac{v_o^+}{u_o} = 215$ and $\frac{v_o^+}{u_o} = 58$, flow patterns similar to the one described above were observed. These photographs also represent pictures of the spinning donut of milky fluid which existed in a stable form for time periods on the order of 100 chamber fill times. The nested series of alternate cells of clear and milky fluid which exist within the donut are also clearly visible in these photographs. It is instructive to note by comparing the photographs of Figures 6.3, 6.4 and 6.5 that the extent of the chamber occupied by the spinning donut of fluid decreases as the ratio of $\frac{v_o^+}{u_o}$ decreases. At a ratio of $\frac{v_o^+}{u_o} = 407$, the donut fills the chamber to a radius of about 0.68 r_o while for $\frac{v_o^+}{u_o} = 215$ the donut fills the chamber to a radius of about 0.61 r_o and for $\frac{v_o^+}{u_o} = 58$, the donut fills the chamber to a radius of about 0.39 r_o. As the ratio of $\frac{v_o}{u_o}$ is decreased, radial flow penetrates further into the chamber in the region near the chamber midplane and the spinning donut of fluid occupies less of the chamber.

In the flow condition corresponding to the photograph of Figure 6.6, $\frac{v_o^+}{u_o} = 24$, a spinning donut of fluid was not observed to exist in the chamber. After milk was injected into the chamber, the complete chamber became milky in appearance and then after a relatively short period of time, 10-20 chamber fill times, the entire

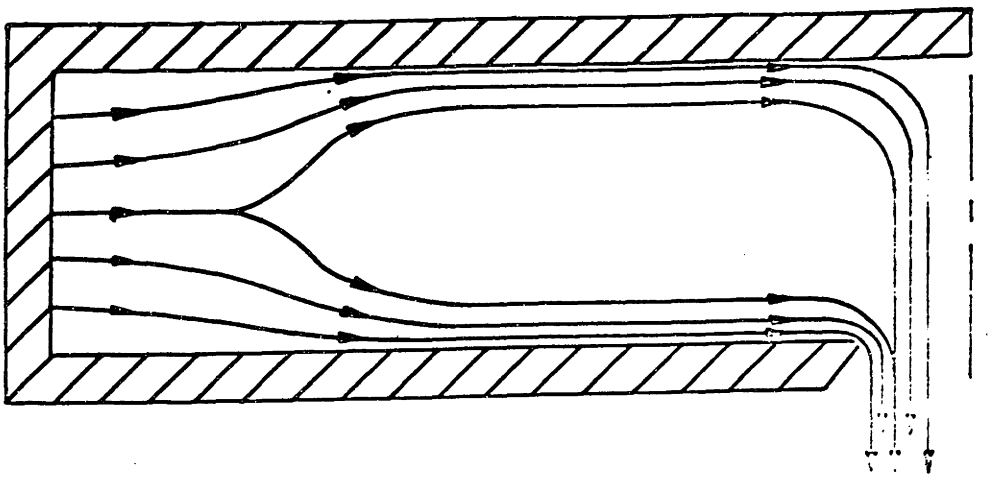

RADIAL STREAMLINES $\frac{V_o+}{U_o} = 407$

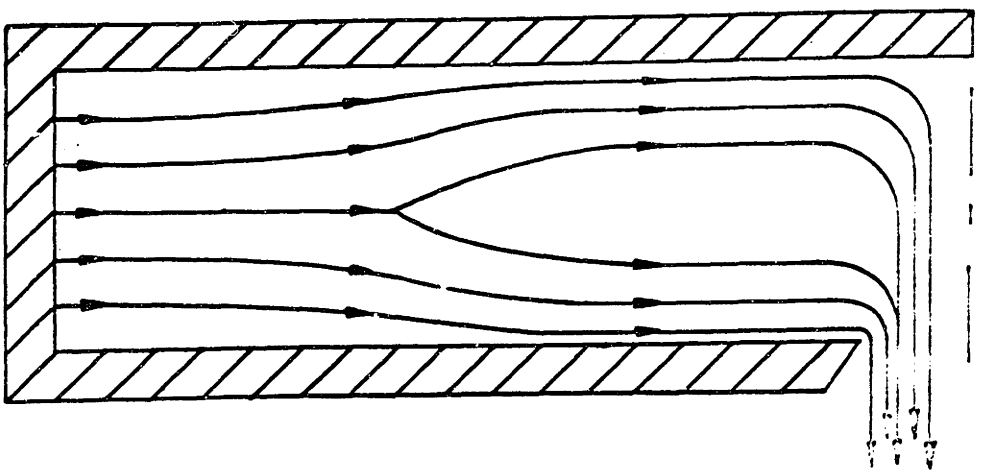

RADIAL STREAMLINES $\frac{V_o+}{U_o} = 58$

Fig 6.7. Intrepretation of the Flow Visualization Photographs.

chamber would simply be clear again. At this low value of $\frac{v_o^+}{u_o} = 24$ sufficient radial flow exists in all regions of the chamber to carry the milk away.

As a result of the flow visualization studies, a "picture" of the flow patterns which exist in the vortex valve at various operating points on a valve characteristic has been obtained. At very low values of $\frac{v_o}{u_o}$, the flow procedes from the outer periphery of the chamber to the inlet with radial flow existing at all axial positions in the valve. As the value of $\frac{v_o}{u_o}$ is increased, a major fraction of the flow passing through the chamber is drawn into the end wall boundary layers. At sufficiently high values of $\frac{v_o}{u_o}$, at some point in the chamber all the radial flow is contained in the end wall boundary layers and the radial velocity in the midplane region of the chamber is essentially zero. As $\frac{v_o}{u_o}$ is further increased, the radial flow is drawn into the chamber boundary layers at a larger radius and a spinning donut of fluid through which no radial flow passes fills a significant portion of the chamber near the chamber midplane region. At very high values of $\frac{v_o}{u_o}$ as represented by Figure 6.3, the spinning donut may extend to a radius approaching 70% of the chamber radius. The "picture" described above of the flow in the vortex chamber under varying flow conditions is used as a basis for the analytical study of the flow field in the vortex chamber outlined in Chapter 7.

6.3 End Wall Static Pressure Distributions

As a part of the experimental investigation, end wall static pressure distributions were measured for several flow conditions in a short vortex chamber with the experimental apparatus shown in

Figure 6.8 operating on air. The apparatus consists of a top plate, a bottom plate and two concentric rings -- a retaining ring and a chamber inlet ring. The chamber inlet ring contains a total of thirty-six 0.125 inch diameter holes drilled tangent to the inside of the ring which is seven inches in diameter. The tangential holes are arranged in 9 groups of 4 holes each, with each group evenly spaced at 40° around the ring. Within each group of 4 holes, each hole is evenly spaced with respect to its neighboring holes so that the holes are evenly spaced over the chamber height which is 1.0 inches. The flow conditions in the chamber may be altered by changing the total inlet hole area which may be accomplished either by selectively plugging a few of the inlet holes or by inserting stainless steel needle tubing into the holes. The ten inch retaining ring forms a plenum with the inlet ring and top and bottom plates into which the apparatus supply flow is injected. The plenum provides a means of maintaining a uniform supply pressure for each of the tangential inlet holes. The bottom plate of the apparatus contains the chamber exit orifice. Several bottom plates with different exit areas were used with the apparatus. In each of the bottom plates the shape of the exit orifice is similar to the orifice sketched in Figure 4.7. Two top plates were used with the apparatus; one contained an exit orifice to allow investigation of dual exit chambers; the other contained no exit. The top plate with no exit contained twenty-nine 0.025 inch diameter pressure taps evenly spaced at 0.125 inch intervals all in a line along a chamber radius. The innermost tap was placed at the center of the top plate, while the outermost tap was

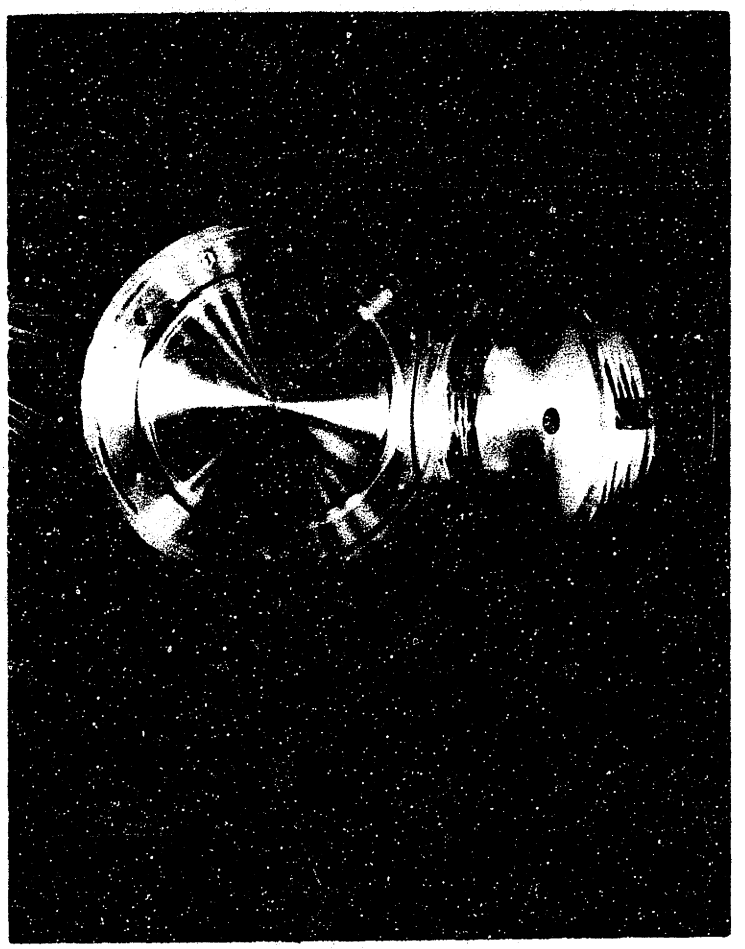

Fig. 6.8 Photograph of the Pressure Profile Test Apparatus

placed at a radius of 3.5 inches. A second series of twenty 0.025 inch diameter taps were placed at 5° intervals in two constant radius arcs; 10 at a radius of 3.375 inches and 10 at a radius of 2.625 inches. This series of pressure taps was used to determine the variation of end wall static pressure along an arc of constant radius around the chamber for an arc length which extended between two of the nine inlet port regions. The top plate with the 0.5 inch diameter exit orifice contained 26 pressure taps evenly spaced at 0.125 inch intervals all in a line along a radius of the valve. The outermost pressure tap in the line of pressure taps was located at a radius of 3.5 inches while the innermost pressure tap was located at a radius of 0.325 inches. The pressure at each of the taps was measured with the aid of a 50 tube water manometer board.

The experimental procedure for the test series consisted in setting up the apparatus with a given exit orifice and a given inlet area, setting the flow rate of air to the apparatus and recording the pressure distribution from the manometer board. The flow rate to the apparatus was measured with the critical orifice set described in Chapter 4. For the complete test series the chamber was operated exhausting to atmosphere. By changing the inlet flow area in the apparatus the inlet flow conditions were altered. The ideal ratio of the tangential to radial velocity at the outer periphery of the chamber may be derived from equation 6.1 by noting in the present apparatus $\bar{W}_c = \bar{W}_o$ and therefore:

$$\left.\frac{v_o}{u_o}\right|_{ideal} = \frac{v_o^+}{u_o} = \frac{A_c}{2\pi r_o h} \qquad (6.2)$$

where A_c is the apparatus tangential inlet area.

In the apparatus the ideal ratio of tangential to radial velocity at the chamber outer periphery depends only on chamber size and the chamber tangential inlet area and not upon the flow rate through the apparatus.

The results of tests to determine the end wall static radial pressure distribution for several exit orifice sizes and selected values of inlet area, i.e. values of $\frac{v_o^+}{u_o}$, are presented in Figures 6.9, 6.10, and 6.11. It is noted that in the Figures the radial pressure distributions have been plotted as $\frac{p}{p_o}$ versus $\bar{r} = \frac{r}{r_o}$ where p_o is the pressure measured at the tap located at $r = r_o = 3.5$ inches. All pressures were measured relative to atmospheric pressure. The test conditions and the value of $\frac{v_o^+}{u_o}$ for each set of test data presented in the Figures is tabulated in Table 6.1.

In Figure 6.9, the pressure distributions measured on the 0.5 inch exit diameter dual exit vortex chamber are presented for two flow conditions -- $\frac{v_o^+}{u_o} = 65$ and $\frac{v_o^+}{u_o} = 323$. The data for the profile corresponding to $\frac{v_o^+}{u_o} = 65$ indicates that as $\frac{r}{r_o}$ increases the pressure gradient in the chamber $\frac{dp}{dr}$ decreases monotonically while for the profile corresponding to $\frac{v_o^+}{u_o} = 323$ the pressure gradient decreases monotonically with increasing r from the valve exit to a point in the chamber at $\bar{r} \simeq 0.85$. In the region from $\bar{r} = 0.85$ to $\bar{r} = 1.0$, the pressure gradient is greater than the gradient at $\bar{r} = 0.85$. For the flow conditions which occur in short vortex chambers the pressure gradient in the chamber may be related to the tangential velocity as shown by equation 7.31 of Chapter 7. Under the condition that

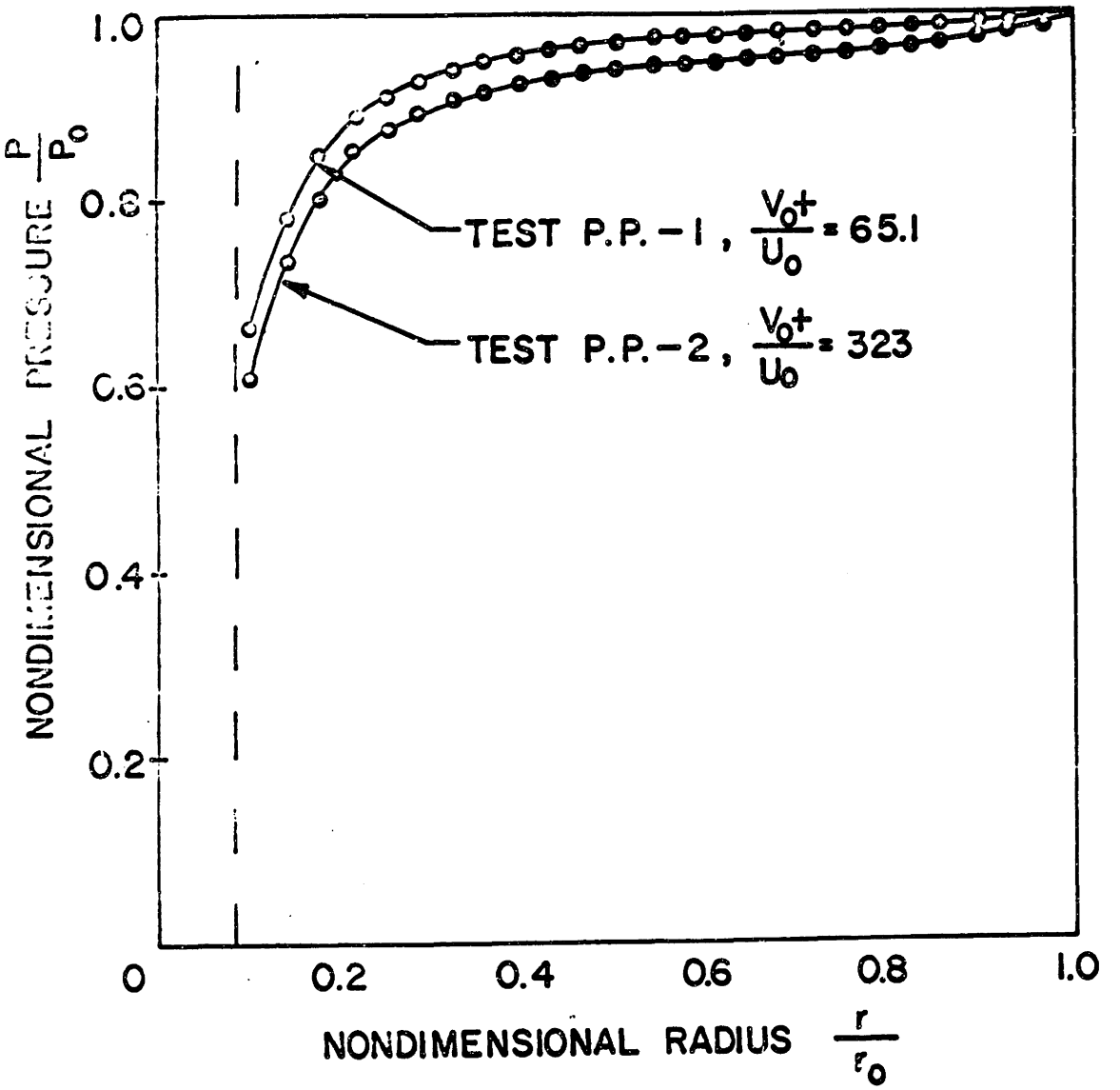

Fig. 6.9. Experimental Pressure Profile in the 0.25 inch Exit Radius Dual Exit Chamber.

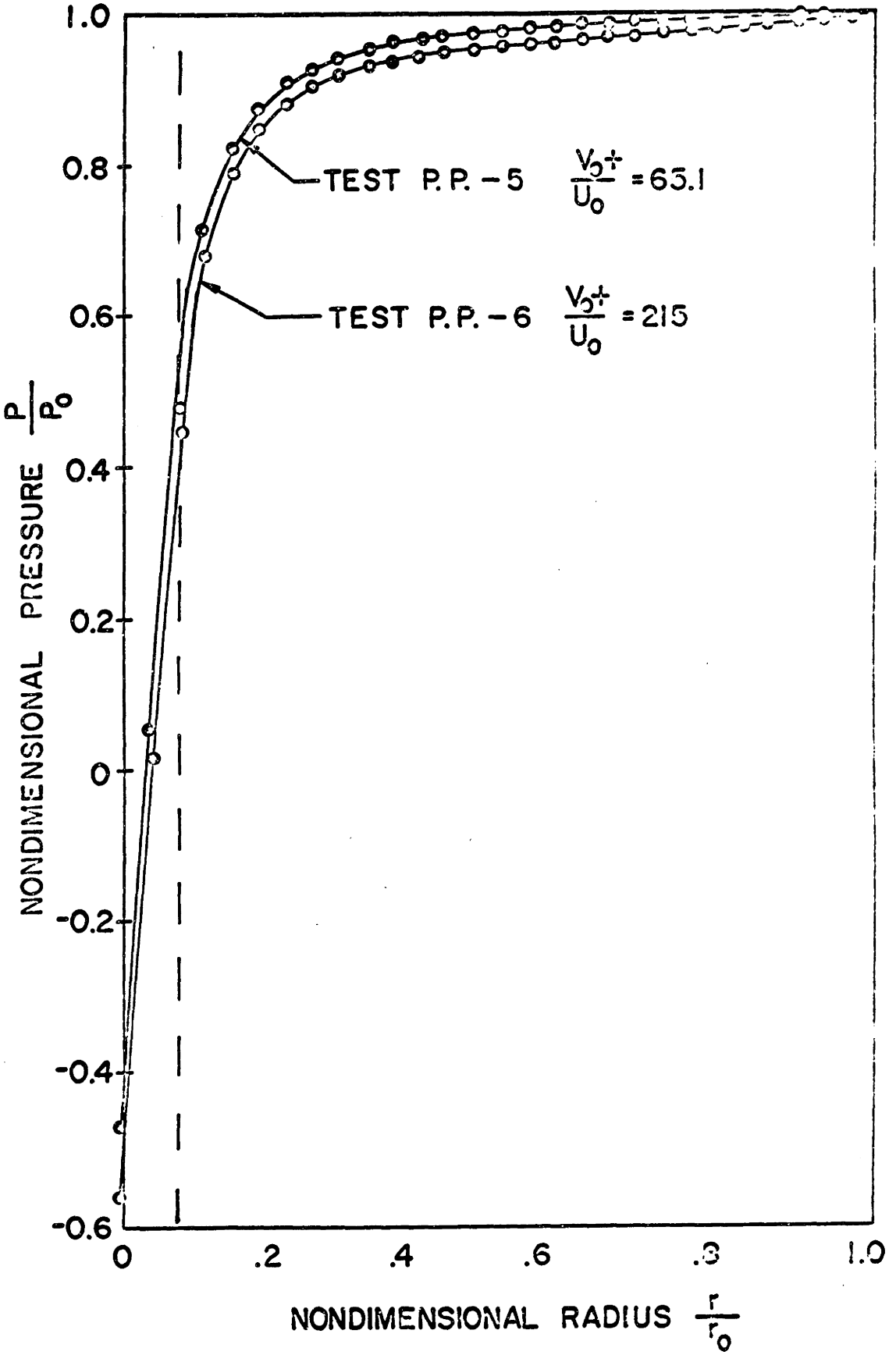

Fig. 6.10. Experimental Pressure Profile in the 0.25 inch Exit Radius Single Exit Chamber.

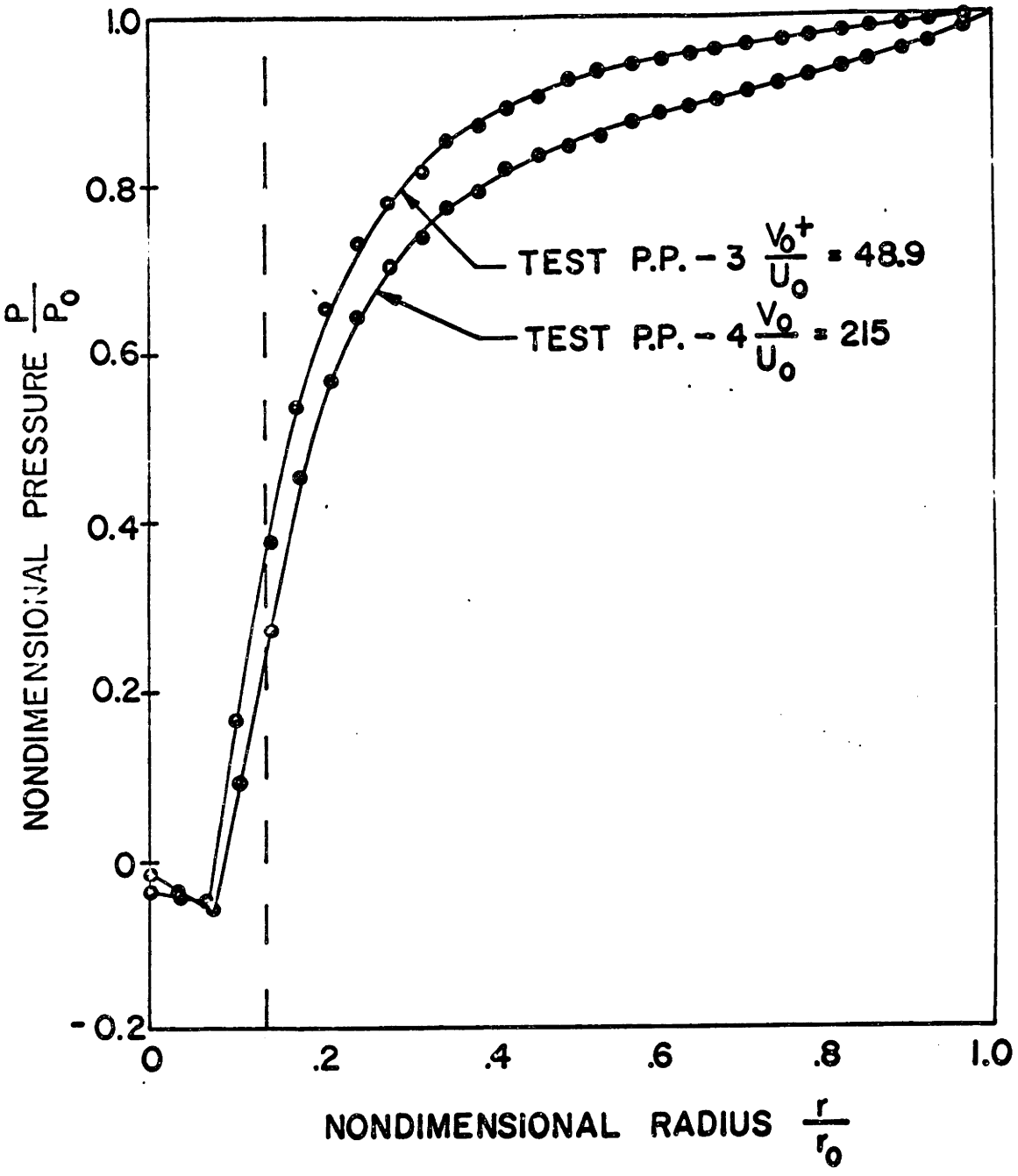

Fig. 6.11. Experimental Pressure Profile in the 0.5 inch Exit Radius Single Exit Chamber.

$\frac{v_o}{u_o} > 10$ in the chamber, the pressure gradient may be expressed as:

$$\frac{dp}{dr} = \frac{\rho V^2}{r} \tag{6.3}$$

Equation 6.3 indicates that as long as the tangential velocity in the chamber increases less rapidly than $\sqrt{r}$ with increasing r, the pressure gradient will decrease with increasing r. For instance, if the tangential velocity in the chamber decreased as $\frac{1}{r}$ with increasing r, as would be the case for a potential vortex, the pressure gradient would decrease with increasing r as $\frac{1}{r^3}$. It may easily be noted that in all of the pressure distributions presented in this section the pressure gradient decreases much less rapidly than $\frac{1}{r^3}$. The observation that the pressure gradient for the data of $\frac{v_o^+}{u_o} = 323$ in the region $\bar{r} = 0.85$ to $\bar{r} = 1.0$ is greater than the gradient at $\bar{r} = 0.85$ indicates that the tangential velocity at $\bar{r} = 0.85$ is less than the tangential velocity at a larger value of $\bar{r}$. The tangential velocity in the vortex chamber actually decreases somewhat with decreasing r in a region near $\bar{r} = 0.85$ under the flow condition of $\frac{v_o^+}{u_o} = 323$. It may be noted from Figures 6.10 and 6.11 that similar results are obtained in these radial pressure profiles. At low values of $\frac{v_o^+}{u_o}$ the pressure gradient in the main vortex chamber excluding the exit region decreases monotonically with increasing r, while at high values of $\frac{v_o^+}{u_o}$, the pressure gradient decreases with increasing r only over a region of the chamber and near the chamber outer periphery increases with increasing r. The explanation for this behavior is found in the analytical work of Section 7.4 which indicates that at

sufficiently high values of $\frac{v_o}{u_o}$ a small region exists in the chamber near the point at which all the flow has entered the end wall boundary layers in which the viscous losses in the boundary layer are sufficient so that the tangential velocity decreases in value with decreasing r. This result is discussed in more detail in Section 7.4

The profiles presented in Figures 6.10 and 6.11 for the single exit chambers include static end wall pressure measurements made on the region of the top plate opposite the chamber exit. It is noted that for all of the flow conditions tested, the vortex strengths were great enough so that within the exit region of the chamber, the end wall static pressures were less than atmospheric pressure. In the 0.5 inch exit diameter chamber, the minimum end wall static pressure occurred at $\bar{r} = 0$ while in the 1 inch exit diameter chamber the minimum end wall static pressure occurred at $\bar{r} \approx 0.072$. These subambient pressures were accompanied by a reversed axial flow pattern in the chamber exit in which some atmospheric flow was drawn into the chamber along the exit centerline. A similar reversed exit flow pattern in vortex chamber exits has been studied in some detail by Kwok (19).

The pressure tap measurements obtained from the series of 20 taps located in two arcs at chamber radii of $\bar{r} = .965$ and $\bar{r} = .75$ indicated that virtually no measurable variation existed in the end wall static pressure measurements over a constant radius arc including two inlet port regions. For example,measurements made on the 1.0 inch exit chamber indicated for the test at $\frac{v_o^+}{u_o} = 48.9$ that each pressure tap measurement differed from all other measurements

at the same radius by less than 1%. The presence of the inlet jet was barely perceptible in the data for $\bar{r} = .965$ by the fact that the pressures at taps in the most immediate vicinity of the jet differed from neighboring static pressures by less than 0.1 "H_2O on a base of 15.20 "H_2O. At the radius of $\bar{r} = 0.75$, the position of the inlet jet could not be detected from the data. Similar results were obtained for higher values of $\frac{v_o^+}{u_o}$.

6.4 Effective Chamber Outer Wall Tangential Velocity

Experimental work reported in References 33 and 36 has indicated that the effective outer wall tangential velocity V_w in the vortex chamber may differ significantly from the ideal outer peripheral tangential velocity v_o^+ calculated from the velocity of the tangential driving jets used in the apparatus. As shown in Chapter 3, if it is assumed that the velocity profile across the inlet hole is uniform and that the mixing of the jet flow with the main chamber flow is lossless and if the shear on the outer chamber wall is neglected, the ideal tangential peripheral velocity v_o^+ is for the present apparatus:

$$v_o^+ = \frac{W}{\rho A_\varepsilon} \tag{6.4}$$

while the ratio of the ideal tangential velocity to the radial velocity has been derived previously in equation 6.2. If the ratio of the ideal to actual effective tangential velocity at the chamber outer wall is defined as:

$$\varepsilon = \frac{V_w}{v_o^+} \tag{6.5}$$

then V_w may be written as:

$$V_w = \varepsilon v_o^+ = \frac{\varepsilon W_o}{\rho A_c} \tag{6.6}$$

where the quantity ε is essentially a jet recovery factor. An indication of the values of the jet recovery factor may be obtained from the radial end wall static pressure profiles. Equation 6.3 has indicated that for the conditions under which the present test data was taken, the tangential velocity at a given radius in the chamber may be determined from the pressure gradient which exists in the chamber. An attempt was made to determine the value of the effective outer wall tangential velocity by differentiating the pressure profile data. This method of determining V_w proved to be very uncertain because it required taking the difference between two small numbers. Another method was adopted. It was assumed that in a region near the outer wall, i.e. a region extending from $\bar{r} = 0.926$ to $\bar{r} = 1.0$, the tangential velocity distribution was given by:

$$\frac{V}{V_w} = \frac{r_o}{r} \tag{6.7}$$

Equation 6.7 represents the distribution of a potential flow. It is noted that the boundary layer analysis of Chapter 7 indicates that for a region very near the outer wall, the midplane tangential velocity distribution is identical to that given by equation 6.7. Combining equations 6.3 and 6.7 and integrating the resultant equation, the pressure distribution valid for $\bar{r} > 0.926$ may be derived as:

$$p = p_o - \frac{\rho V_w^2}{2}\left[\frac{r_o^2}{r^2} - 1\right] \tag{6.8}$$

Equation 6.8 may be written in terms of the test-apparatus geometries, the flow condition, and jet recovery factor as:

$$p = p_o - \frac{\varepsilon^2 W_o^2}{2\rho A_c^2}\left[\frac{r_o^2}{r^2} - 1\right] \tag{6.9}$$

For each of the test conditions given in Table 6.1, the pressure distribution of equation 6.9 was matched to the experimental distributions over the region $\bar{r} = .926$ to $\bar{r} = 1.0$ by finding the value of the jet recovery factor ε which resulted in a good fit of the experimental data. For the series of test data the range of ε which provided the fit varied from 0.55 to 0.95. The fit was obtained by plotting the distribution given in equation 6.9 for several values of ε with the experimental data and choosing the value which resulted in the best fit. It was found that with this technique, the value of ε could be determined easily to within a range of variation which was less than 0.02. It was felt that a more sophisticated curve fitting technique was not justified in the present case. The results of applying this method to the data presented in Figures 6.9, 6.10 and 6.11 are presented in Figure 6.12 as a plot of jet recovery factor ε versus the ideal ratio of tangential to radial velocity calculated from equation 6.2 for each test condition. Data is also included in the Figure which was obtained on the test apparatus for some flow conditions not included in Table 6.1.

The plot of ε versus $\frac{v_o^+}{u_{ov_o}^+}$ in Figure 6.12 indicates that for each exit configuration tested as $\frac{v_o^+}{u_o}$ is increased the jet recovery factor decreases. At a value of $\frac{v_o^+}{u_o} \simeq 50$, the jet recovery factor approaches 0.95 while for $\frac{v_o^+}{u_o} \simeq 325$ the recovery factor approaches

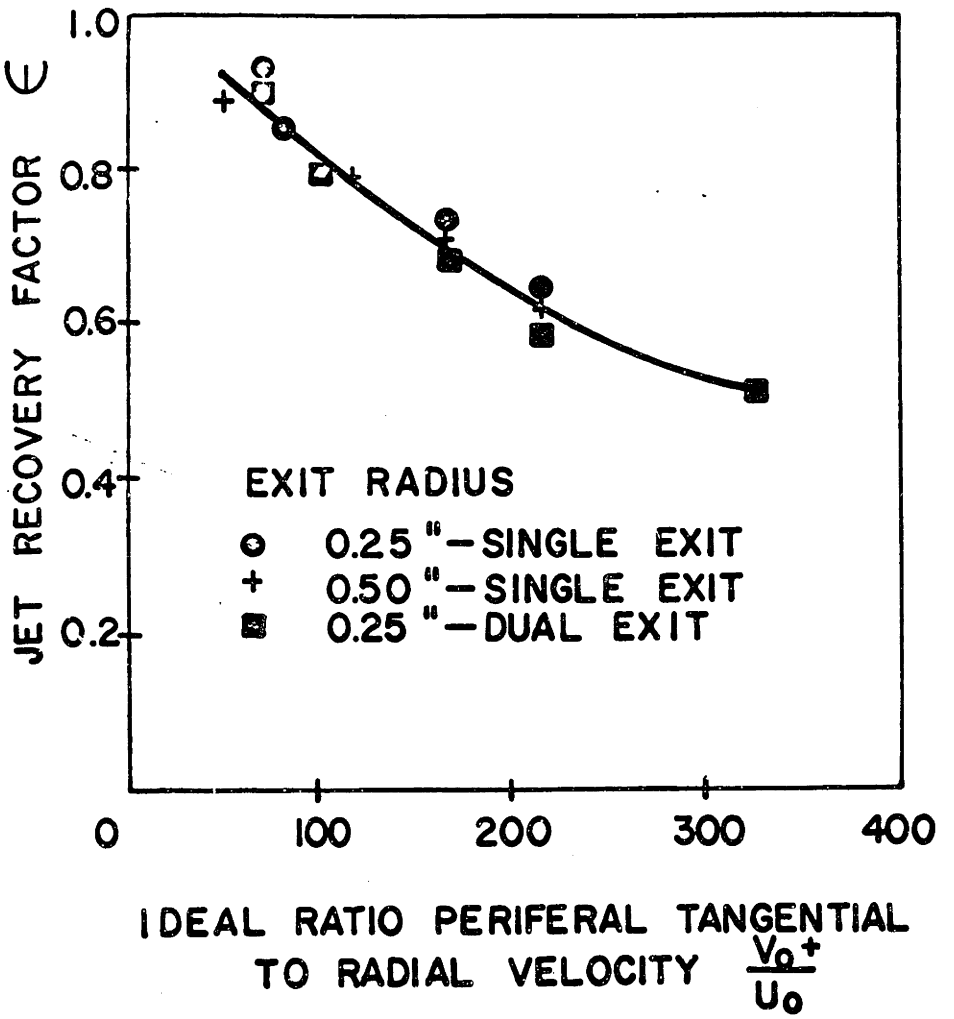

Fig. 6.12. Influence of the Ideal Ratio of Peripheral Tangential to Radial Velocity on the Jet Recovery Factor.

0.55. The data indicates that the size and configuration of the chamber exit do not markedly affect the value of the recovery factor. The most important result of the data is simply the fact that a substantial loss of inlet jet momentum occurs in a vortex chamber at high values of $\frac{v_o^+}{u_o}$. A complete model of the vortex chamber which is to be valid for flow conditions including high values of $\frac{v_o^+}{u_o}$ must include a consideration of the loss in inlet jet momentum. The data of Figure 6.12 suggest, however, that an empirical correlation for jet recovery factor in which the jet recovery factor is expressed as a function of $\frac{v_o^+}{u_o}$ might be successful for a range of exit conditions. This possibility would merit further investigation in future studies of the vortex chamber.

CHAPTER 7

ANALYTICAL INVESTIGATION OF THE FLOW FIELD IN SHORT VORTEX CHAMBERS

7.1 Introduction

At the present time a complete analysis of the flow fields which exist in a vortex chamber inlet, main chamber, and exit regions is not available even though considerable time and effort has been devoted to the study in the last decade. The many facets of the three dimensional flow patterns and the interdependence of the flows in each of the regions of the chamber have posed a difficult analytical problem.

In this chapter an analysis of the flow in the vortex main chamber region is developed which considers the viscous losses that occur in the boundary layers on the chamber end walls. As a result of the analysis it is possible to predict the pressure distribution across the vortex chamber to the chamber exit, given the conditions at the chamber outer periphery. The analysis serves as one step toward a complete vortex valve model. An investigation which includes a comprehensive study of each of the three regions of the valve was not feasible within the scope of the present study. Effort was concentrated in the investigation of the valve main chamber region because an adequate understanding of this region appeared at the onset of the investigation to be a prerequisite for future studies of the valve exit region or of vortex valve dynamic behavior. In the

frequency response ranges of interest in vortex valve dynamic behavior, the main chamber region of the valve may be the predominate factor influencing vortex valve dynamic behavior and an adequate valve dynamic model over much of the frequency range of interest might well incorporate a dynamic model of the main chamber region coupled with static models of the valve inlet and exit regions which could possibly be formulated from static experimental measurements. The analysis described in this chapter has provided a "picture" of the character of the internal flow in the main chamber and in so doing has provided a basis for future studies of the flow in the chamber exit region and for the study of vortex chamber dynamic behavior.

A large number of previous analytical studies of confined vortex flows have been conducted because of interest in a variety of vortex-type devices. Many studies (20, 21, 22, 23, 24) starting with those of Taylor (29) have considered the development of the boundary layer on a finite disk or vortex chamber end wall for a vortex-like free stream flow in which the free stream tangential velocity distribution across the disk is specified as a function of radius. Only a few studies (30, 31) have considered the interaction which exists between the flow in the end wall boundary layers and the main vortex flow. The result of these studies indicates that in a confined vortex flow such as occurs in a vortex valve the boundary layers on the vortex chamber end walls can carry a substantial amount of the flow through the vortex chamber and may have a significant influence on the main flow tangential velocity and pressure

distributions. The analysis in this chapter has been based upon a model formulated from the flow visualization photographs of Chapter 6 in which a spinning donut of fluid that served as an impenetrable barrier to radial flow was observed to exist in the chamber under sufficiently high swirl conditions. The present analysis differs with respect to other analyses of vortex chambers primarily in its treatment of this impenetrable spinning donut of fluid. In the vortex chambers considered in this investigation all of the radial flow passing through the vortex chamber may be contained in the end wall boundary layers at sufficiently high vortex strengths.

7.2 Formulation of the Flow Model

A model for the axisymmetric, steady, incompressible flow in the vortex main chamber may be formulated with the aid of Figure 7.1. In Figure 7.1 the flow is assumed to consist of two flow regions -- a developing flow region and a developed flow region. The developing flow region in which the boundary layers on the chamber end walls develop extends from the chamber outer perifery to the point in the chamber at which all the radial flow through the chamber has entered the chamber end wall boundary layers. The developed flow region extends from the point at which all the flow has entered the boundary layers to the chamber exit radius. First the model for the developing flow region is considered.

7.2.1 The Developing Flow Region

In the developing flow region of the chamber, the flow is subdivided into a boundary layer flow on the chamber end wall and a core flow at the chamber midplane as illustrated in Figure 7.1. It is assumed that the tangential and radial velocity components in the core are functions only of r while they are assumed to be functions of both r and y in the boundary layer. The core is assumed to be inviscid and it is assumed that the boundary layer starts from zero thickness at the chamber outer perifery. The thickness of the "tangential boundary layer" and the "radial boundary layer" are assumed to be equal. The continuity and momentum equations for both the inviscid core and the boundary layer region may be derived as outlined below.

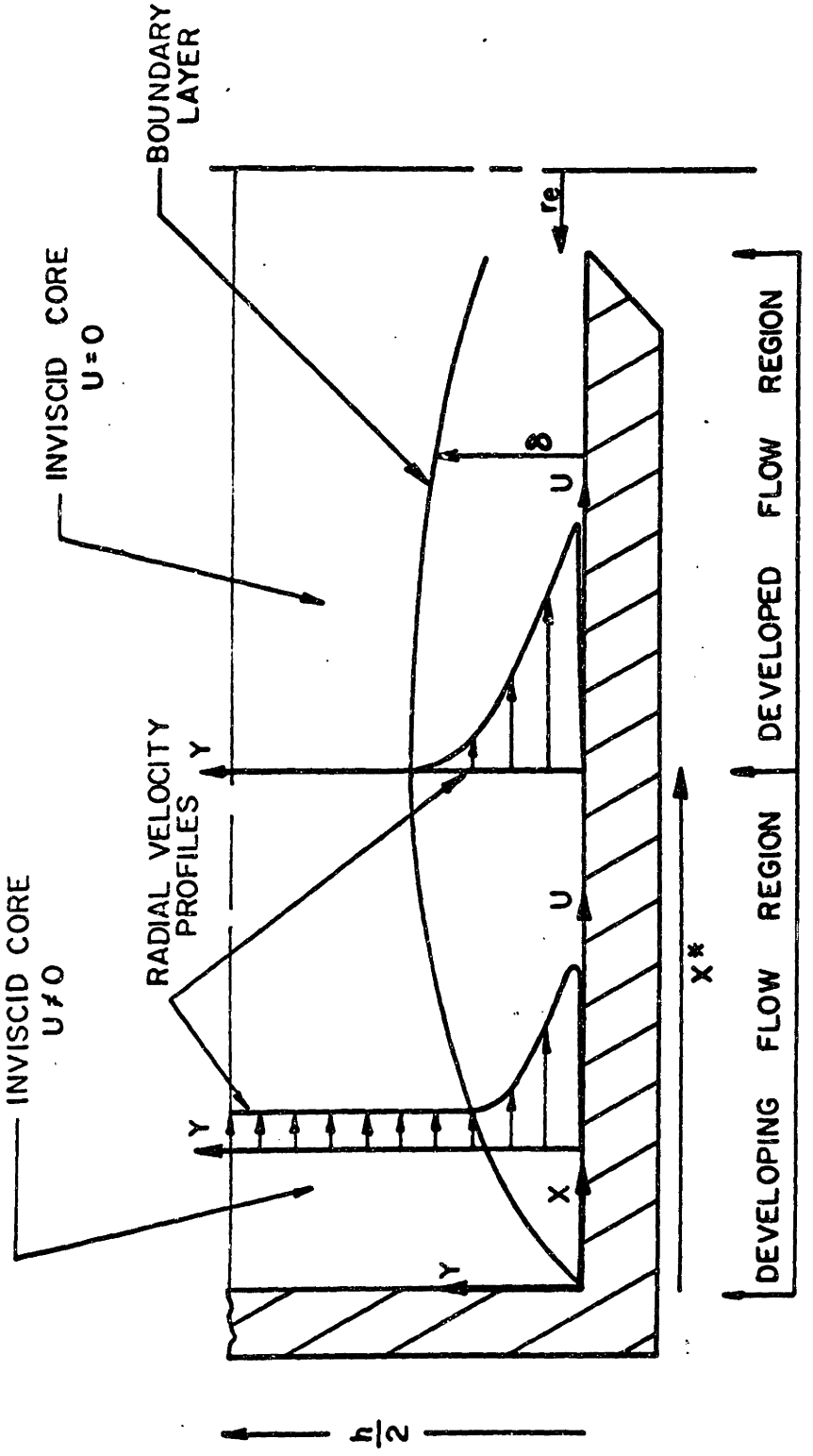

Fig. 7.1. The Developing and Developed Flow Regions.

For the case of axisymmetric, incompressible flow, the continuity equation may be written as

$$\frac{\partial u}{\partial r} + \frac{u}{r} + \frac{\partial w}{\partial r} = 0 \tag{7.1}$$

while the radial and tangential momentum equations in the inviscid core where the tangential and radial velocity components are functions only of r may be written as:

$$u \frac{\partial u}{\partial r} - \frac{v^2}{r} = - \frac{1}{\rho} \frac{\partial p}{\partial r} \tag{7.2}$$

$$u \frac{\partial v}{\partial r} + \frac{uv}{r} = 0 \tag{7.3}$$

where:

u,v,w = the respective velocity components in the radial, tangential and axial directions

r = radial displacement

y = axial displacement

p = pressure

ρ = fluid density

In deriving the tangential and radial momentum equations for the boundary layer it is also assumed that the axial velocity component is small compared to the tangential and radial velocity components and that the axial coordinate y is small compared with r. Under these additional conditions the radial and tangential momentum equations which apply to the boundary layer become:

$$u \frac{\partial u}{\partial r} - \frac{v^2}{r} + w \frac{\partial u}{\partial y} = - \frac{1}{\rho} \frac{\partial p}{\partial r} + \frac{1}{\rho} \frac{\partial \tau_r}{\partial y} \tag{7.4}$$

$$u \frac{\partial v}{\partial r} + \frac{uv}{r} + w \frac{\partial v}{\partial y} = \frac{\partial \tau_t}{\partial y} \tag{7.5}$$

where:

y = axial coordinate

τ_r, τ_t = the respective shear stresses in the radial and tangential directions

If the analysis is restirсted to short vortex chambers, i.e., $\frac{h}{r_o} << 1$, the zeroth order axial momentum equation has been shown in Reference 24 to reduce to:

$$\frac{\partial p}{\partial y} = 0 \tag{7.6}$$

Equation 7.6 states that the pressure in a short vortex chamber is essentially constant across the chamber in the axial direction.

When the flow is assumed to be symmetric about the chamber midplane, the boundary conditions for the problem are:

$$\text{at } y = 0, \quad u = w = v = 0 \tag{7.7}$$

$$\text{at } y = \frac{h}{2}, \quad w = \frac{\partial u}{\partial y} = \frac{\partial v}{\partial y} = 0 \tag{7.8}$$

$$\text{at } r = r_o, \quad u = -u_o, \quad v = v_o, \quad p = p_o, \quad w = 0 \tag{7.9}$$

where it is recalled that u_o was defined in Chapter 3 as positive in the -r direction while u is positive in the +r direction.

The method used in this investigation to solve equations 7.1-7.6 subject to the boundary conditions of 7.7-7.9 is the well known (25) momentum integral method of solution.

The appropriate form of the continuity equation for the momentum integral method may be obtained by integrating equation 7.1 over the chamber half width subject to the boundary conditions of equations 7.7 and 7.8.

$$\int_0^{\frac{h}{2}} \frac{\partial u}{\partial r}\, dy + \int_0^{\frac{h}{2}} \frac{u}{r}\, dy = 0 \tag{7.10}$$

The momentum integrals for the boundary layer equations may be obtained by formally integrating equations 7.4 and 7.5 across the boundary layer. When the integration is performed subject to the boundary conditions of equations 7.7 and 7.8 and where it is assumed that the shear stresses vanish at the inviscid core boundary, the equations become:

$$\int_c^{\delta} \frac{\partial u^2}{\partial r}\, dy - \frac{1}{r} \int_o^{\delta} (v^2 - u^2)dy - u_\delta \int_o^{\delta} (\frac{\partial u}{\partial r} + \frac{u}{r})dy = -\frac{\delta}{\rho} \frac{\partial p}{\partial r} - \frac{\tau_r}{\rho}\Big|_{y=o} \tag{7.11}$$

$$\int_o^{\delta} \frac{\partial (uv)}{\partial r}\, dy + 2 \int_o^{\delta} \frac{uv}{r}\, dy - v_\delta \int_o^{\delta} (\frac{\partial u}{\partial r} + \frac{u}{r})dy = -\frac{\tau_t}{\rho}\Big|_{y=o} \tag{7.12}$$

where:

δ = boundary layer thickness

u_δ, v_δ = the values of u, v at $y = \delta$

The momentum equations for the inviscid core in which u and v are functions only of r become simply:

$$u_\delta \frac{du_\delta}{dr} - \frac{v_\delta^2}{r} = -\frac{1}{\rho} \frac{dp}{dr} \tag{7.13}$$

$$u_\delta \frac{dv_\delta}{dr} + u_\delta \frac{v_\delta}{r} = 0 \qquad (7.14)$$

where the velocity components in the inviscid core have been matched to those at the edge of the boundary layer by setting $u = u_\delta$ and $v = v_\delta$. It is noted that u_δ and v_δ are functions only of r.

In order to obtain a solution to the set of equations 7.10 to 7.14, the velocity distributions of u and v across the vortex chamber must be determined.

In the case of flow in vortex chambers, there is very little experimental data available to guide in the choice of the distributions. Velocity profiles have been measured in long vortex chambers, $\frac{h}{r_o} > 1.0$, by Kendall (26) while measurements have been made by Donaldson and Williamson (27) and by Savino and Keshock (28) for short vortex chambers. The most complete data is given by Savino and Keshock who measured the radial and tangential velocity distributions in a short vortex chamber $\frac{h}{r_o} \approx 0.17$, for a ratio of tangential to radial velocity at the outer wall of about 15.0. A typical set of velocity distributions measured by Savino and Keshock is reproduced in Figure 7.2 Both the radial and tangential distributions contain a boundary layer region in which the profiles are strongly dependent on y, i.e. $0 \leq \frac{y}{h} \leq 0.22$ and $0.78 \leq \frac{y}{h} \leq 1.0$ and a core region in which the profiles are relatively independent of y. In the tangential direction in which the pressure gradient is zero, the velocity distribution in the boundary layer is similar to the power law velocity distribution for the turbulent flow over a flat plate with zero pressure gradient; the velocity increases rapidly from zero at the edge chamber wall to a maximum value at the

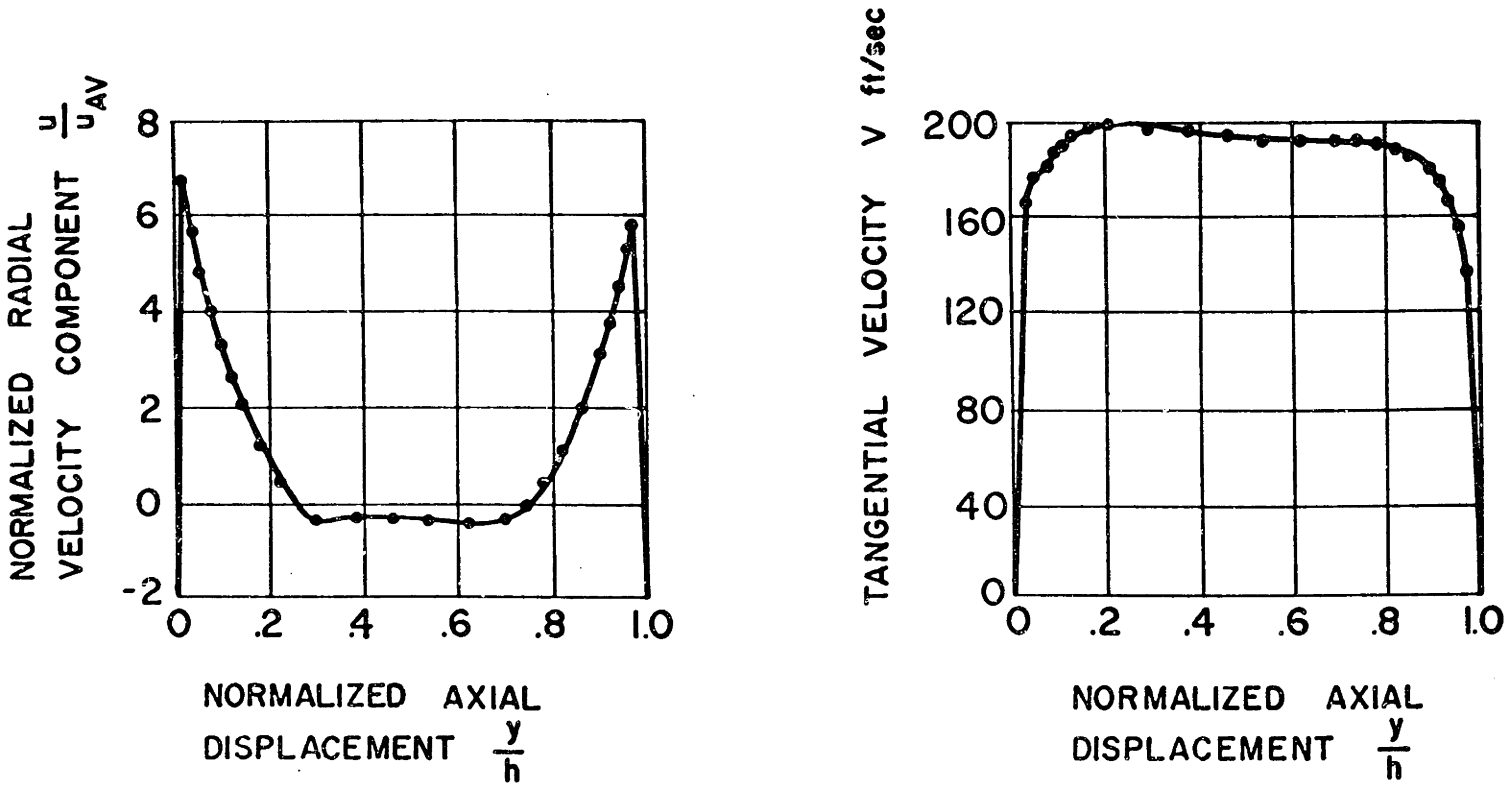

Fig. 7.2. Experimental Velocity Profiles from the Data of Savino and Keshock, Ref. 28.

edge of the boundary layer. The radial velocity distribution in the boundary layer is triangular in shape rising very rapidly from zero at the wall to a maximum value near the edge of the wall and then decreasing to a value near zero at the edge of the boundary layer. In the core region the radial velocity component is small in value and is in a direction opposite to the main flow through the chamber. Some recirculation takes place in the vortex chamber under the condition in which the data was taken, i.e. $\frac{v_o}{u_o} \approx 15$. Tests conducted at a higher value of $\frac{v_o}{u_o}$ by Kendall (26) showed the radial core velocity to be zero at nondimensional chamber radii of 0.34 and 0.71. The flow visualization photographs of Chapter 6 also indicate that at higher values of $\frac{v_o}{u_o}$, the radial core velocity is also zero.

Using the experimental data of References 26, 27, and 28 as a guide, the assumption is made that the form of the radial velocity distribution is:

$$\begin{aligned} 0 \le y \le \delta \qquad & u = u_\delta f(\eta) + u_s g(\eta) \\ \delta \le y \le \frac{h}{2} \qquad & u = u_\delta \end{aligned} \tag{7.15}$$

where $g(\eta)$ is assumed to be a function only of $\eta = \frac{y}{\delta}$ and must satisfy the conditions:

$$g(0) = 0, \qquad g(1) = 0 \tag{7.16}$$

and where $f(\eta)$ is a function only of η and must satisfy the conditions:

$$f(0) = 0.0, \quad f(1) = 1.0 \tag{7.17}$$

The radial velocity profile has been assumed to consist of two separate profiles where the primary and secondary velocity coefficients u_δ and u_s are to be determined from a solution of the continuity and momentum equations. The part of the profile $u_\delta f(\eta)$ represents the contribution of the radial flow profile which occurs due to radial flow in the core and represents the velocity profile which would occur in the chamber if the tangential velocity were zero. The profile $u_s g(\eta)$ represents the contribution of the secondary flow which is induced into the boundary layer by the strong inward pressure gradient existing in the chamber at values of $\frac{v_o}{u_o} > 1.0$.

The form of the tangential velocity distribution is assumed to be:

$$\begin{aligned} 0 \leq y \leq \delta \qquad & v = v_\delta f(\eta) \\ \delta \leq y \leq \tfrac{h}{2} \qquad & v = v_\delta \end{aligned} \tag{7.18}$$

where the conditions on $f(\eta)$ are given in equation 7.17.

The numerical forms of $f(\eta)$ and $g(\eta)$ are specified in Section 7.2.3. When the velocity distributions specified in equations 7.15 and 7.17 are substituted into the continuity (7.10) and momentum equations (7.11 and 7.12) and the indicated differentiations and integrations are performed, the following equations may be derived:

Continuity equation:

$$[\alpha_5 u_\delta + \alpha_4 u_s - u_\delta] \frac{d\delta}{dr} + [\alpha_5 \delta + (\tfrac{h}{2} - \delta)] \frac{du_\delta}{dr} + \alpha_4 \delta \frac{du_s}{dr}$$

$$= -\frac{1}{r} [\alpha_5 \delta u_\delta + \alpha_4 \delta u_s + (\tfrac{h}{2} - \delta) u_s] \tag{7.19}$$

Boundary layer radial momentum equation:

$$[\alpha_1 u_s^2 + 2\alpha_2 u_\delta u_s + \alpha_5 u_s^2 - \alpha_4 u_\delta u_s + \alpha_3 u_s^2] \frac{d\delta}{dr} + [2\alpha_1 \delta u_s + 2\alpha_2 \delta u_s - \alpha_5 \delta u_\delta] \frac{du_\delta}{dr}$$

$$+ [2\alpha_3 \delta u_s + 2\alpha_2 \delta u_\delta - \alpha_4 \delta u_\delta] \frac{du_s}{dr} = \frac{1}{r} [\alpha_1 \delta v_\delta^2 - \alpha_1 \delta u_\delta^2 - 2\alpha_2 \delta u_s u_\delta - \alpha_3 \delta u_s^2$$

$$+ \alpha_5 \delta u_\delta^2 + \alpha_4 \delta u_\delta u_s] - \frac{\delta}{\rho} \frac{dp}{dr} - \frac{\tau_r}{\rho}\Big|_{y=o} \qquad (7.20)$$

Boundary layer tangential momentum equation:

$$[\alpha_1 u_\delta v_\delta + \alpha_2 u_s v_\delta - \alpha_5 u_\delta v_\delta - \alpha_4 u_s v_\delta] \frac{d\delta}{dr} + [\alpha_1 \delta v_\delta - \alpha_5 \delta v_\delta] \frac{du_\delta}{dr}$$

$$+ [\alpha_2 \delta v_\delta - \alpha_4 \delta v_\delta] \frac{du_s}{dr} = [-\alpha_1 \delta u_\delta - \alpha_2 \delta u_s] \frac{dv_\delta}{dr} - \frac{2}{r} [\alpha_1 \delta u_\delta v_\delta + \alpha_2 \delta u_s v_\delta]$$

$$+ \frac{1}{r} [\alpha_5 \delta u_\delta v_\delta + \alpha_4 \delta u_s v_\delta] - \frac{\tau_t}{\rho}\Big|_{y=o} \qquad (7.21)$$

where the α's are defined in terms of the velocity profiles as:

$$\alpha_1 = \int_o^1 f^2(\eta)\, d\eta \qquad (7.22)$$

$$\alpha_2 = \int_o^1 f(\eta) g(\eta) d\eta \qquad (7.23)$$

$$\alpha_3 = \int_o^1 g^2(\eta) d\eta \qquad (7.24)$$

$$\alpha_4 = \int_o^1 g(\eta) d\eta \qquad (7.25)$$

$$\alpha_5 = \int_o^1 f(\eta) d\eta \qquad (7.26)$$

Before further consideration of the set of equations which have been derived for the vortex chamber, it is convenient to

introduce the following dimensionless variables:

$$\Gamma = \frac{v_\delta r}{v_o r_o} \quad , \quad U = -\frac{u_\delta}{u_o} \quad , \quad U_s = -\frac{u_s}{u_o}$$

$$\bar{\delta} = \frac{\delta}{\frac{h}{2}} \quad , \quad \lambda = \frac{v_o}{u_o} \quad , \quad x = 1 - \frac{r}{r_o} \tag{7.27}$$

$$\bar{\tau}_{tw} = \left.\frac{\tau_t}{\rho u_o^2}\right|_{y=o} \quad , \quad \bar{\tau}_{rw} = \left.\frac{\tau_r}{\rho u_o^2}\right|_{y=o} \quad , \quad \bar{P} = \frac{p}{\rho u_o^2}$$

It is noted that the normalized circulation Γ and the normalized coordinate x have been introduced. It is also noted that U and U_s have been defined as positive in the + x direction.

When the nondimensional quantities in equation 7.27 are introduced into the continuity (7.19) and momentum equations (7.13, 7.14, 7.20, 7.21), the following set of five normalized equations are obtained:

Continuity equation:

$$[\alpha_5 U + \alpha_4 U_s - U] \frac{d\bar{\delta}}{dx} + [\alpha_5 \bar{\delta} + (1 - \bar{\delta})] \frac{dU}{dx} + \alpha_4 \bar{\delta} \frac{dU_s}{dx}$$
$$= \frac{1}{(1 - x)} [\alpha_5 \bar{\delta} U + \alpha_4 \bar{\delta} U_s + (1 - \bar{\delta}) U] \tag{7.28}$$

Boundary layer radial momentum equation:

$$- [\alpha_1 U^2 + 2\alpha_2 U U_s - \alpha_5 U^2 - \alpha_4 U U_s + \alpha_3 U_s^2] \frac{d\bar{\delta}}{dx} - [2\alpha_1 \bar{\delta} U + 2\alpha_2 \bar{\delta} U_s - \alpha_5 \bar{\delta} U] \frac{dU}{dx}$$
$$- [2\alpha_2 \bar{\delta} U - \alpha_4 \bar{\delta} U + 2\alpha_3 \bar{\delta} U_s] \frac{dU_s}{dx}$$
$$= \frac{1}{(1 - x)} \left[\frac{\alpha_1 \bar{\delta} \lambda^2 \Gamma^2}{(1 - x)^2} - \alpha_1 \bar{\delta} U^2 - 2\alpha_2 \bar{\delta} U U_s - \alpha_3 \bar{\delta} U_s^2 + \alpha_5 \bar{\delta} U^2 + \alpha_4 \bar{\delta} U U_s\right]$$
$$+ \bar{\delta} \frac{dp}{dx} + \left(\frac{r_o}{\frac{h}{2}}\right) \bar{\tau}_{rw} \tag{7.29}$$

Boundary layer tangential momentum equation:

$$+ [\alpha_1 U + \alpha_2 U_s - \alpha_5 U - \alpha_4 U_s] \frac{d\bar{\delta}}{dx} + [\alpha_1 \bar{\delta} - \alpha_5 \bar{\delta}] \frac{dU}{dx} + [\alpha_2 \bar{\delta} - \alpha_4 \bar{\delta}] \frac{dU_s}{dx}$$

$$= - \frac{[\alpha_1 \bar{\delta} U + \alpha_2 \bar{\delta} U_s]}{\Gamma} \frac{d\Gamma}{dx} - \frac{[-\alpha_1 \bar{\delta} U - \alpha_2 \bar{\delta} U_s + \alpha_5 \bar{\delta} U + \alpha_4 \bar{\delta} U_s]}{(1 - x)} - \frac{(1 - x)}{\Gamma \lambda} \left(\frac{r_o}{\frac{h}{2}}\right) \bar{\tau}_{tw} \tag{7.30}$$

Inviscid core radial momentum equation:

$$- U \frac{dU}{dx} - \frac{\lambda^2 \Gamma^2}{(1 - x)^3} = \frac{d\bar{P}}{dx} \tag{7.31}$$

Inviscid core tangential momentum equation:

$$+ U \frac{d\Gamma}{dx} = 0 \tag{7.32}$$

These five equations contain the following five unknowns which are functions only of x: U, U_s, Γ, $\bar{P}$, $\bar{\delta}$. The values of these variables at $x = 0$ are:

$$U(0) = 1.0 \tag{7.33}$$

$$U_s(0) = 0.0 \tag{7.34}$$

$$\Gamma(0) = 1.0 \tag{7.35}$$

$$\bar{P}(0) = \frac{P_o}{\rho u_o^2} \tag{7.36}$$

$$\bar{\delta}(0) = 0.0 \tag{7.37}$$

The parameters which enter the set of equations are the chamber aspect ratio $h/2r_o$, the α's which are a set of numbers obtained from the assumed velocity profiles, the nondimensional end wall shear stresses $\bar{\tau}_{tw}$ and $\bar{\tau}_{rw}$ and the ratio of the tangential to radial velocity at the chamber outer wall λ.

The circulation distribution in the developing flow region may be obtained directly from the inviscid core tangential momentum equation (7.32), $U \frac{d\Gamma}{dx} = 0$. When it is noted that the developing flow region has been defined by the condition $U \neq 0$, the solution to equation 7.32 is simply that the circulation is a constant, $\Gamma = 1.0$, for the full extent of the developing flow region in the vortex chamber. The solution to the complete set of equations for the developing flow region extending from $x = 0$ to $x = x^*$ at which point all the flow through the chamber is contained in the end wall boundary layer is discussed in Section 7.3.

7.2.2 The Developed Flow Region

The developed flow region in the chamber is assumed to start at $x = x^*$ where all the radial flow in the chamber is contained in the end wall boundary layers. The condition at $x = x^*$ can be achieved either by the end wall boundary layers meeting $\bar{\delta} = 1.0$, or by the inviscid core radial velocity reaching zero, $U = 0$, with $\bar{\delta} < 1$. In all cases considered in this analysis, i.e. $\frac{h}{2r_o} > 0.02$, it was found that all of the radial flow is drawn out of the developing flow region inviscid core before the end wall boundary layers have met. The condition in which the end wall boundary layers meet will

not be given further consideration.

Once all the flow is drawn out of the inviscid core into the boundary layers, the assumption is made that the flow will remain in the boundary layers until the chamber exit is reached. In the developed flow region, the flow in the chamber consists of an inviscid core with no radial flow, U = 0.0, and the boundary layers which contain all the radial flow passing through the chamber. The support for the assumption that there is no radial flow through the inviscid core in the developed flow region is provided by the flow visualization photographs of Chapter 6. It is recalled that a spinning donut of fluid which served as an impenetrable obstacle to radial flow was observed to exist in the chamber midplane region at sufficiently high values of $\frac{v_o}{u_o}$. The spinning donut region of the photographs corresponds to the developed flow region of this analysis and the assumption is made that in the developed flow region the radial flow outside of the boundary layers is zero, i.e. U = 0.0.

Under the condition that U = 0.0, the solution for the circulation distribution may no longer be obtained from the inviscid core tangential momentum equation which indicated that $\Gamma = 1.0$ for $U \neq 0$, but must be found from the boundary layer tangential momentum equation by applying the condition that all the radial flow remain in the boundary layer. The equations which describe the flow in the developed flow region may be derived directly from the developing flow set of equations by setting U = 0.0 in each of the equations. When U = 0.0, the tangential momentum equation for the inviscid core region vanishes and the continuity and remaining momentum equations become:

Continuity equation:

$$U_s \frac{d\bar{\delta}}{dx} + \bar{\delta} \frac{dU_s}{dx} = \frac{\bar{\delta} U_s}{(1 - x)} \tag{7.38}$$

Boundary layer radial momentum equation:

$$- \alpha_3 U_s^2 \frac{d\bar{\delta}}{dx} - [2\alpha_3 \bar{\delta} U_s] \frac{dU_s}{dx} = \frac{1}{(1 - x)} \left[\frac{\alpha_1 \bar{\delta} \lambda^2 \Gamma^2}{(1 - x)^2} - \alpha_3 \bar{\delta} U_s^2\right] + \bar{\delta} \frac{dp}{dx}$$

$$+ \left(\frac{r_o}{\frac{h}{2}}\right) \bar{\tau}_{rw} \tag{7.39}$$

Boundary layer tangential momentum equation:

$$(\alpha_4 - \alpha_2) U_s \frac{d\bar{\delta}}{dx} + (\alpha_4 - \alpha_2) \bar{\delta} \frac{dU_s}{dx} = \frac{(\alpha_4 - \alpha_2)\bar{\delta} U_s}{(1 - x)} + \frac{\alpha_2 \bar{\delta} U_s}{\Gamma} \frac{d\Gamma}{dx}$$

$$+ \frac{(1 - x)}{\lambda \Gamma} \left(\frac{r_o}{\frac{h}{2}}\right) \bar{\tau}_{tw} \tag{7.40}$$

Inviscid core radial momentum equation:

$$- \frac{\lambda^2 \Gamma^2}{(1 - x)^3} = \frac{d\bar{p}}{dx} \tag{7.41}$$

The set of four equations 7.38 - 7.41 contain as unknowns $\bar{\delta}$, U_s, Γ, and $\bar{P}$. The initial values of these unknowns at $x = x^*$ are determined from the values computed at $x = x^*$ in the solution to the developing flow set of equations. The parameters which enter equations 7.38 - 7.41 are identical to those in the developing flow set of equations, i.e. the α's, Γ, $\frac{2r_o}{h}$, and the end wall shear stresses $\bar{\tau}_{rw}$ and $\bar{\tau}_{tw}$.

When the continuity equation (7.38) is combined with the boundary layer tangential momentum equation (7.40), the following equation may be derived for the circulation distribution in the developed flow region.

$$\frac{d\Gamma}{dx} = - \frac{2r_o\alpha_4(1 - x)^2}{h\,\alpha_2\,\lambda} \bar{\tau}_{tw} \tag{7.42}$$

While in the developing flow region the circulation in the chamber is a constant, in the developed flow region the circulation is not a constant but is a strong function of the shear stress on the chamber end wall.

7.2.3 Specification of the Velocity Profile Functions and the Shear Law

Before a solution to the sets of equations derived above may be obtained, the velocity profile functions $f(\eta)$ and $g(\eta)$ as well as the chamber wall shear stresses must be specified. For the flow conditions in vortex valves which are of primary interest, i.e. the high strength vortex region of the characteristic, the tangential Reynolds numbers, $\frac{\rho v_o \bar{r}_o}{\mu}$, are commonly in the range of 10^4 to 10^6. Because of these high tangential Reynolds numbers, the selection of the velocity profile functions $f(\eta)$ and $g(\eta)$ and the selection of the shear law are based upon the premise that the end wall boundary layers are turbulent.

For the numerical calculations included in this chapter the functions $f(\eta)$ and $g(\eta)$ are assumed to be:

$$f(\eta) = \eta^{1/7} \tag{7.42}$$

$$g(\eta) = 1.69\ \eta^{1/7}\ (1 - \eta)^2 \tag{7.43}$$

It is noted that the function $f(\eta)$ is the familiar power law velocity profile commonly used in the investigation of turbulent flow over flat plates. The function $g(\eta)$ is somewhat triangular in shape being zero at $\eta = 0$ and $\eta = 1$ and has been normalized to have a maximum value of 1.0 at $\eta = 0.067$.

The radial and tangential profile functions specified in equations 7.15 and 7.17 were selected because they were found to be the simplest profile functions which provided a reasonable fit to the experimental data of Savino and Keshock. A comparison is made between the analytical profiles and Savino and Keshock's measured profiles in Figure 7.3 where it has been assumed that: $\frac{\delta}{h} = 0.22$, $V_\delta = 200\ \frac{\text{feet}}{\text{sec}}$, $U_\delta = 0.0$, $\frac{U_s}{U_{av}} = 6.8$. It is noted that the analytical profiles provide a reasonable fit to the experimental profiles.

With the specification of the velocity profile functions $f(\eta)$ and $g(\eta)$ by equations 7.42 and 7.43, the values of the constants $\alpha_1 \ldots \alpha_5$ defined in equations 7.27 to 7.26 may be determined to be:

$$\alpha_1 = 0.778 \qquad \alpha_2 = 0.350$$

$$\alpha_3 = 0.313 \qquad \alpha_4 = 0.439 \tag{7.44}$$

$$\alpha_5 = 0.875$$

The shear law adopted in this investigation is similar to the shear law used by Prandtl in the study of turbulent flow over a flat plate:

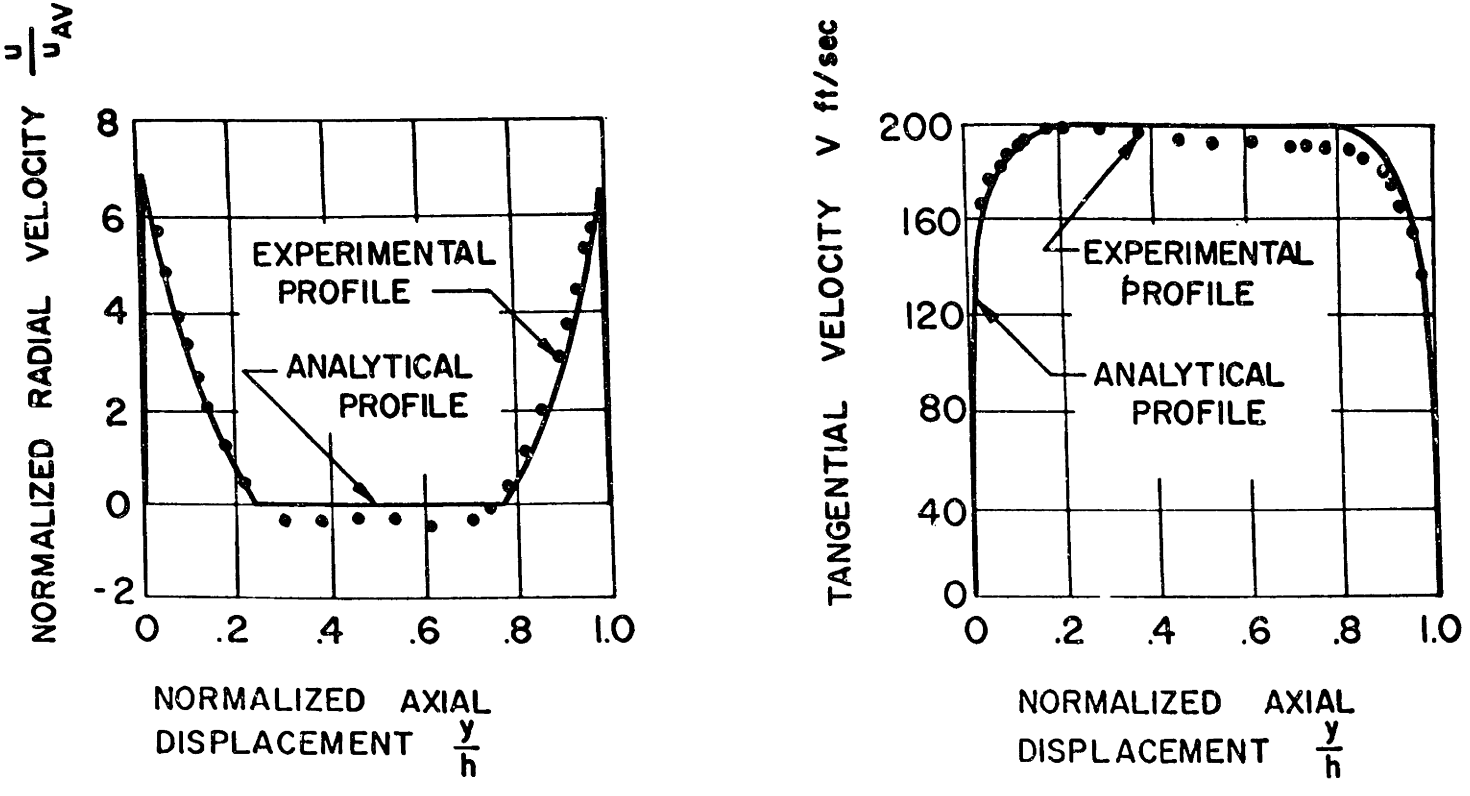

VELOCITY PROFILE DATA TAKEN AT $\frac{r}{r_o} = 0.44$

Fig. 7.3. Comparison of Analytical Velocity Profiles with the Data of Savino and Keshock, Ref. 28.

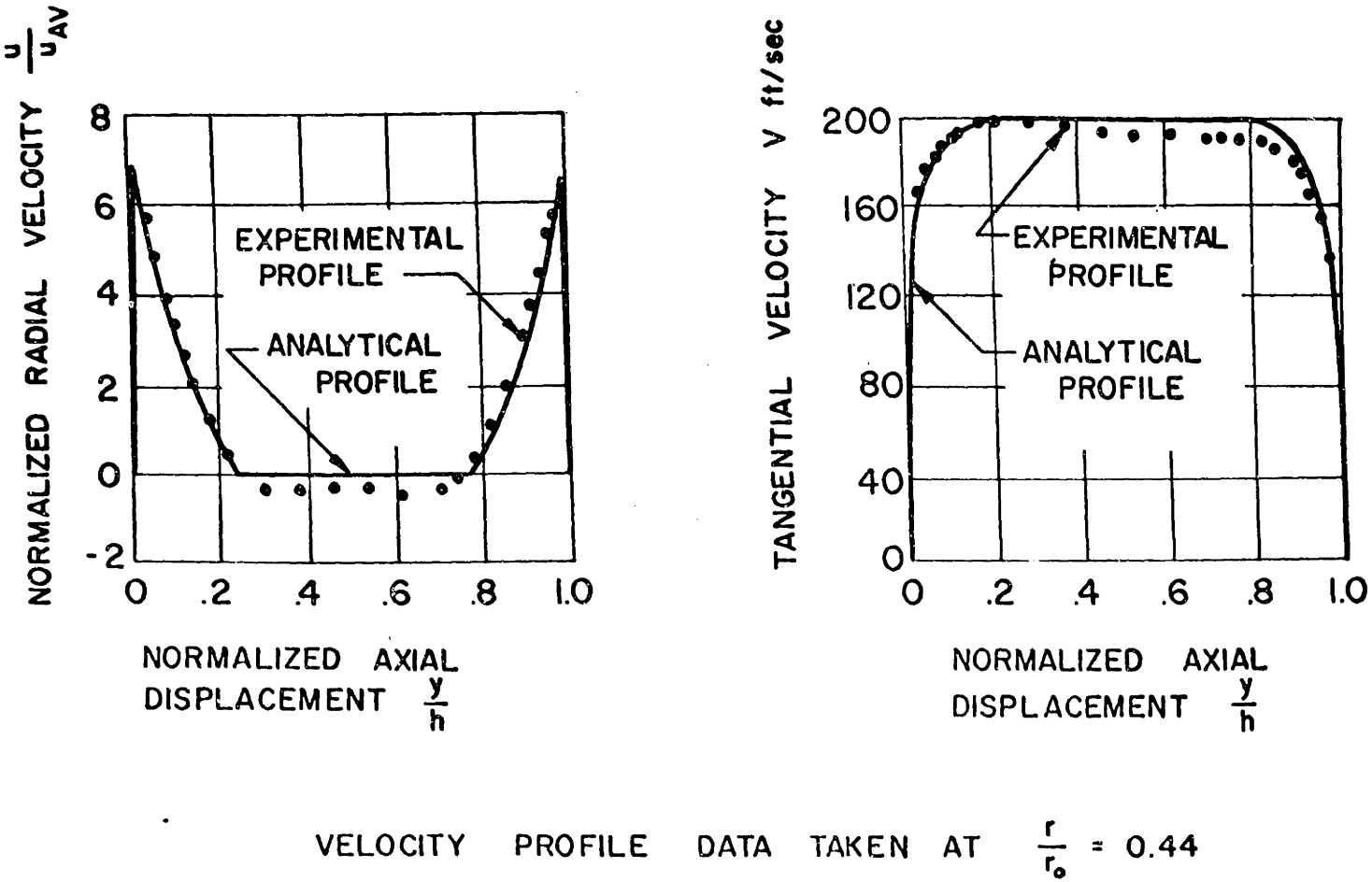

Fig. 7.3. Comparison of Analytical Velocity Profiles with the Data of Savino and Keshock, Ref. 28.

$$\tau_w = \frac{f\rho V_\infty^2}{\left(\frac{\rho V_\infty \delta}{\mu}\right)^{1/4}} \tag{7.45}$$

where:

τ_w = wall shear stress in free stream direction

f = friction coefficient

V_∞ = free stream velocity

In the case of a smooth flat plate the friction coefficient f is usually assumed to be 0.0225.

When the wall shear stresses in the vortex chamber are assumed to be similar to τ_w given in equation 7.45, the shear stresses $\bar{\tau}_{tw}$ and $\bar{\tau}_{rw}$ are:

$$\bar{\tau}_{tw} = \frac{C_f \lambda \Gamma V_f}{(1 - x)(\bar{\delta} V_f)^{1/4}} \tag{7.46}$$

$$\bar{\tau}_{rw} = \frac{C_f U V_f}{(\bar{\delta} V_f)^{1/4}} \tag{7.47}$$

where:

$$C_f = f/\left(\frac{\rho \frac{h}{2} u_o}{\mu}\right)^{1/4}$$

$$V_f = \sqrt{U^2 + \frac{\Gamma^2 \lambda^2}{(1 - x)^2}}$$

and where it is noted that V_f is the equivalent nondimensional total velocity in the core region of the vortex chamber and that C_f is an equivalent friction factor which is constant for a given flow condition.

7.3 Solution of the Vortex Chamber Equations

With the specification of the velocity profile functions and the shear law, the solution to the sets of equations derived for the developing flow region (7.28 - 7.32) and the developed flow region (7.38 - 7.41) may be solved subject to the boundary conditions at $x = 0$ given in equations 7.33 - 7.37. Solutions to the sets of equations which are ordinary, nonlinear, first order, differential equations, for the unknowns $\bar{\delta}$, Γ, U, U_s, and $\bar{P}$ were obtained by numerically integrating the equations for the developing flow region from $x = 0$ to $x = x^*$ defined by the point at which $U = 0.0$ and then integrating the developed flow region equations from x^* to the chamber exit x_e using the values of $U_s(x^*)$, $\Gamma(x^*)$, $\bar{\delta}(x^*)$ and $\bar{P}(x^*)$ provided by the solution to the developing flow set of equations. A simple step-wise integration technique was used in the integration. The step size used in the integration from $x = 0$ to $x = x^*$ was $\Delta x = 0.0005$ while the step-size used in the integration from $x = x^*$ to $x = x_e$ was 0.001. Doubling or halfing these step sizes resulted in less than 0.5% change in any computed value.

It is noted that a problem exists at $x = 0$ in starting the solution because of the factor of $\bar{\delta}^{1/4}$ in the denominator of the shear stress terms in the equations. The values of the unknowns at $x = 0.0005$ were obtained from the work of Rott (22) who derived expressions valid for small x for the total secondary flow in the boundary layer and the boundary layer thickness by integrating a reduced form of the boundary layer equations which have been derived as equations 7.4 and

7.5 in this chapter. The starting values of $\bar{\delta}$, U, and U_s appropriate for the values of the velocity profile coefficients listed in equation 7.44 and valid for $x << 1$ and $\lambda > 10$ are:

$$\bar{\delta} = \left(18.1 \left(\frac{2r_o}{h}\right) \frac{C_f\sqrt{x}}{\lambda^{1/4}}\right)^{4/5} \tag{7.48}$$

$$U_s = .686\ \lambda\sqrt{x} \tag{7.49}$$

$$U = \frac{(1.0 + .439\ \bar{\delta}U_s)}{(1.0 - .115\ \bar{\delta})} \tag{7.50}$$

where it is noted that x is to be replaced by 0.0005 to obtain the values at the first step in the integration. It is noted that the solution to the set of equations was not found to depend critically upon the exact values of $\bar{\delta}$, U_s and U used to start the solution at $x = 0.0005$. For example, it was found that the value of $\bar{\delta}$ at $x = 0.0005$ could be changed by more than 25% for solutions exhibited in Figures 7.4 and 7.5 and the values of $\bar{\delta}$, U_s, U and Γ for the two different initial values of $\bar{\delta}$ differed by less than 2% by $\bar{x} = 0.02$ and became indistinguishable for large values of x.

If consideration is restricted to obtaining the solution to the sets of equations for $\bar{\delta}$, Γ, U and U_s, then the pressure $\bar{P}$ may be eliminated by substitution from four of the equations for the developing flow region and from three of the equations for the developed flow region. This reduced set of equations may be solved for $\bar{\delta}$, Γ, U and U_s when the α's are given by equation 7.44 with the specification of only two parameters $\lambda = \frac{v_o}{u_o}$ and BLC where:

$$BLC = \frac{2r_o}{h} \frac{f}{\left(\frac{\rho u_o h}{2\mu}\right)^{1/4}} \tag{7.51}$$

The reduced sets of equations have been solved for selected values of the parameters λ and BLC. Solutions for Γ, $\bar{\delta}$, U, and U_s for selected values of λ and BLC are plotted in Figures 7.4 and 7.5.

It is noted from Figure 7.4 in the plot for BLC = 0.01 and $\lambda = 10$ that the developing flow region exists completely across the chamber, the circulation in the chamber is constant, and the boundary layer thickness grows monotonically. At these low values of λ and BLC, the inviscid core region extends completely across the chamber and the midplane circulation distribution is essentially that of a potential vortex. At low values of BLC and λ the solution for the midplane circulation distribution is similar to that derived from a two dimensional inviscid valve model such as described in Chapter 3. When the ratio of the tangential to radial velocity at the outer edge of the chamber is increased as shown in the plots for $\lambda = 50$ and $\lambda = 100$, the developing flow region no longer extends completely across the chamber. In the case of $\lambda = 50$, all the flow has entered the end wall boundary layers by $x = 0.57$ while for the case of $\lambda = 100$ all the flow has entered the end wall boundary layers by $x = 0.24$. As the ratio of $\lambda = \frac{v_o}{u_o}$ is increased, the developed flow region in which the inviscid core velocity is zero extends over a greater portion of the chamber; this occurrence corresponds closely with the observed increase in the size and extent of the spinning donut of fluid as the ratio of $\frac{v_o}{u_o}$ was increased in the flow visualization

$$BLC = 2r_0 f/h \left(\frac{\rho u_0 h}{2\mu}\right)^{1/4}$$

$$\lambda = \frac{V_o}{U_o}\ ,\quad \Gamma = \frac{Vr}{V_o r_o}\ ,\quad \bar{\delta} = \frac{2\delta}{h}\ ,\quad U_{pn} = \frac{r U_\delta}{r_o U_o}\ ,\quad U_{sn} = \frac{r U_s}{r_o U_o}\ ,\quad X = 1 - \frac{r}{r_o}$$

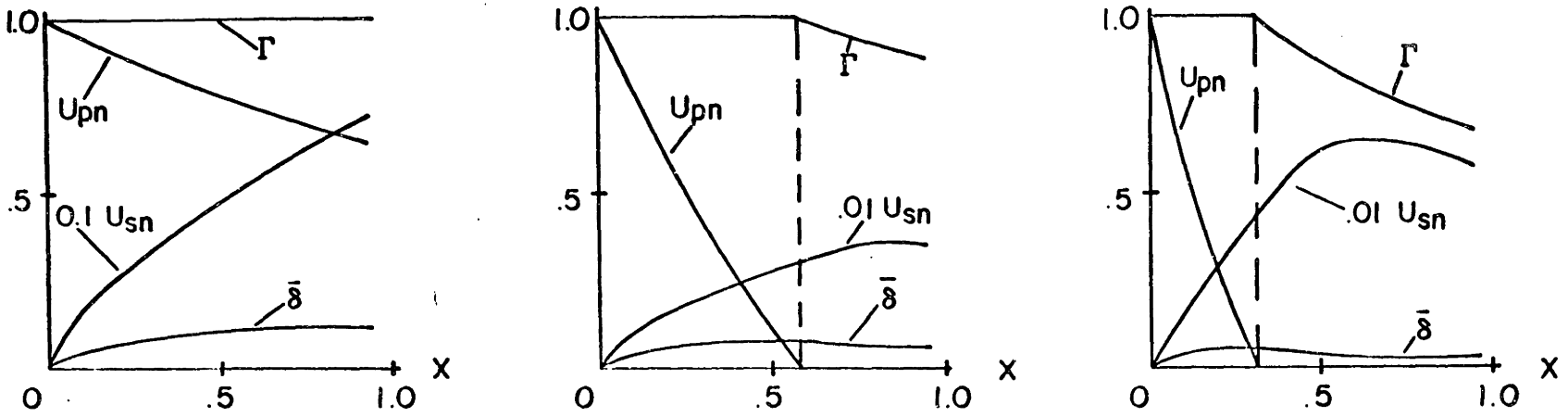

Fig. 7.4. Analytical Flow Properties of a Vortex Chamber for BLC = 0.01.

$$BLC = 2r_o f / h \left(\frac{\rho U_o h}{2\mu}\right)^{1/4}$$

$$\lambda = \frac{V_o}{U_o}, \quad \Gamma = \frac{Vr}{V_o r_o}, \quad \bar{\delta} = \frac{2\delta}{h}, \quad U_{pn} = \frac{r U_\delta}{r_o U_o}, \quad U_{sn} = \frac{r U_s}{r_o U_o}, \quad X = 1 - \frac{r}{r_o}$$

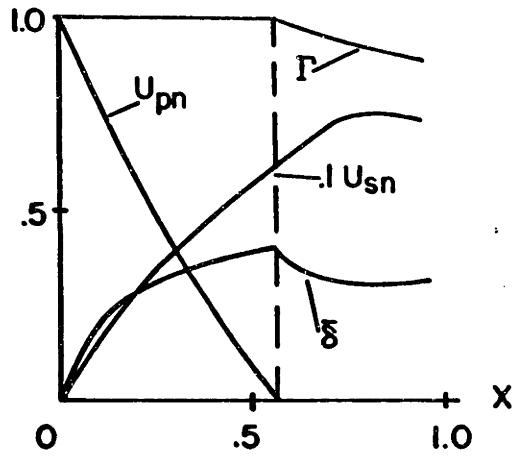

PLOT FOR BLC = 0.05,
λ = 10

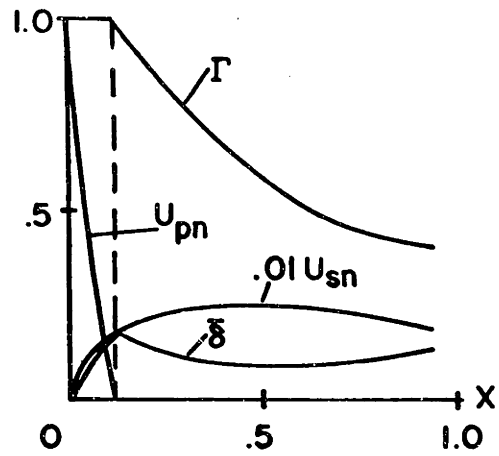

PLOT FOR BLC = 0.05,
λ = 50

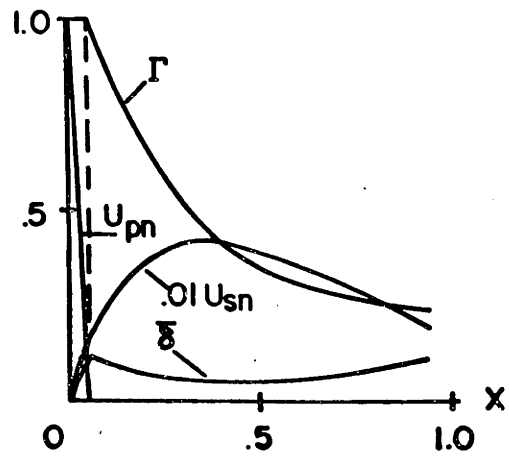

PLOT FOR BLC = 0.05
λ = .00

Fig. 7.5. Analytical Flow Properties of a Vortex Chamber for BLC = 0.05.

photographs of Chapter 6.

The nondimensional circulation $\frac{v_\delta r}{v_o r_o}$ in the plots of Figure 7.4 is constant in the developing flow region of the chamber and decreases in value in the developed flow region of the chamber reaching a value at x = 0.95 of 0.89 for $\lambda = 50$ and a value of 0.75 for $\lambda = 100$. The boundary layer grows monotonically in the developing flow region of constant Γ and decreases with increasing x for further increases in x until a point near the chamber center at which point it begins to grow again due to the fact that the flow area is decreasing rapidly with increasing x at small x. It should be noted that a factor of $\frac{r}{r_o}$ has been included in the definition of the normalized primary and secondary flow velocities, $U_{p\eta}$ and $U_{s\eta}$ plotted in Figures 7.4 and 7.5.

Plots similar to those of Figure 7.4 are shown in Figure 7.5 for BLC = 0.05. It may be noted by comparing the results at identical values of λ of Figures 7.4 and 7.5 that as BLC increases, i.e. the chamber aspect ratio decreases or the chamber friction coefficient increases, the developed flow region extends over a greater portion of the chamber and the circulation distribution is constant over a smaller region of the chamber and decreases more rapidly with increasing x. A comparison between the plots for BLC = 0.01, $\lambda = 50$ and BLC = 0.05, $\lambda = 10$ is of particular interest. The circulation distributions in these two plots are almost identical while the boundary layer thickness in the plot of $\lambda = 50$ is about 20% of the boundary layer thickness for the plot with $\lambda = 10$ at the same value of x and the secondary flow velocity $U_{s\eta}$ in the plot with λ equal to 50 is about 5 times the value of $U_{s\eta}$ in the plot for $\lambda = 10$ at the same value of x. The comparison of these plots suggests that the circulation

distribution in the chamber is dependent primarily on the product of λ and BLC which is designated as BLC^*:

$$BLC^* = BLC\ \lambda = \frac{2r_o}{h}\ \frac{v_o}{u_o}\ \frac{f}{\left(\frac{\rho u_o h}{2\mu}\right)^{1/4}} \tag{7.52}$$

The circulation distribution across the chamber has been plotted for selected values of the parameter BLC^* in Figure 7.6 and for $\lambda = 10$ and $\lambda = 200$. The plots in the Figure indicate that the circulation distribution across the chamber is essentially a function of the single parameter BLC^* when the shear law and the velocity profile functions have been specified as described above. At values of BLC^* less than 0.25, the circulation distribution across the valve chamber is constant and the developing flow region extends completely across the chamber. As the value of BLC^* increases, i.e. $\frac{v_o}{u_o}$, $\frac{r_o}{2h}$, or f increases, the circulation is constant over a smaller portion of the chamber and decays more rapidly with increasing x. It is noted that for flow conditions in which $\frac{v_o}{u_o} > 10.0$, the pressure distribution across the vortex chamber is essentially determined by the circulation distribution; therefore, the result is obtained that the pressure distribution in the vortex chamber is essentially determined by the parameter BLC^* for the choice of velocity profiles and shear law specified above. It is interesting to determine the implications of this result with respect to the observed characteristics of vortex valves. The quantity BLC^* may be rewritten in terms of valve geometry, valve nondimensional total flow $\bar{W}_o$ and valve nondimensional control flow $\bar{W}_c$ as:

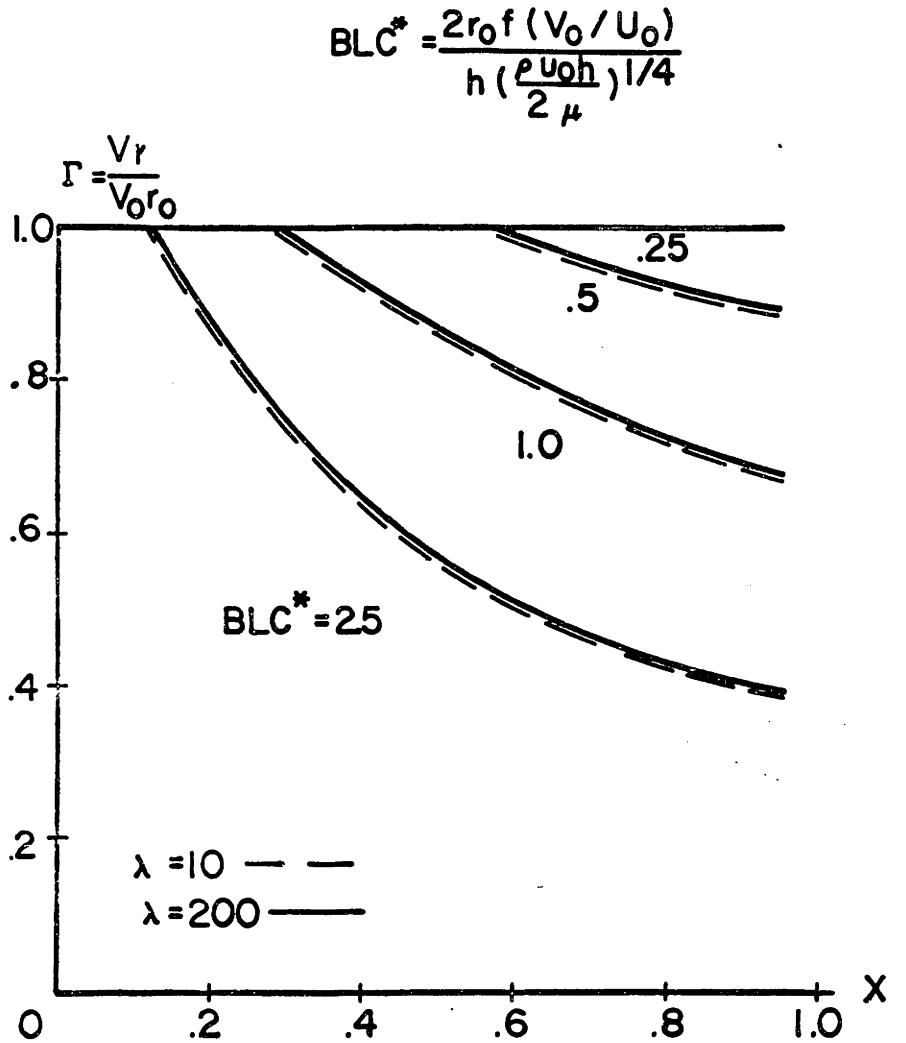

Fig. 7.6. Circulation Distribution in a Vortex Chamber.

$$BLC^* = \frac{4\pi r_o^2 \varepsilon}{A_c (\bar{W}_o)^{1/4}} \frac{\bar{W}_c^2}{\bar{W}_o^2} \frac{f}{\left(\frac{R_w}{2}\right)^{1/4}} \tag{7.53}$$

where following the work of Chapter 3 u_o has been replaced by $\frac{W_o}{2\pi h r_o \rho}$ and v_o has been replaced by $\varepsilon v_o^+ = \frac{\varepsilon W_c^2}{\rho A_c W_o}$ and where it is recalled that R_w is the maximum flow Reynolds number. In terms of valve parameters BLC^* depends strongly upon chamber radius, control port area, and the nondimensional valve total and control flows and depends weakly upon the maximum flow Reynolds number. As the value of $\bar{W}_c$ is increased and $\bar{W}_o$ decreased, the value of BLC^* increases. At a point on a valve characteristic near the maximum flow condition BLC^* would tend to be small and the flow in the chamber would tend to be nearly inviscid. At a point near cutoff on the valve characteristic BLC^* would tend to be large and the influence of the viscous losses in the end wall boundary layers would become of major importance in the valve. The quantity BLC^* does not depend upon valve chamber length. The analysis indicates that the pressure distribution in a vortex valve depends primarily upon BLC^* and is therefore essentially independent of valve chamber length and weakly dependent upon maximum flow Reynolds number. The experimental investigation described in Chapter 4 has indicated that vortex valve characteristics are essentially independent of valve chamber length and maximum flow Reynolds number. The analytical model developed in this chapter for predicting vortex chamber pressure distributions has a dependence upon geometry and fluid properties which is very similar to that observed in the characteristics of vortex valves.

7.4 Comparison of Predicted and Experimental Pressure Profiles

The analysis developed in this chapter can be used to predict the pressure distribution across the vortex chamber, given the chamber geometry (r_o, r_e, h), the flow conditions at the outside of the chamber (u_o, v_o, p_o) and the operating fluid (ρ, μ).

Pressure profiles predicted by the analysis are compared in Figures 7.7, 7.8 and 7.9 with the profiles measured experimentally in Chapter 6. The input data required by the analysis for the chamber geometry and flow conditions of each test is available from Table 6.1. The value of the end wall friction coefficient f was assumed to be 0.021 for each test. This value for f was selected because it provided a good correlation for <u>all</u> of the data taken on the apparatus. It is noted that this value of f is quite close to the value of friction coefficient of 0.0225 commonly used in flat plate work. The value of the outer periphery tangential velocity used in the analysis was the actual value V_w determined in the work of Chapter 6. In the analysis v_o was set equal to $V_w = \varepsilon v_o^+$ where it is recalled that ε and v_o^+ are the jet recovery factor and ideal tangential velocity. For each set of pressure profile data $v_o = \varepsilon v_o^+$ was determined from equation 6.6 and ε was determined from Figure 6.12. The value of u_o required by the analysis was determined from equation 7.54

$$u_o = \frac{W_o}{\rho 2\pi r_o h} \tag{7.54}$$

Data is presented in Figure 7.7 for the double exit vortex chamber in which the flow should tend to be symmetric about the chamber midplane. It is noted that close agreement exists between

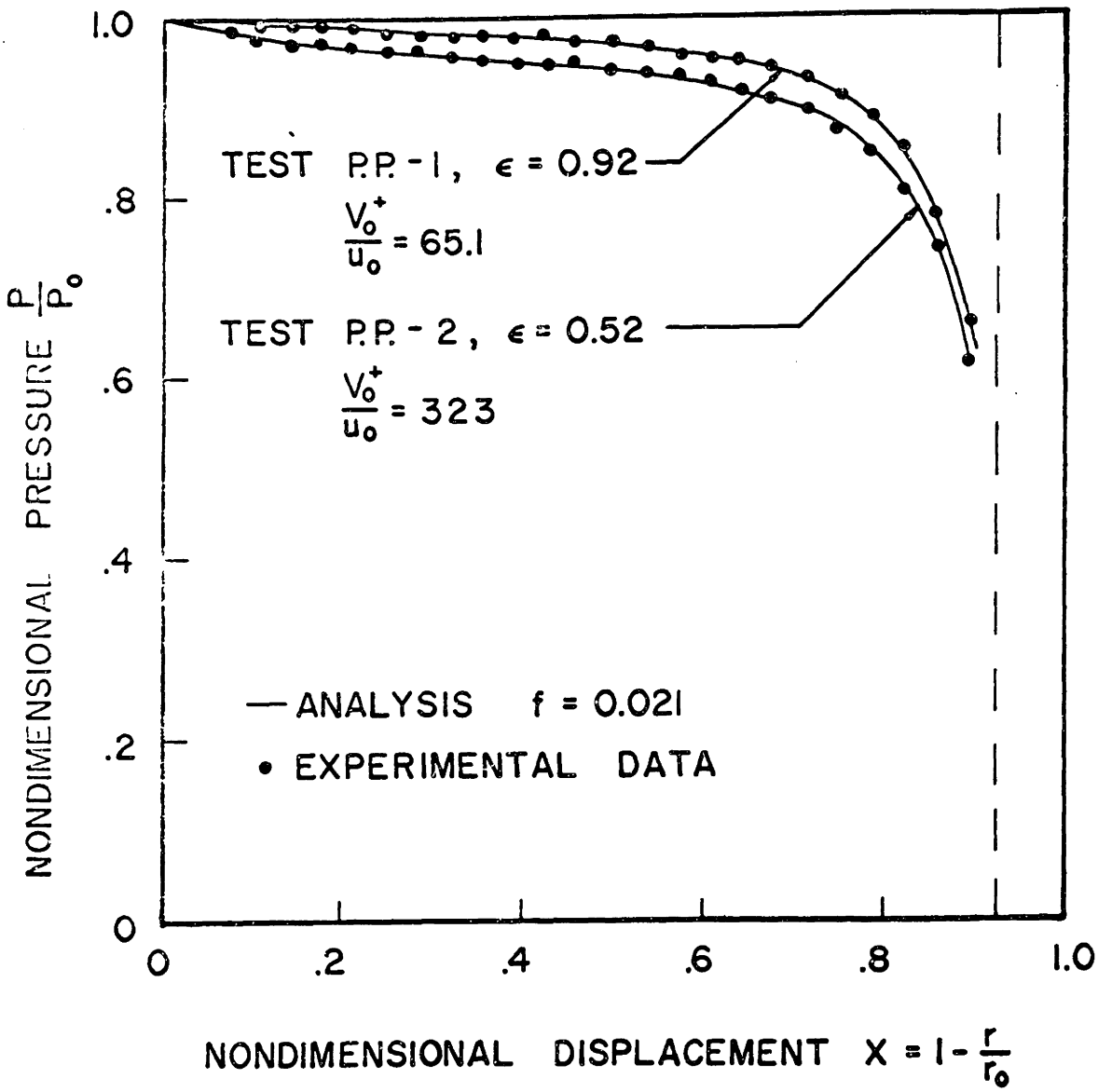

Fig. 7.7. Comparison of the Analytical and Experimental Pressure Profiles for the 0.25 inch Exit Radius Dual Exit Chamber.

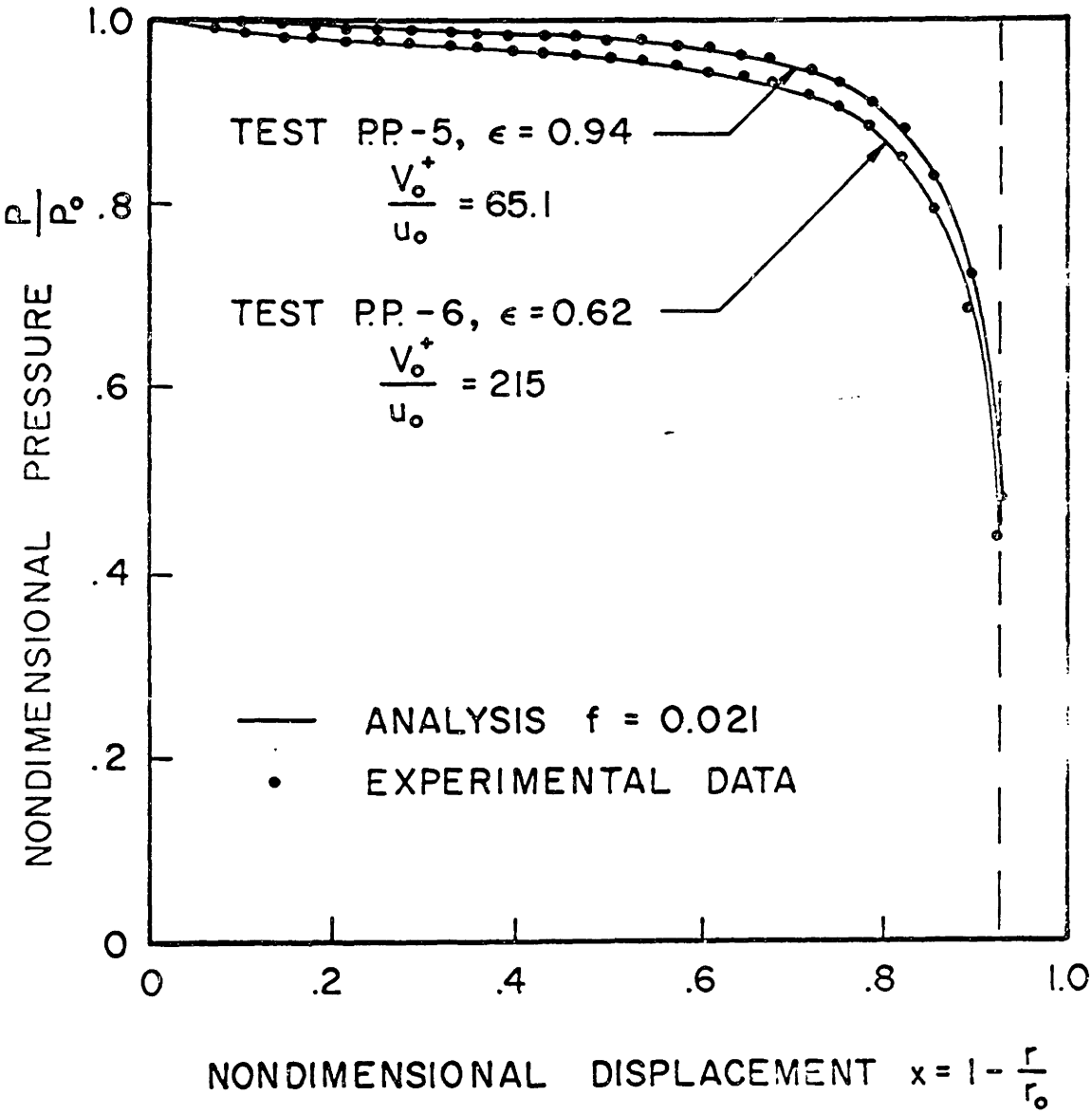

Fig. 7.8. Comparison of the Analytical and Experimental Pressure Profiles for the 0.25 inch Exit Radius Single Exit Chamber.

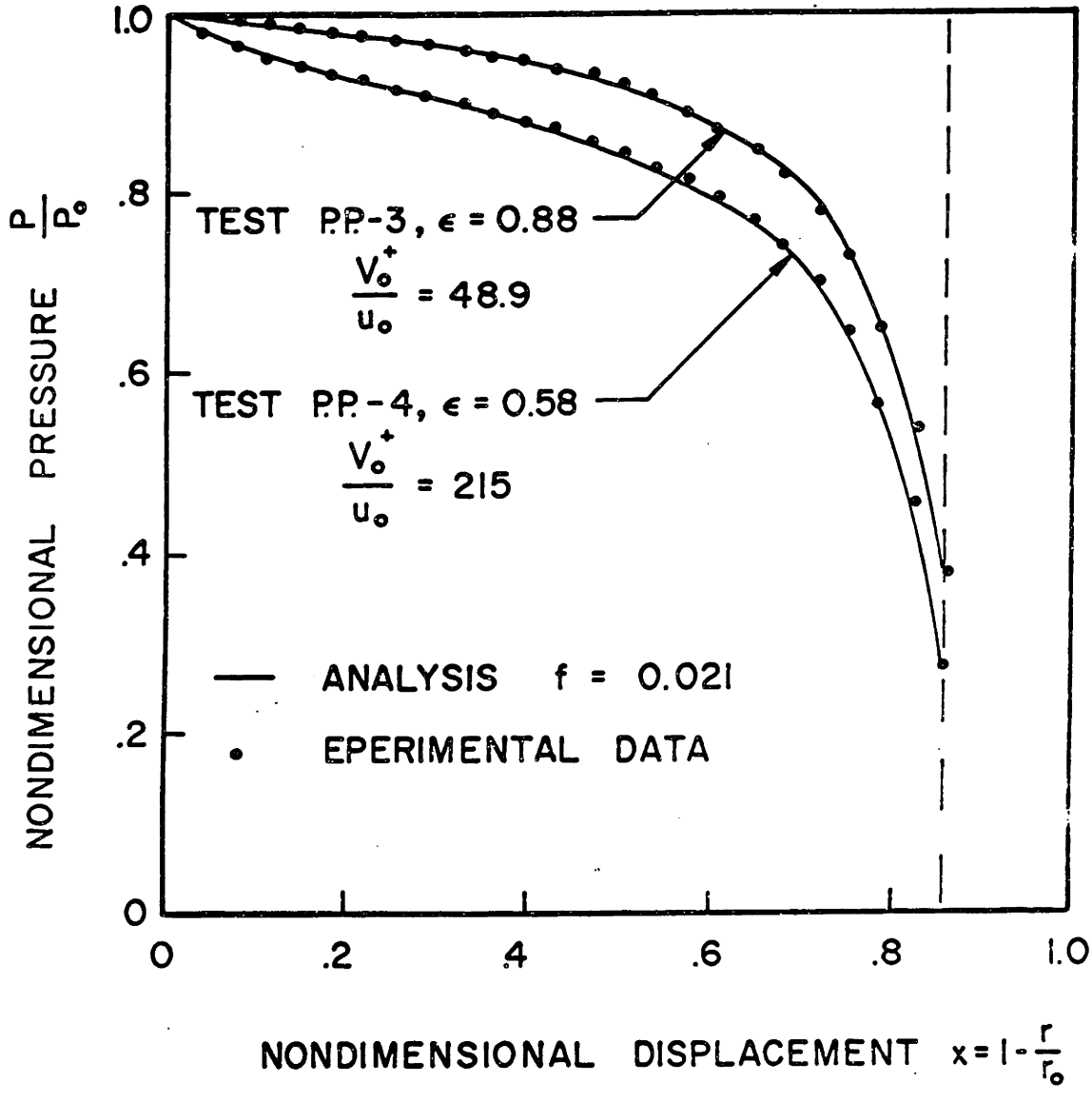

Fig. 7.9. Comparison of the Analytical and Experimental Pressure Profiles for the 0.5 inch Exit Radius Single Exit Chamber.

the analytical and experimental data for profiles at both values of $\frac{v_o}{u_o}$. In Figures 7.8 and 7.9 a comparison is made between analytical and experimental profiles for single exit vortex chambers with 0.5 and 1.0 inch diameter exit orifices. It is noted that in the cases of single exit chambers, the agreement between the analysis and the experimental data is also quite good. The effects of asymmetry in the valve exit configuration do not appear to radically influence the vortex chamber nondimensional pressure distribution.

In each of the sets of data presented in the Figures it is noted that at low values of $\frac{v_o}{u_o}$ both the analytical and experimental pressure profiles indicate that $\frac{dp}{dr}$ decreases monotonically with increasing $\bar{r} = 1 - x$ while at high values of $\frac{v_o}{u_o}$ both the analytical and experimental pressure profiles indicate that the pressure gradient $\frac{dp}{dx}$ decreases monotonically with increasing $\bar{r}$ only over a region of the chamber. At high values of $\frac{v_o}{u_o}$ in a region near the chamber outer periphery ($\bar{x} \approx .05 - .15$ for the data of the Figure) the pressure gradient $\frac{dp}{dr}$ increases with increasing r. In each case presented, the region of the chamber near the outer periphery in which the pressure gradient begins to increase in magnitude with increasing r corresponds to the transition from the developed flow region of varying circulation in which $\frac{d\Gamma}{dx} \alpha \tau_{tw}$ to the developing flow region in which the circulation is constant. As shown by equation 7.41, for the pressure gradient $\frac{dp}{dr}$ to increase with increasing radius requires that the midplane tangential velocity decrease with decreasing radius. In the developing flow region $\bar{r} = 1 - x > 1 - x^*$, the midplane tangential velocity is proportional to $\frac{1}{r}$ and $\frac{dp}{dr}$ is proportional to $\frac{1}{r^3}$. In the developed flow region $\frac{d\Gamma}{dx}$ decreases with increasing x proportional

to the end wall shear (equation 7.42) which is approximately proportional to $(\frac{v_o}{u_o})^2$ for small x. At very high values of $\frac{v_o}{u_o}$ the circulation distribution decreases rapidly enough at the beginning of the developed flow region so that the midplane tangential velocity decreases with decreasing r. (Note the circulation distribution in Figure 7.5 for $BLC^* = 0.05$, $\frac{v_o}{u_o} = 100$). Thus both the experimental data and the analytical pressure profile data tend to confirm that for sufficiently high values of $\frac{v_o}{u_o}$ a small region exists in the chamber near the chamber outer periphery in which the midplane tangential velocity decreases with decreasing radius.

In conclusion it is noted that analysis developed in this chapter has been quite successful in predicting pressure distributions across both single and dual exit vortex chambers for a variety of flow conditions including conditions with $\frac{v_o}{u_o}$ greater than 150.

7.5 Requirements of an Analytical Method of Predicting Vortex Valve Characteristics

The analysis which has been outlined in the previous sections of this chapter has considered only the flow in the vortex main chamber. In order to predict vortex valve characteristics adequate models are required for the valve inlet region and the valve exit region. In the inlet region of the valve the mixing losses can be substantial and these losses must be considered in formulating a model for this region. In the outlet region of the valve the nonuniform flow profiles approaching the exit region, the possible ejection of boundary layer flow into the exit cone, and the presence of reversed axial flow from the atmosphere pose a difficult problem.

It is apparent that to gain a complete understanding of vortex valve behavior and to be able to predict valve characteristics in detail a basic study of the valve inlet and exit regions is required. It is noted that the results of such a basic study would be useful in understanding the behavior of a broad variety of vortex-type devices.

APPENDIX A

TABULATION OF TEST CONDITIONS

The test conditions for each of the tests conducted on the four and seven inch vortex valves which are referred to in Chapter 4 are tabulated in Table A1 of this appendix.

TABLE A 1

TABULATION OF TEST CONDITIONS

TEST	CHAMBER DIAMETER	EXIT DIAMETER	CHAMBER LENGTH	CONTROL AREA	SUPPLY AREA	SUPPLY PRESSURE	MAXIMUM FLOW
	In.	In.	In.	10^{-2} In.	In^2	In. Hg. gage	lbm/sec
1	7	.500	.500	3.17	.89	3.2	.031
2	7	.500	.500	3.17	.89	6.4	.045
3*	7	.500	.500	3.17	.89	8.8	.66
4	4	.500	.75	6.34	1.62	2.0	.030
5	4	.500	.75	3.17	1.62	2.1	.031
6	4	.500	.75	1.66	1.62	5.0	.045
7	4	.500	.75	0.83	1.62	5.0	.047
8	4	.354	.75	1.66	1.62	9.0	.030
9	4	.707	.75	1.66	1.62	1.4	.043
10	4	1.00	.75	1.66	2.33	0.48	.045
11**	4	.354	.75	1.66	1.62	2.95	.033
12	4	.707	.375	0.83	0.20	5.0	.035
13	4	.707	.375	0.83	0.39	3.0	.041
14	4	.707	.375	0.83	0.78	2.0	.046
15	7	.500	2.25	3.17	3.56	3.1	.031
16	7	.500	1.25	3.17	1.78	3.2	.031
17	7	.500	.75	3.17	.89	3.2	.031
18*	7	.500	.500	3.17	.89	1.46	.27

*Test run on water at 52°F - all other tests run on air nominally at 65°F.

**Dual Exit Valve.

APPENDIX B

CONTROL PORT PRESSURE FLOW CHARACTERISTICS

The pressure flow characteristics of each of the control port areas referenced in Chapter 4 for the four inch valve are plotted in Figure B1 of this appendix. The data for the 0.0083 and 0.0166 in^2 areas correspond to control port areas which were formed by (6 and 12 respectively) 0.042 in. internal diameter steel needle tubing. The data for the 0.0317 and 0.0634 in^2 areas correspond to control port areas which were formed by (6 and 12 respectively) 0.082 inch diameter drilled holes.

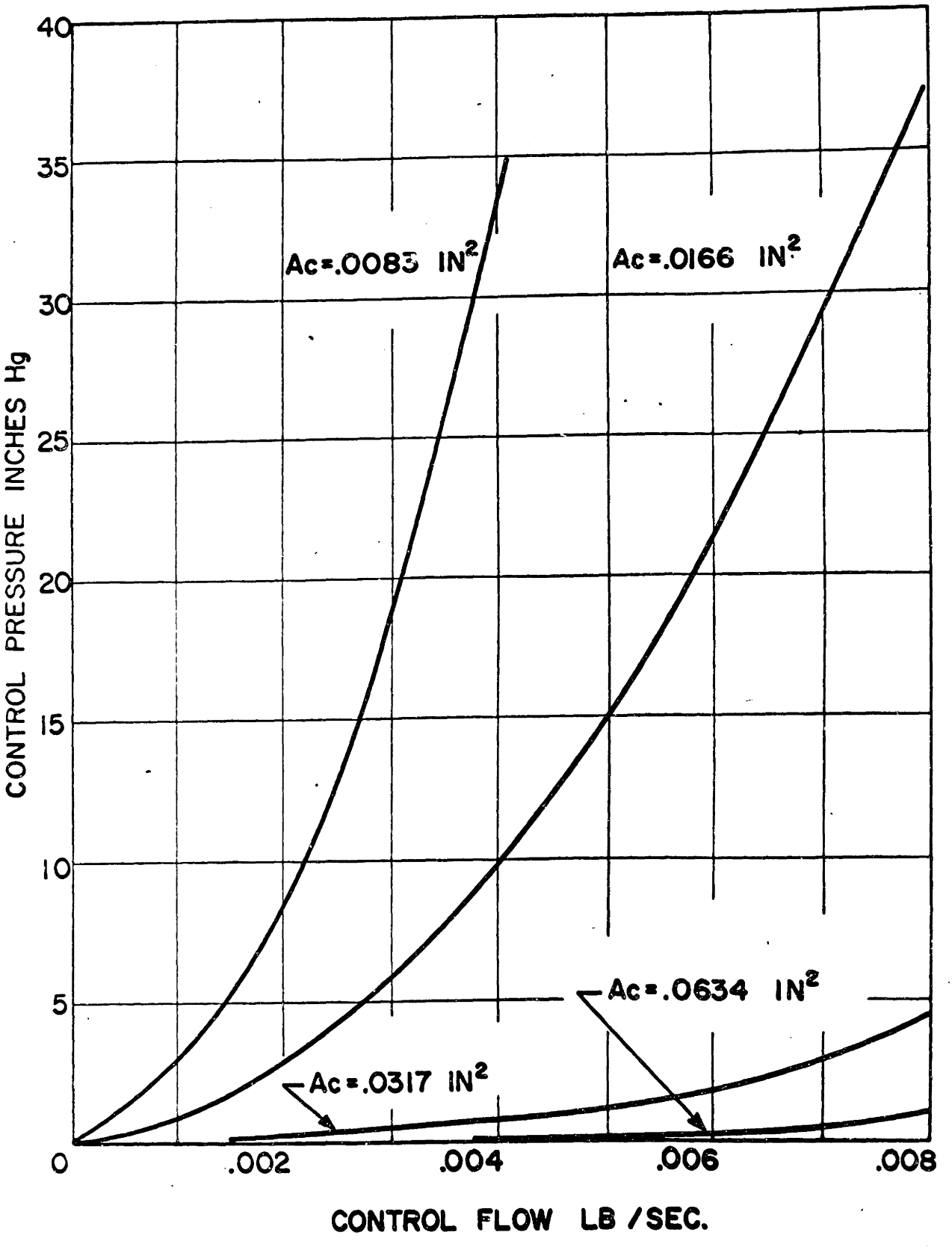

Fig. B.1. Pressure Flow Characteristics of Inlet Orifices.

BIBLIOGRAPHY

1. Gebben, V.D., "Vortex Valve Performance Power Index", Advances in Fluidics, ASME, 1967.

2. Koerper, P.E., "Design of an Optimized Vortex Amplifier", E.D.C. Report 7-65-6, Control Systems Synthesis Laboratory, Case Institute of Technology, Cleveland, Ohio, 1965.

3. Howland, G.R., "Performance Characteristics of Vortex Amplifiers", Proceedings of the Fluid Amplification Symposium", Vol. II, Harry Diamond Laboratories, Washington, D.C., 1965.

4. Rivard, J.G., Walberer, J.C., "A Fluid State Vortex Hydraulic Servovalve", Paper presented at 21st National Conference on Fluid Power, Chicago, Illinois, 1965.

5. Cardon, M.H., "Design, Fabrication, and Test of a Fluid Interaction Servovalve", NASA CR-54463, 1965.

6. Vos, C.E., "Design, Fabrication, and Test of a Flueric Servovalve", NASA CR-54783, 1965.

7. Larson, R.H., "Vortex Amplifier Parameters", Instruments and Control Systems, Vol. 39, No. 10, pg. 105-110, October 1966.

8. Otsap, B.A., "Experimental Study of a Proportional Vortex Fluid Amplifier", Proceedings of the Fluid Amplification Symposium, Vol.II, Harry Diamond Laboratories, Washington, D.C., 1964.

9. Kasselman, J.T., Rivard, J.G., "Development of an All-Fluid Amplifier Control System for Liquid Rocket Applications", NASA CR-54446, 1965.

10. Mayer, E.A., "Large-Signal Vortex Valve Analysis", Advances in Fluidics, ASME, 1967.

11. Bell, A.C., "Optimization of a Vortex Valve", S.M. Thesis, Department of Mechanical Engineering, Massachusetts Institute of Technology, December, 1965.

12. Taplin, L.B., "Phenomenology of Vortex Flow and its Application to Signal Amplification", Summer Engineering Seminars, Pennsylvania State University, University Park, Pennsylvania, July, 1965.

13. Taplin, L.B., "Small Scale Signal Analysis of Vortex Amplifiers", Bendix Research Laboratories, Southfield, Michigan, 1966.

14. Blackburn, J.F., Reethof, G., Shearer, J.L., et.al., Fluid Power Control, The M.I.T. Press, Cambridge, Massachusetts, 1960.

15. Smith, J.L., Jr., "An Experimental Study of the Vortex in the Cyclone Separator", Journal of Basic Engineering, Tran. ASME, Series D, Vol. 84, 1962.

16. Hilsch, R., "The Use of the Expansion of Gases in a Centrifugal Field as a Cooling Process", Review of Scientific Instruments, Vol. 18, 1947.

17. Kerrebrock, J.L., Meghreblian, R.V., "Vortex Containment for the Gaseous Fission Rocket", Journal of Aerospace Sciences, Vol. 28, 1961.

18. Vonnegut, B., "A Vortex Whistle", Journal of the Acoustical Society of America, Vol. 26, 1954.

19. Kwok, C.C.K., "Vortex Flow in a Thin Cylindrical Chamber and its Applications in Fluid Amplifier Technology", Report No. 66-8, Department of Mechanical Engineering, McGill University, Montreal, Quebec, Canada, 1966.

20. Mack, L.M., "Laminar Boundary Layer on a Disk of Finite Radius in a Rotating Flow, Part I", Jet Propulsion Lab. Rept. TR-32-224, 1962.

21. King, W.S., "Momentum Integral Solutions for the Laminar Boundary Layer on a Finite Disk in a Rotating Flow", Aerospace Corp. Rept., ATN-63(9227)-3, 1963.

22. Rott, N., "Turbulent Boundary Layer Development on the End Walls of a Vortex Chamber", Aerospace Corp. Rept., ATN-62(9202)-1, 1962.

23. Weber, H.E., "Boundary Layer Inside a Conical Surface Due to Swirl", Journal of Applied Mechanics, Trans. ASME, Series E, Vol. 23, 1956.

24. Ostrach, S., Loper, D.E., "An Analysis of Confined Vortex Flows", AIAA Paper No. 66-88, 1966.

25. Schlichting, H., Boundary Layer Theory, McGraw-Hill, N.Y., 1955.

26. Kendall, J.M., Jr., "Experimental Study of a Compressible Viscous Vortex", Jet Propulsion Laboratory Rept. TR-32-290, 1962.

27. Donaldson, C. du P., Williamson, G.G., "An Experimental Study of Turbulence in a Driven Vortex", Aeronautical Research Associates of Princeton Rept. ARAP Tech. Memo. 64-2, 1964.

28. Savino, J.M., Keshock, E.G., "Experimental Profiles of Velocity Components and Radial Pressure Distributions in a Vortex Contained in a Short Cylindrical Chamber", NASA TN D-3072, 1965.

29. Taylor, G.I., "The Boundary Layer in the Converging Nozzle of a Swirl Atomizer", Quarterly Journal of Mechanics and Applied Mathematics, Vol. 3, 1950.

30. Rosenzweig, M.L., Lewellen, W.S., Ross, D.H., "Confined Vortex Flows with Boundary Layer Interaction", AIAA Journal Vol. 2, 1964.

31. Anderson, O., "Theoretical Solutions for the Secondary Flow on the End Wall of a Vortex Tube", United Aircraft Corp. Rept. R-2494-1, 1961.

32. Pivirotto, T.J., "Radial Static Pressure Distributions in Confined Compressible Vortex Flow Fields", Jet Propulsion Laboratory Rept. 32-1076, 1967.

33. Roschke, E.J., "Experimental Investigation of a Confined, Jet-Driven Water Vortex", Jet Propulsion Laboratory Rept. 32-982, 1966.

34. Roschke, E.J., "Flow-Visualization Studies of a Confined, Jet-Driven Water Vortex", Jet Propulsion Laboratory Rept. 32-1004, 1966.

35. Ross, D.H., "An Experimental Study of Secondary Flow in Jet-Driven Vortex Chambers", Aerospace Corporation Rept. ATN-64(9277)-1, 1964.

36. Lee, S-Y, Richardson, H.H., et.al., "Basic Applied Research in Fluid Power Control", Department of Mechanical Engineering, Engineering Projects Laboratory, Massachusetts Institute of Technology, Cambridge, Massachusetts, 1967.

37. Williamson, G.G., McCune, J.E., "A Preliminary Study of the Structure of Turbulent Vortices", Aeronautic Research Associates of Princeton Rept. ARAP No. 32, 1961.

38. Savino, J.M., Ragsdale, R.G., "Some Temperature and Pressure Measurements in Confined Vortex Fields", ASME Paper No. 60-SA-4, 1960.

39. Sarpkaya, T., "Characteristics of Counter Vortex Oscillators", Proceedings of the Fluid Amplification Symposium, Vol. II, Harry Diamond Laboratories, Washington, D.C., 1964.

40. Rodely, A.E., White, D.F., Chanaud, R.C., "A Digital Flowmeter without Moving Parts", ASME Paper No. 65-WA-FM-6, 1965.

41. Sarpkaya, T., Goto, J.M., Kirshner, J.M., "A Theoretical and Experimental Study of Vortex Rate Gyro", Advances in Fluidics, ASME, 1967.

BIOGRAPHICAL NOTE

The author was born in Moline, Illinois on September 1, 1939. After graduating from Heidelberg Armed Forces High School in Heidelberg, Germany, he entered the Massachusetts Institute of Technology in 1958. He received a S.B. Degree in Mechanical Engineering in June, 1962.

The author entered the M.I.T. Department of Mechanical Engineering Graduate School in 1962 and received the degree of S.M. in Mechanical Engineering in February, 1964. The author has been a member of the Systems and Design Division of the Mechanical Engineering Department since entering graduate school and has held appointments as a Teaching Assistant in the Department of Electrical Engineering and as a Research Assistant and Instructor in the Department of Mechanical Engineering. He has been actively involved in the teaching of laboratory and course work in the areas of design, automatic control, fluid power control, dynamic systems, experimental engineering, and electromechanical systems and components. The author served for one year as the Coordinator of the Engineering Projects Laboratory, an interdisciplinary laboratory facility in which undergraduate and graduate student projects and research programs are conducted. The author's research activities have been primarily in the area of automatic control and fluid power control.

The author is a member of Sigma Xi and Pi Tau Sigma.